2012

Thermal Performance Study of a Prototype Multiport Heat Exchanger

Shahram Fotowat
University of Windsor

Thermal Performance Study of a Prototype Multiport Heat Exchanger

by

Shahram Fotowat

A Thesis
Submitted to the Faculty of Graduate Studies
through Mechanical, Automotive, and Materials Engineering
in Partial Fulfillment of the Requirements for
the Degree of Master of Applied Science at the
University of Windsor

Windsor, Ontario, Canada

2012

Thermal Performance Study of a Prototype Multiport Heat Exchanger

by

Shahram Fotowat

APPROVED BY:

_____
Dr. Xueyuan Nie
Department of Civil and Environmental Engineering

_____
Dr. Nader Zamani
Department of Mechanical, Automotive and Materials Engineering

_____
Dr. Amir Fartaj, Advisor, Advisor
Department of Mechanical, Automotive and Materials Engineering

_____
Dr. Bill Zhou, Chair of Defense
Department of Mechanical, Automotive and Materials Engineering

June 12, 2012

DECLARATION OF ORIGINALITY

I hereby certify that I am the sole author of this thesis and that no part of this thesis has been published or submitted for publication.

I certify that, to the best of my knowledge, my thesis does not infringe upon anyone's copyright nor violate any proprietary rights and that any ideas, techniques, quotations, or any other material from the work of other people included in my thesis, published or otherwise, are fully acknowledged in accordance with the standard referencing practices. Furthermore, to the extent that I have included copyrighted material that surpasses the bounds of fair dealing within the meaning of the Canada Copyright Act, I certify that I have obtained a written permission from the copyright owner(s) to include such material(s) in my thesis and have included copies of such copyright clearances to my appendix.

I declare that this is a true copy of my thesis, including any final revisions, as approved by my thesis committee and the Graduate Studies office, and that this thesis has not been submitted for a higher degree to any other University or Institution.

ABSTRACT

Great efforts have been made to investigate the thermal performance and fluid flow behaviour in Minichannel Heat Exchangers (MICHX), however, the examination of air side in a multiport serpentine slab heat exchanger is rare. In the current investigation, experiments were conducted on air heating via a prototype multiport MICHX. Hot DI-water at different mass flow rates and a constant inlet temperature of 70°C was passed through the channels. The water side Reynolds numbers were varied from 255 to 411. The airside Reynolds numbers were calculated based on the free mean stream velocity and varied from 1750 to 5250, while, the air inlet temperatures were in the range of 22.5°C to 34.5°C. The effects of dimensional parameters, such as Reynolds number, Nusselt number, Prandtl number, Brinkman number, and Dean number on the heat transfer performance were investigated. The effect of the serpentine on the enhancement of DI water thermal performance behaviour was studied. Heat transfer correlations were established and compared to the results in the open literature.

Dedicated to

my family,

who sacrificed a lot,

and has been a great source of motivation and inspiration.

ACKNOWLEDGEMENT

TABLE OF CONTENTS

CHAPTER IV

IV.   EXPERIMENTAL SETUP

LIST OF PUBLICATIONS

S. Fotowat, A. Fartaj, M. Ismail, M. A. Quaiyum, and Askar S. "Experimental study on air-heating through a cross-flow minichannel heat exchanger", CSME Biennial International Conference, 2012, Winnipeg, Manitoba, Canada (Published).

M. Ismail, A. Fartaj, M. Karimi, S. Fotowat, and Saadi M. "Numerical investigation of heat transfer & fluid flow characteristics through minichannel heat exchanger", CSME Biennial International Conference, 2012, Winnipeg, Manitoba, Canada (Published).

LIST OF TABLES

LIST OF FIGURES

NOMENCLATURE

A   Area (m^2)

A_a Airside total heat transfer area (m^2)

Ac   Channel cross sectional area (m^2)

A_f Fin surface area (m^2)

$A_{a,fr}$ Airside frontal area (m^2)

$A_{a,min}$ Airside minimum free flow area (m^2)

A_s Heat transfer surface area (m^2)

Br   Brinkman number

$c_{p,a}$ Specific heat capacity at constant pressure $\left(\frac{J}{kg.K}\right)$

D_{ch} Channel inside diameter (m)

De   Dean number

$D_{h,a}$ Airside hydraulic diameter (m)

$D_{h,w}$ Water side hydraulic diameter (m)

Di   Channel inside diameter

Do   Channel outside diameter

Ec   Eckert number

F   LMTD correction factor for cross-flow and multi pass heat exchanger

G_a Airside mass velocity $\left(\frac{kg}{m^2.s}\right)$

h_a Airside heat transfer coefficient $\left(\frac{W}{m^2.K}\right)$

h_w Waterside heat transfer coefficient $\left(\frac{W}{m^2.K}\right)$

k	Thermal conductivity $\left(\frac{w}{m.k}\right)$
L	Flow length (m)
L_{th}	Thermal entrance length
L_{hy}	Hydrodynamic entrance length
M	Axial conduction number
m	Fin parameter
MICHX	Minichannel heat exchanger
$\dot{m}$	Mass flow rate $\left(\frac{kg}{s}\right)$
NTU	Number of transfer unit
Nu	Nusselt number
P	Pressure (pa)
P	Perimeter (m)
Pr	Prandtl number
ΔP	Pressure difference (pa)
$\dot{Q}$	Heat transfer rate (w)
rad	Radiant heat transfer
R	Radius of serpentine curvature
R_{total}	Total thermal resistance $\left(\frac{°k}{w}\right)$
Re	Reynolds number
T	Temperature (ºC)
$\Delta T_{lm,cf}$	Log mean temperature difference (ºC)
U	Overall heat transfer coefficient $\left(\frac{W}{m^2.k}\right)$

v	Volume (m^3)
V	Velocity $\left(\frac{m}{s}\right)$
v_i	Viscous dissipation number

GREEK LETTERS

δ	Thickness (m)
Δ	Differential
ε	Effectiveness
η	Efficiency
μ	Fluid dynamic viscosity $\left(\frac{Kg}{m.s}\right)$
ρ	Density (kg/m^3)
σ	Standard deviation

SUBSCRIPTS

a	Airside
abs	Absolute
avg	Average
b	Bulk
f	Fin
ht	Heat transfer
lm	Log mean temperature
i	Inlet
o	Outlet
s	Channel surface
w	Water side

CHAPTER I

INTRODUCTION

1.1 <u>Introduction</u>

Energy exists in several forms such as heat, kinetic, mechanical, potential, electrical, etc. According to the law of conservation of energy, the total energy of a system remains constant, however, it may transform into different forms. The United States Energy Information Administration reported that the world's electrical demand will increase by almost 50% from the year of 2007 to 2035 in its International Energy Outlook (IEO), U.S. Energy Information Administration (2010).

While the actual rate at which population and electrical demands will increase is a point for debate, the idea that they will definitely be raised is widely agreed upon. A boost in electrical demand will result from such a population growth, which will require new power sources that are recently not under development.

According to the EC's Joint Research Centre (2009), heating, ventilating and air conditioning systems in the 27 European Union member countries were approximated to account for nearly 313 terawatt-hours (TWh) of electricity use in 2007, about 11% of the whole 2800 TWh of electricity which was consumed in Europe that year. North American countries have similar consumption level. Therefore, improving HVAC system performance can be a key contributor towards energy savings if the west is to achieve its goal of 20% reduction in energy use by 2020. As an example, minichannel heat exchanger (MICHX) can play an immense role in future design of the HVAC&R system to save energy through improving the heat exchanger performance.

Using more surface area and/or higher flow velocity will improve the heat exchanger performance, which essentially increases the heat transfer capacity. An abundant amount of energy savings can be achieved by the use of MICHX compared to the traditional heat exchangers.

A heat exchanger is a device used to facilitate the transfer of heat from one fluid to another without a direct contact between the fluids. Heat exchangers generally maximize the transfer of heat by increasing the contact surface area between the fluids. A conventional heat exchanger has an area density of 700 m^2/ m^3, while the MICHX are density is in the order of about 5000 m^2/ m^3.

Air to water cross flow heat exchangers that consist of flow passes of various shapes have been frequently used in many applications. Therefore, a proper choice of the air and water side heat transfer correlations in the relevant design and applications is essential. To design such heat exchangers, some basic parameters have to be considered which include: the geometry and the shape of the fins, air and water flow rates, and the heat exchanger size. In addition, the economic and environmental issues in the industry place the need for system compactness and further performance improvement. These requirements lead to the improvement of thermal performance, minimization of pressure drop, and easy fabrication.

The heat exchangers are being developed for innovative applications and have been shown to be capable of handling heat loads of up to 100 W/cm^2. A vastly efficient heat exchanger that is considered a potential alternative to substitute the conventional fin and tube heat exchanger is the mini-channel heat exchanger (MICHX). Louvered or wavy fins, flat tubes or slabs are used in the construction of mini channel heat exchangers. In

fin tube heat exchangers, the thermal resistance on the air-side is considered a limitation of the heat transfer. The louver and wavy fins in mini channel heat exchangers have been studied by a number of researchers where most of them used a numerical approach. It is found that the convective heat-transfer coefficient (h) between the substrate and the coolant is the primary obstruction to achieve low thermal resistance. Heat transfer coefficient on the air side is lower than that of the liquid side; as a result, large area density is expected from the air side [Kays and London (1984)].

Genhart (1962) designed a MICHX to boost the heat transfer rate from liquid to gas. Modern manufacturing industries are capable of making narrow channels heat exchangers due to the advancement in materials and methodology for a wide range of applications, especially in the areas of HVAC-R condensers, evaporators, automotive, and aerospace.

The heat transfer process in minichannel heat exchangers depends on the heat transfer surface area (A_s), which is proportional to the channel hydraulic diameter (D_h). The liquid flow rate depends on the cross sectional area of the channel (A_c) which is proportional to $D_h{}^2$. Thus, the ratio of the heat transfer surface area to volume (A_s/v) corresponds to $1/D$. As D decreases, the A_s/v increases (further compactness). On the other hand, Nusselt number for fully developed laminar flow is equal to $Nu=(h.D_h)/k$, an increase in h is obtained by decreasing D_h since, h is inversely proportional to the channel diameter. Therefore, by decreasing the heat exchanger channel diameter (D_{ch}), the heat transfer coefficient (h) will increase providing further compactness of the heat exchanger.

1.2 Motivations

MICHXs are used in different types of industrial applications with various geometries. Their enhanced heat transfer and small passage channels are the main characteristics that

differentiate them from other heat exchangers. A multiport flat slab minichannel heat exchanger (MICHX) is becoming more prevalent among heat exchangers. This aluminum multiport slab MICHX is predicted to be a superior candidate over conventional heat exchangers for the following reasons:

- Higher thermal performance.

- Compactness: Its area density is nearly 4000 m^2/m^3, almost six times higher than the traditional compact heat exchangers, Carrier (2006) and Kim and Groll (2003).

- Diminished both air and water sides pressure drop for a given heat duty, Kang et al. (2002) and Fan (2008).

- Lower pressure drop reduces fan size, hence decreases the energy consumption for driving the fan and its noise (environmentally friendly).

- More structural robustness since the slab structure is monolithic and more reliable compared to the tube row with the connection joints.

- It prevents structural failure due to its resistance to the vortex induced vibration and is environmentally friendly (sound pollution). Therefore, it is recommended for the HVAC-R applications, Carrier (2006).

- The serpentine effect leads to the axial heat conduction phenomenon which in turns causes a secondary flow and develops new boundary layer that result in an increase in the heat transfer rate, Dehghandokht et al. (2011).

1.3 Objectives

The objective of the present study is to investigate the heat transfer characteristics of heating the air-side and cooling the liquid-side of a serpentine slab minichannel heat exchanger. The investigation determines the effect of the serpentine bend, the presence of

the axial heat conduction, and viscous dissipation in the MICHX. The heat transfer correlation found from this current study is compared to the other available correlations. The following are the key objectives of this investigation.

- Experimentally analyze the heat transfer characteristics (h, Nu) of the airside heating and DI water cooling in a minichannel heat exchanger.

- Examine the prototype heat exchanger performance, overall thermal conductance (UA), heat exchanger effectiveness (ε), and the number of transfer units (NTU)

- Obtain the general correlations of both air and water side heat transfer and fluid flow such as Nu, h, NTU with Re, Nu with Br, and Nu with De.

- Compare the established correlations Nu_a-Re_a-Pr_a of air heating with the correlations of air cooling obtained by Dasgupta (2011).

- Possible scope of improvements in the multiport prototype MICHX.

High flux heat removal with light weight and low area density is a roadmap of challenges and opportunities. Watchful achievements of such investigation objectives provide a source of information for forthcoming research.

CHAPTER II

REVIEW OF LITERATURE

The heat exchanger design is a field of thermal engineering that involves the conversion or exchange of thermal energy and heat between two or more fluids by various mechanisms such as by; conduction, convection, radiation and phase change. In recent years, considerable research and several investigations were applied to optimize the design of compact heat exchangers with narrow channels. However, the literatures studying the air side characteristics using a minichannel heat exchanger with circular channels are rare. The Nu number found for minichannel heat exchangers is 0.21 to 16 times higher than that for conventional heat exchangers. Kandlikar and Shah (2006) classification is based on the channel size, which is widely used nowadays, is outlined in Table 1.1.

Table 1.1 Channel classifications, Kandlikar and Shah (2006)

Conventional passages	> 3 mm
Minichannels	3 mm $\geq$ D $\geq$ 200 μm
Microchannels	200 μm $\geq$ D $\geq$ 10 μm
Transitional Microchannels	10 μm $\geq$ D $\geq$ 1μm
Transitional Nanochannels	1μm $\geq$ D $\geq$ 0.1μm
Nanochannels	0.1μm $\geq$ D

2.1 Scaling Effect

The scaling effect describes the scale invariance found in many natural phenomena. Considering the scaling effect, some correlations used in conventional heat exchangers can be applied to minichannel heat exchangers working in the laminar regime. On the

other hand, the applicability of other heat transfer characteristics is still under debate. Tuckerman and Pease (1981) initially investigated the use of microchannels in a heat sink to cool the silicon integrated circuits. Inspired by Tuckerman and Pease's work, Morini (2004) investigated several experiments on single phase convective heat transfer in microchannels. Although a literature exists that covers the correlation used for a developing laminar flow in conventional pipes, the correlations concerned with the developing laminar flow in circular serpentine multi-slab MICHX are rare. Khan et al. (2010) established a correlation for a single slab mini channel heat exchanger using 50% ethylene glycol-water mixture as the working fluid. The correlation found for that study was $Nu = 0.152 \, Re_g^{0.4912} Pr_g^{0.33}$, for Reynolds number range of $1400 \geq Re_a \geq 400$, which is higher than that for a fully developed flow in conventional heat exchangers. Dasgupta (2011) studied the air side of a mini channel heat exchanger using DI-water as the working fluid. The correlation was found from his study is $Nu_a = 0.3972 \, Re_a^{0.3766}$, he noticed that Nu is higher than Tang and Tailor's (2005). The main advantages minichannel heat exchangers provide over conventional compact heat exchangers considering the same heat transfer duty are: smaller size, lighter weight, larger heat transfer area density (m²/m³), lower fluid waste and less pollution for some fluids like Freon, higher heat transfer coefficient and energy efficiency.

2.2 Axial Heat Conduction in the Channel Wall

Gamrat et al. (2005) numerically analyzed the entrance and conduction effects in rectangular micro channel heat sinks. Two and three dimensional numerical models with 1mm and 0.1 mm channel spacing were studied. In their study, water was used as the working fluid with Reynolds number range of 200 to 3000. The numerical simulation

results found to have a good agreement with the published data on flow and heat transfer in two dimensional channels. Results show that the entrance effect is dependent on Reynolds number and the channel spacing, which are not the same found for the reference case of uniform inlet velocity and temperature profiles reported by Shah and London (1978). The numerical models used in their work assumed some simplifications, e.g. viscous heating was not taking into account, which can decrease the Nusselt number especially for channels of smaller spacing than those investigated in the current work. There was no size effect on heat transfer showed when the channel spacing is reduced from 1mm down to 0.1 mm. As a result, the strong reduction in Nusselt number observed in the experiments cannot be explained due to conduction effects such as the axial conduction in the walls or deficient of two-dimensionality of the heat flux distribution since the geometry is complex.

Tiselj and Hetsroni (2004) experimentally and numerically investigated heat transfer characteristics of water flowing in silicon micro channels with the length (L) of 10mm, D_h of 160 μm, Re=3.2~64, and the L_{th} =0.13~3.3 mm. It was shown that the bulk water and wall temperatures do not change linearly along the channel. The local Nu range varied from 1.5 ~ 2.5. The Nu number along the channel had a particular point at which the difference between the temperatures of the wall and the bulk water becomes negative, the flux changes its sign, and is directed from the fluid to the wall. There are significant changes in the temperature gradient in the flow direction. Close to the channel outlet, the temperature gradients change sign. This value depends on Reynolds number and shifts to the channel outlet with the increase in Re. The non-monotonic behavior of the fluid and heated wall temperatures is due to high values of axial heat flux in the silicon wafer. The

axial heat flux has a maximum near the inlet collector and decreases in the flow direction up to zero. Zhuo et al. (2007) experimentally and numerically investigated 3 different rough tubes and 3 other different soft tubes with $D_h = 50 \sim 1570$ and de-ionized water to cool the water at Re= $20 \sim 2400$. Axial heat conduction (AHC) was studied numerically. The effect of AHC weakened as Re increased and relative tube wall thickness decreased, thus the local Nu approached the conventional theory prediction. Axial heat conduction number M is a dimensionless number that was used to express the relative importance of the axial heat conduction in the tube wall over the convective heat transfer of the fluid flow in the tube. M is not the only criterion for judging whether the axial heat conduction can be neglected. When increasing Re to more than 100, the results agreed with the traditional heat transfer characteristics.

$$M = \frac{\emptyset_{cond}}{\emptyset_{conv}} = \frac{A_{c,o} K_s \Delta T_s / L_h}{A_{c,i} \, \rho \, C_p u_{ave} \Delta T_l} \tag{2-1}$$

Where

$$A_{c,i} = \pi R_i^2, \text{ and } A_{c,o} = \pi (R_o^2 - R_i^2)$$

$$\Delta T_l = T_{b,avg} - T_{in} \tag{2-3}$$

$$\Delta T_s = T_{s,out} - T_{in}$$

The heat conduction of water in mini-micro channels was numerically investigated by Maranzana et al. (2004). The wall heat flux density, for small Reynolds numbers, can become strongly non-uniform: most of the flux is transferred to the fluid flow at the entrance of the mini–micro-channel. Another finding was that axial heat conduction in the walls of a mini–micro counter-flow heat exchanger yielded a loss of efficiency: an optimal wall conductivity that maximized this efficiency existed. A new non-dimensional number, axial conduction number (M) quantifying the relative part of conductive axial

heat transfer in walls has been introduced. Disregarding this effect can lead to very large bias in the experimental estimation of heat transfer coefficients, especially for small Reynolds numbers. Even if the non-dimensional numbers (Br_w, and NTU) and boundary conditions have an effect on axial conduction too, it has been noticed that in the simulation of most cases that were studied, axial conduction can be neglected as soon as the M number becomes smaller than 10^{-2}. Axial conduction in the walls has to be considered for the design of mini channel heat exchangers. There existed an optimal conductivity for the wall which maximized the exchanger efficiency.

Cole and Cetin (2011) numerically studied axial conduction both in the fluid and in the adjacent wall for heating using a parallel-plate microchannel. A uniform heat flux was applied to the outside of the channel wall. The fluid was liquid with constant properties and a fully-developed velocity distribution. The study included obtaining numerical results for the local and average Nusselt number for various flow velocities, heating lengths, wall thicknesses, and wall conductivities. These results have applications in the optimal design of small-scale heat transfer devices in areas such as biomedical devices, electronic cooling, and advanced fuel cells. It was found that the effect of the axial conduction in the channel wall is important when: (i) the microchannel has a small length-over-height ratio; (ii) the Peclet number (Pe) is small; (iii) the wall thickness relative to the channel height is large; and, (iv) the wall conductivity of the wall material is high relative to the thermal conductivity of the working fluid. For high Pe flow (e.g. Pe> 100) along with a low thermal conductivity wall, the effect of the axial conduction in the wall is negligible.

2.3 <u>Viscous Dissipation</u>

Viscous dissipation is defined as the transformation of kinetic energy to internal energy (heating up the fluid) due to viscosity. These energies include both turbulent kinetic energy and mean flow kinetic energy. Viscous dissipation in fluid dynamics usually means dissipation of energy, although it can be dissipation of vortices etc. In a viscous fluid flow, the viscosity of the fluid will take energy from the motion of the fluid (kinetic energy) and transform it into internal energy of the fluid which leads to temperature rise of the fluid. This process is partially irreversible and is referred to as dissipation, or viscous dissipation. Dissipation is high in regions with large gradients (boundary layers, shear layers etc.) and also in regions with very high turbulence levels (wakes etc.). At high Mach numbers (air Reynolds number is also an important parameter) there is a considerable amount of temperature rise in the boundary layer due to "viscous dissipation".

The energy transferred to heat will raise the temperature of the fluid. Viscous dissipation is also important in high viscosities fluid flows where the temperature of the fluid increases with the increase of viscosity. Viscous dissipation is considered here for vertical surfaces subject to both isothermal and uniform-flux surface conditions.

Viscosity is a measure of the resistance of a fluid which is being deformed by either shear or tensile stress. In everyday terms (and for fluids only), viscosity is the "thickness" or the "internal friction". Thus, water is "thin", having a lower viscosity, while honey is thick. Koo and kleinstreuer (2004) numerically and experimentally examined the viscous dissipation effects in microchannels and micro tubes using three common working fluids water, methanol and isopropanol in different conduit geometries. It was established that in microchannels viscous dissipation is a strong function of the channel aspect ratio,

Reynolds number, Eckert number, Prandtl number and conduit hydraulic diameter. Thus, ignoring viscous dissipation can affect the accuracy of the flow simulations and measurements in micro conduits.

The viscous dissipation effect on the friction factor was found to increase as the system size decreases. Specifically, for water flow in a tube with D < 50 μm, viscous dissipation becomes significant and hence should be taken into consideration for all experimental and computational analyses.

Channel size, Reynolds number, and the Brinkman number (or the Eckert number and the Prandtl number) are the key factors which determine the impact of viscous dissipation. Viscous dissipation effect can be very important for fluids with low specific heat capacities and high viscosities, even in relatively low Reynolds number flows.

The effect of viscosity change, caused by variations in fluid temperature, on viscous dissipation was found to be measurable for flows in a long channel with a small hydraulic diameter. For liquids, the viscous dissipation effect decreases as the fluid temperature increases. The aspect ratio of a channel, i.e., height vs. width plays an important role in viscous dissipation. Specifically, as the aspect ratio deviates from unity, the viscous dissipation effect increases. Viscous dissipation increases rapidly with a decrease in channel size and hence should be considered along with imposed boundary heat sources. Ignoring the viscous dissipation effect could ultimately affect friction factor measurements for flows in micro conduits.

Morini (2005) analytically studied viscous heating of liquid flow in micro-channels. The viscous dissipation effect was demonstrated to be a typical ''scaling effect'' for micro-channel flows. This effect can become very important for liquid flows when the hydraulic

diameter is less than 100 μm. The temperature rise in an adiabatic micro-channel has been expressed as a function of the Eckert, and Reynolds numbers. The theory of heat transfer in microtubes with viscous dissipation effect has been studied by Tunc and Bayazitoglu (2001) considering steady state laminar flow with uniform temperature and uniform heat flux boundary conditions. Herwig and Hausner (2003) explained the deviation of minichannel heat exchangers from the conventional heat exchangers as scaling effects since the minichannel used in the study is relatively short (<150 D).

Variable property effects due to axial temperature and pressure drops probably are of minor importance. Therefore, the focus would be first on axial heat conduction and the conjugate effect. CFD calculations with adequate grid resolution are a proper tool, since the flow is laminar so that there is no turbulence modeling problem. It is demonstrated that the bulk temperature is not distributed linearly between the inlet and outlet values. Physically, this corresponds to the strong conjugate effects and considerable axial heat conduction.

Xu et al. (2002) theoretically analyzed and examined the effects of viscous dissipation in microchannel liquid flows. The parameters affecting the viscous dissipation in microtubes included D, L, ρ, c_p, k, μ, U_m, and ΔT. From the Buckingham Pi theorem, for a case with eight parameters and four primary dimensions, four independent dimensionless groups exist, $\Pi 1$, $\Pi 2$, $\Pi 3$ and $\Pi 4$ in descriptions of the relationships of these eight parameters.

$$G\ (\Pi 1,\ \Pi 2,\ \Pi 3,\ \Pi 4) = 0 \qquad\qquad (2\text{-}5)$$

Adopting the standard approach in dimensional analysis, and choosing ρ, c p, U, and D as the repeated parameters, the remaining four parameters may be expressed in terms of the repeated parameters as,

$$[k]\frac{ML}{t^3 T} = [\rho U_m C_p D] \tag{2-6}$$

$$[\mu] = \frac{M}{Lt} = [\rho U_m D] \tag{2-7}$$

$$[\Delta T] = T = \frac{U_m^2}{C_p} \tag{2-8}$$

$$[L] = L = D \tag{2-9}$$

$$\Pi_1 = \frac{\rho . U_m . C_p . D}{K} \tag{2-10}$$

$$\Pi_2 = \frac{\rho U_m D}{\mu} \tag{1-11}$$

$$\Pi_3 = \frac{C_p \Delta T}{U_m^2} \tag{2-12}$$

$$\Pi_4 = \frac{L}{D} \tag{2-13}$$

$$\Pi_2 = Re \tag{2-14}$$

$$Pr = \frac{\Pi_1}{\Pi_2} \tag{2-15}$$

$$\Pi_5 = \frac{C_p T_{ref}}{U_m^2} \tag{2-16}$$

$$v_i = \frac{\Pi_4}{\Pi_2 \Pi_5} = \frac{\mu U_m^2 L}{\rho U_m C_p T_{ref} D^2} \tag{2-17}$$

$$\Delta T^* = A.(v_i)^a.(Re)^b.(Pr)^c.\left(\frac{L}{D}\right)^d \tag{2-18}$$

$$\Delta T^* = \frac{93.419 \, v_i . Pr^{-0.1}}{5.2086 + v_i . Pr^{-0.1}} \tag{2-19}$$

v_i can be referred to as the viscous number and it measures the viscous dissipation energy relative to fluid energy rise as in the following equations,

$$v_i . Pr^{-0.1} \leq 0.056 \quad No \; viscous \; dissipation \; effect \tag{2-20}$$

$$v_i . Pr^{-0.1} \geq 0.056 \quad significant \; dissipation \; effect \tag{2-21}$$

It was found that the viscous dissipation effect becomes significant and influences the temperature, the pressure, and velocity distribution of the flow. Therefore, relationships between the average friction factor and the Reynolds number change when the hydraulic diameter of the microchannel is very small. The viscous dissipation effect is shown in the rise of the velocity gradient as the hydraulic diameter reduces for a constant Reynolds number. Choosing water as an example, the criterion for the significance of the viscous dissipation effect on flows has been established. This criterion can be used to evaluate the possibilities of the viscous dissipation effect on flows in micro geometries. The method employed can also be used to discuss the effects of the viscous dissipation for other fluids flowing in micro geometries.

TSO et al. (1998) surveyed the convective heat transfer in microchannels where Brinkman number (Br) is proposed as a parameter for correlating the convective heat transfer parameters. Principal dimensional analysis using inputs from the survey showed that in addition to Re, Pr, and a dimensionless geometric parameter of the micro-channels, Nu can be correlated with Br in the form of equation (4) generally, and in the form of equation (16) specifically for rectangular microchannels. Br is not only a measure of the relative importance of viscous dissipation in microchannels, but also decides the fundamental limit for the reduction of the microchannel dimension. It should be more important in the laminar regime compared to the transition and turbulent regimes. For the case of heating, the exponent of Br is positive as it is confirmed by experimental data. From the present analysis, the exponent of Br is negative for cooling. The unusual behavior of the decrease in Nu with the increase in Re in the laminar regime can be explained using Brinkman number.

TSO et al. (2000) experimentally investigated the unusual behavior of Nusselt number with Brinkman number in the laminar regime using water flow in a microchannel test specimen. The laminar single-phase forced convective heat transfer in microchannels correlates with Brinkman number at constant wall heat flux boundary condition. The global correlation for Br followed a good trend quantitatively for constant wall heat flux boundary condition as the data was obtained along the flow. The Brinkman number is associated with the convection heat transfer. Variations in the Brinkman number captured the variation in the change in viscosity both over the cross section and along the flow, and the momentum transfer and conduction heat transfer across the flow. The viscosity variations combined with the temperature and velocity fields cause a change in the temperature profile along and across the flow which in turns affect the rate of convection. This effect is generally observed in microchannels and identified here as the secondary effect of Br.

2.4 The Minichannel Heat Exchanger (MICHX)

Forced convection heat transfer in a cross-flow microchannel heat exchanger was experimentally investigated by Cao et al. (2010). The maximum volumetric heat transfer coefficient found with DI-water as the working fluid reached $11.1 MW.m^{-3}.K^{-1}$ with a corresponding pressure drop of less than 6 kPa when Reynolds number in the microchannels was ~64. Furthermore, the maximum volumetric heat-transfer coefficient using air as the working fluid was $0.67 MW.m^{-3}.K^{-1}$ at a corresponding pressure drop of ~30 kPa when Re ≈ 1026. Correlations of the average Nusselt number and Re values were obtained from the main cryogenic heat exchanger (MCHE) with 2 plates and their validity was confirmed by other MCHEs with 2 and 10 plates.

CHAPTER III

DESIGN AND METHODOLOGY

3.1 Key Assumptions

The following assumptions were made to facilitate data reduction and proper evaluation.

- Experiments were conducted at steady state.

- Heat transfer due to radiation is negligible.

- No heat loss from the test chamber to the surrounding.

- No condensation on the surface of the heat exchanger.

3.2 Bulk and Wall Temperatures

The use of the fluid bulk mean temperature to evaluate the fluid thermo-physical properties was suggested by Shah and Sekulic (2003). Their book provides a detail explanation of why calculating the fluid properties at the bulk temperature. Muzychka, (2011) also suggested the use of the bulk temperature for calculating the fluid properties in heat exchangers.

Muzychka (2011) explained the use of the fluid temperature based on the application such as using the fluid inlet temperature for single fluid application as in heat sinks and fluid Bulk mean temperature for two fluids application as in heat exchangers. In the current study, the mean bulk temperature was considered as the representative temperature for finding the properties of the working fluids.

The thermo-physical properties of DI-water were found which basically include; specific heat, thermal conductivity, density, dynamic viscosity, etc. The bulk mean temperatures of DI-water and air are calculated from the following formulas,

$$\text{Bulk temperature for the DI} - \text{water} \quad T_{b,w} = \frac{T_{w,i} + T_{w,o}}{2} \qquad (3\text{-}1)$$

$$\text{Bulk temperature for the air} \quad T_{b,a} = \frac{T_{a,i} + T_{a,o}}{2} \qquad (3\text{-}2)$$

Inner surface wall temperature ($T_{s,i}$) and outer surface wall temperature ($T_{s,o}$) are used in the calculation of the dimensionless numbers such as Eckert Number (Ec), and other parameters such as the heat transfer coefficient (h). Thermocouples were installed at the outer surface of the channel wall to provide the temperatures readings. While, the inner surface temperature is calculated as,

$$T_{s,i} = T_{s,o} + (Q_{avg} \times R_{wall}) \qquad (3\text{-}3)$$

Where, R_{wall} is wall thermal resistance and can be computed as,

$$R_{wall} = \frac{Ln(\frac{D_o}{D_i})}{2\pi \, k_{wall} L} \qquad (3\text{-}4)$$

3.3 Dimensionless Numbers

A dimensionless number is a quantity disassociated from any physical dimension. Dimensionless quantities are broadly used in physics, mathematics, and engineering. The well-known dimensionless quantities in the field of heat transfer which are explained below are Re, Pr, and Nu. A summary of the most important dimensionless numbers follows hereafter.

3.3.1   Reynolds Number (Re)

Reynolds number (Re) is a dimensionless number named after the founder Osborne Reynolds. It is the most significant dimensionless number defined as the ratio of the inertia forces over viscous forces. Re is used to characterize different flow regimes such as: laminar, transition, and turbulent flows. Laminar flow occurs at low Reynolds numbers, where viscous forces are governed, and is characterized by smooth and constant fluid movement. Turbulent flow occurs at high Reynolds numbers and is governed by

inertial forces, which incline to produce messy eddies, vortices and other flow instabilities. Re definition is shown as follows,

$$Re_w = \frac{Inertia\ force}{Viscous\ force} = \frac{\rho_w V_w D_{h,w}}{\mu_w} = \frac{G_w D_{h,w}}{\mu_w} = \frac{\dot{m}_w}{51\rho\pi\mu D_h} \qquad (3\text{-}5)$$

$$Re_a = \frac{Inertia\ force}{Viscous\ force} = \frac{\rho_a V_a D_{h,a}}{\mu_a} = \frac{G_a D_{h,a}}{\mu_a} = \frac{4\dot{m}_a L}{\mu_a A_a} \qquad (3\text{-}6)$$

Where

$$G(mass\ flux) = \frac{mass\ flow\ rate}{cross\ section\ area} = \frac{\dot{m}}{A_{min}} \qquad (3\text{-}7)$$

D_h is a characteristic length or a hydraulic diameter, and is shown as

$$D_h = \frac{4A}{P} \qquad (3\text{-}8)$$

P is the wetted perimeter. For circular cross section geometry, the equation becomes as,

$$D_h = \frac{4(\pi D^2)}{4\pi D} \qquad (3\text{-}9)$$

Where, the hydraulic diameter is the channel diameter.

Muzychka, et al. (2009) investigated non circular cross section geometry in a laminar developing flow. They presented a new characteristic length, which is the square root of the channel cross sectional area. Bahrami et al. (2009) concluded that the square root of the channel cross sectional area can convey better results in fluid flow studies when expressing the hydraulic diameter of the geometry.

$$D_h = \sqrt{A} \qquad (3\text{-}10)$$

For the current study, Re is shown as,

$$Re = \frac{\dot{m}}{51\rho\pi\mu D_h} \qquad (3\text{-}11)$$

3.3.2 Prandtl Number (Pr)

The Prandtl number is a dimensionless number named after Ludwig Prandtl who introduced the concept of the thermal boundary layer. Prandtl number is defined as

$$Pr = \frac{Momentum\ diffusivity}{thermal\ diffusivity} = \frac{\nu}{\alpha} = \frac{\mu\ c_p}{k} \tag{3-12}$$

The heat transfer rate depends on the thermal boundary layer as well as the velocity boundary layer. The thermal boundary layer is thicker compared to the velocity boundary layer when Pr<<1 and thinner when Pr>>1. Prandtl number < 1 indicates higher thermal diffusion in heat transfer.

3.3.3 Nusselt Number (Nu)

Nusselt number reveals how much faster the convective heat transfer can occur. It is named after Erst Kraft Wilhelm Nusselt, a German scientist. This dimensionless number is the ratio of convection to conduction heat transfer. It is expressed as,

$$Nu = \frac{Convective\ heat\ transfer\ coefficient}{condtative\ heat\ transfer\ coefficient} = \frac{hD_h}{k} \tag{3-13}$$

$$Nu_a = \frac{h_a D_{h,a}}{k_a} \tag{3-14a}$$

$$Nu_w = \frac{h_w D_{h,w}}{k_w} \tag{3-14b}$$

3.3.4 Dean Number (De)

The Dean number (De) is another dimensionless number. It was found while W.D. Dean, its creator, was investigating a fully developed laminar flow in a curved circular cross section tube. It shows the ratio of the viscous force on a fluid flowing in a curved pipe or a serpentine channel to the centrifugal force. Furthermore, it represents Re and the ratio of the square root of tube radius to the radius of the curvature.

$$De = \frac{viscous\ force\ acting\ on\ a\ fluid\ flowing\ in\ a\ curved\ pipe}{centerifugal\ force} \tag{3-15}$$

$$De = \frac{\rho VD}{\mu}\left(\frac{D}{2R}\right)^{\frac{1}{2}} \tag{3-16}$$

$$De = Re\left(\frac{D}{2R}\right)^{\frac{1}{2}} \tag{3-17}$$

For a Newtonian flow, the curvature of the pipe path creates centrifugal forces on the fluid flow which produce a secondary flow. The velocity vector begins to change towards the outside of the curvature due to the centrifugal force vector resulting in a secondary flow. This causes the separation near the inner bend of the curved tube. Consequently, vortices are created due to the return of the flow along the upper and lower curved surfaces. Low Dean numbers point out that the axial-velocity profile stays parabolic similar to the fully developed straight tube's flow. Higher Dean numbers demonstrate that the velocity profile is broken. The magnitude of the Dean number is affected by the curvature ratio: for low curvature ratios, the intensity of the secondary flow becomes higher. The developing length also increases with the increase in Dean Number.

The augmentation of heat-transfer occurs upon the formation of Dean Vortices. Dehghandokht et al. (2011) fulfilled a numerical investigation on similar heat exchangers for a Reynolds number range of $850 < Re_w < 2200$ for water and $400 < Re_a < 1700$ for glycol-water mixture. They figured out that the velocity and thermal boundary layers broke down at the serpentine and new boundary layers start redeveloping.

3.3.5   Brinkman Number (Br)

Brinkman number (Br) is a dimensionless number that has an important role in viscous fluids. It is the ratio of viscous heating over conductive heat transfer. It can also be presented as the ratio of the heat production caused by viscous forces to the heat transferred through the wall as follows,

$$\text{Br} = \frac{Viscous\ dissipation}{thermal\ conduction} = \frac{\mu V^2}{k_w(T_b - T_{wall})} \qquad (3\text{-}18)$$

It is shown when the temperature of the viscous fluid rises due to viscous dissipations. In the current investigation, the effect of viscous dissipation due to viscosity and Re_w will be investigated.

3.3.6   Axial Heat Conduction Number (M)

Axial heat conduction in the channel wall of a MICHX is evaluated by a non-dimensional number (M). It is defined as the ratio of the axial heat conduction in the tube wall to the convection heat transfer of the fluid inside the channel.

$$M = \frac{Axial\ heat\ conduction\ in\ the\ tube\ wall}{convective\ heat\ transfer\ of\ the\ flowing\ fluid\ inside\ tube}$$

$$M = \frac{\dot{Q}_{cond.}}{\dot{Q}_{conv}} = \frac{k_{wall} A_{wall} \frac{\Delta T_{wall}}{L}}{m_w c_{p,w} \Delta T_w} \qquad (3.19)$$

Where, $\dot{Q}_{cond.}$ is the conductive heat transfer through the wall. As for ΔT_{wall}, it is experimentally difficult to measure the accurate temperature difference of the channel wall, therefore, it was taken to be equal to the ΔT_{water}. The ΔT_{wall} cannot be measured precisely through experiments, therefore, Li et al. (2007) numerically determined the wall and liquid temperature difference. The above equation can be simplified as,

$$M = \left(\frac{K_{wall}}{K_{water}}\right)\left(\frac{D_o^2 - D_i^2}{D_{i,L}}\right)\left(\frac{1}{RePr}\right) \qquad (3\text{-}20)$$

3.4 Heat Transfer Characteristics

3.4.1   Heat Transfer Rate (Q)

The basic heat transfer parameters for both fluids were calculated based on the principle of energy conservation equations. The common equation is in the form of,

$$Q = mc_p\ \Delta T \qquad (3\text{-}21)$$

$$\dot{Q} = \dot{m}c_p(T_i - T_o) \tag{3-22}$$

Where, T_i and T_o are the inlet and outlet temperatures of the fluids, respectively. Thus, the heat transfer rate equations of the DI-water and air are expressed as,

$$\dot{Q}_w = \dot{m}_w c_{p,w}(T_{w,i} - T_{w,o}) \tag{3-23}$$

$$\dot{Q}_a = \dot{m}_a c_{p,a}(T_{a,i} - T_{a,o}) \tag{3-24}$$

The heat transfer rate can be determined by means of convection using the bulk temperature of the fluid and the surface temperature as,

$$\dot{Q}_w = h_w A_{ht}(T_{b,w} - T_{s,w}) \tag{3-25}$$

$$\dot{Q}_a = h_a A_{ht}(T_{b,a} - T_{s,a}) \tag{3-26}$$

The heat transfer rate can also be found using the LMTD method as,

$$\dot{Q}_{oa} = UAF\Delta T_{lm,cf} \tag{3-27}$$

Where, $\Delta T_{lm,cf}$ is the log mean temperature difference, U is the overall thermal coefficient, A is heat transfer surface area, and F is the correction factor. The $\Delta T_{lm,cf}$ can be evaluated as,

$$\Delta T_{lm} = \frac{\Delta T_1 - \Delta T_2}{ln(\frac{\Delta T_1}{\Delta T_2})} \tag{3-28}$$

$$\Delta T_1 = T_{coolant,i} - T_{a,o} \tag{3-29}$$

$$\Delta T_2 = T_{coolant,o} - T_{a,i} \tag{3-30}$$

The correction factor F is equal to $\frac{\Delta T_m}{\Delta T_{lm}}$ where, ΔT_m is the average of the inlet and outlet temperature differences expressed as $\Delta T_m = \frac{\Delta T_1 + \Delta T_2}{2}$. For different configuration and flow arrangements, ΔT_{lm} usually stays unchanged. The value of F can be found using the

charts if P, the effectiveness of temperature loading and R, the capacity rate ratio are known as,

$$P = \frac{t_2 - t_1}{T_1 - t_1}, \text{ and } R = \frac{T_1 - T_2}{t_2 - t_1} \tag{3-31}$$

The heat transfer rate due to radiation between the thermal wind tunnel and the room is ignored due to the negligible temperature difference between them $T_{wall,\ inner} \approx T_{a,i}$. The heat transfer coefficient between the thermal wind tunnel wall and the room is calculated from the following formula,

$$h_{rad} = \tau\sigma\left(T_{a,i}^2 + T_{s,o}^2\right)\left(T_{a,i} + T_{s,o}\right) \tag{3-32}$$

For emissivity of $\varepsilon = 0.15$, the h_{rad} found is $0.8\ \frac{W}{m^2.°C}$ in this case, the h_{rad} will not be more than 0.1% of the convectional heat transfer rate. Therefore, the effect of the radiant heat transfer was ignored.

3.4.2 Heat Balance (HB)

It is assumed that the test chamber is well insulated and there is no heat loss between the test chamber and the surrounding. In other words, the heat transfer from the airside and the liquid side should be considered equal. As this assumption is not valid for a practical case, it is necessary to estimate the heat balance based on the percentage of liquid-side heat transfer compared to the ideal case. In real applications, HB cannot be zero and its equation can be written as,

$$HB = \left(\frac{\dot{Q}_w - \dot{Q}_a}{\dot{Q}_w}\right) * 100 \tag{3-33}$$

For more accurate results, the HB can be calculated based on the average heat transfer rate instead of the liquid heat transfer rate and the equation is expressed as,

$$HB_{avg} = \left(\frac{\dot{Q}_w - \dot{Q}_a}{\dot{Q}_{avg}}\right) * 100 \tag{3-34}$$

The average heat transfer rate is found as,

$$\dot{Q}_{avg} = \frac{\dot{Q}_a + \dot{Q}_w}{2} \tag{3-35}$$

It is worthy to note that the ASME PTC 30-1991 acceptance of the heat balance HB range is limited to $\pm 15\%$.

3.4.3 Heat Transfer Coefficient (h)

Heat transfer coefficient is a significant parameter that plays a role in the heat exchanger design and analysis. It represents the convection heat transfer rate between a fluid and a surface.

$$h = \frac{\dot{Q}_{ave}}{A_{ht}(T_b - T_s)} \tag{3-36}$$

Where, $\dot{Q}_{avg}$ is the average heat transfer rate, A_{ht} is the heat transfer surface area, and T_b is the fluid bulk temperature, and T_s is the temperature of the inner or outer heat transfer surface. Heat transfer coefficient can also be calculated from Nusselt number correlation as,

$$h = \frac{Nu.K}{D_h} \tag{3-37}$$

3.5 Heat Transfer Performance

3.5.1 Overall Thermal Conductance (UA)

The thermal resistance is a material property and a measure of the resistance of the material to the heat flow. The total thermal resistance can be calculated as,

$$R_{total} = R_a + R_{wall} + R_w \tag{3-38}$$

Where, $R_a = \frac{1}{(nhA)_a}$, $R_{wall} = \frac{ln\left(\frac{d_o}{d_i}\right)}{2\pi k_{al}L}$, $R_w = \frac{1}{(hA)_w}$, are the thermal resistances of air, wall

and water, respectively. The notation η_a is the fin effectiveness or the fin airside extended

surface efficiency. It is calculated as,

$$\eta_a = 1 - \frac{A_f}{A_a}\left(1 - \eta_f\right) \qquad (3\text{-}39)$$

Where, η_f is the fin efficiency and it depends on the fin geometry and arrangement. A_f is

the fin area and A_a is the total heat transfer surface area of the airside.

Accordingly, the overall thermal resistance can be estimated as,

$$UA = \frac{\dot{Q}_{avg}}{F\Delta T_{LMTD}} \qquad (3\text{-}40)$$

Where, UA is the overall heat coefficient based on the surface area and F is the log mean

temperature difference correction factor for a cross flow heat exchanger. In this study, F

has been considered as a unity.

3.5.2   Effectiveness (ε)

The heat exchanger performance is usually characterized by its effectiveness (ε) and

number of transfer units (NTU). Effectiveness can be calculated as,

$$\varepsilon = \frac{\dot{q}}{\dot{q}_{max}} = \frac{\dot{q}}{(\dot{m}c_p)_{min}\Delta T_{max}} \qquad (3\text{-}41)$$

In the current investigation, the minimum heat capacity rate was found on the waterside

and the maximum temperature difference is between water inlet ($T_{w,i}$) and air inlet ($T_{a,i}$).

Rearranging the above equation, ε can be rewritten as;

$$\varepsilon = \frac{\dot{q}}{(\dot{m}c_p)_w(T_{w,i}-T_{a,i})} \qquad (3\text{-}42)$$

3.5.3   Number of Transfer Units (NTU)

The number of transfer units (NTU) is defined as the ratio of the overall thermal conductance (*UA)* to the minimum heat capacity rate C_{min} as,

$$NTU = \frac{UA}{C_{min}} = \frac{UA}{(\dot{m}C_p)_w} \qquad (3\text{-}43)$$

It is considered a design parameter for heat exchangers and it is an indication of the non-dimensional thermal size rather than the physical size of exchangers.

3.5.4   Pressure Drop

The pressure drop is considered a vital factor that plays an important role in the heat exchanger performance. The total pressure drop through the heat exchanger core depends on the geometric parameters, the fluid types, and the thermodynamic properties. Hereafter, some important parameters such as the friction factor (f), entrance effect, and pressure drop in the straight tube and the curved tube are expressed.

3.5.5   Friction Factor (f):

In fluid dynamics, the Darcy–Weisbach equation for the friction factor relates the head loss and the pressure loss due to friction along a given length of a pipe to the average velocity of the fluid flow. Darcy's friction factor is referred to as f.

$$f_d = \Delta P \frac{D}{L} \frac{2}{\rho V^2} \qquad (3\text{-}44)$$

The friction factor is used to determine the pressure drop for fully developed or developing laminar flow as illustrated below,

$$\Delta P = \frac{f_d L \rho V^2}{2D} \qquad (3\text{-}45)$$

Where, p is the channel circumference. The Hagen Poiseuille theory expresses the pressure drop in a fluid flowing through a long cylindrical pipe. It is mentioned that after

a fluid enters a channel or a tube, the velocity profile begins to develop through the channel until it is fully developed. The velocity is assumed to be uniform at the entrance and the pressure drop in the minichannels is substantial. Hence, the pressure drop caused by the entrance effect should be taken into consideration. If the entrance length is very small in comparison to the total length, the entrance effect may be ignored.

3.5.6 Pressure Drop in the Straight Tube:

There are two significant lengths in the tubes: the hydrodynamic entrance length and the thermal entrance length. The entrance lengths indicate the flow character. For a laminar flow, the hydrodynamically developing length is proportional to Re and D_h and can be found through the following equation,

$$L_{hy} = 0.05 Re D_h \tag{3-46}$$

The thermal entrance length can be estimated as,

$$L_{th} = 0.05 Re Pr D_h \tag{3-47}$$

Or

$$L_{th} = 0.05 \frac{\rho V c_p D_h^2}{k} \tag{3-48}$$

For fully developed flow, the pressure drop is found as,

$$\Delta P = \frac{128 \mu L A V}{\pi D^4} \tag{3-49}$$

$$\Delta P = \frac{L}{D} \frac{32 \mu V}{D} \tag{3-50}$$

Where, D is the channel diameter, L is the flow length, V is the flow velocity, and μ is the dynamic viscosity.

CHAPTER IV

EXPERIMENTAL SETUP

The current experiments were conducted through a well-designed and instrumented experimental setup as shown in Fig. 4.1. It consists of a closed-loop integrated thermal wind tunnel, test chamber, liquid circuit with heater, various measuring and monitoring instruments, a built-in heat exchanger that maintains the inlet-air temperature, wavy-finned serpentine cross-flow minichannel heat exchanger, variable speed gear pump that provides the flow of the fluid, and a 16 bit LabView data acquisition system that monitors and records all data. The largest component of the setup is the integrated closed-loop thermal wind tunnel.
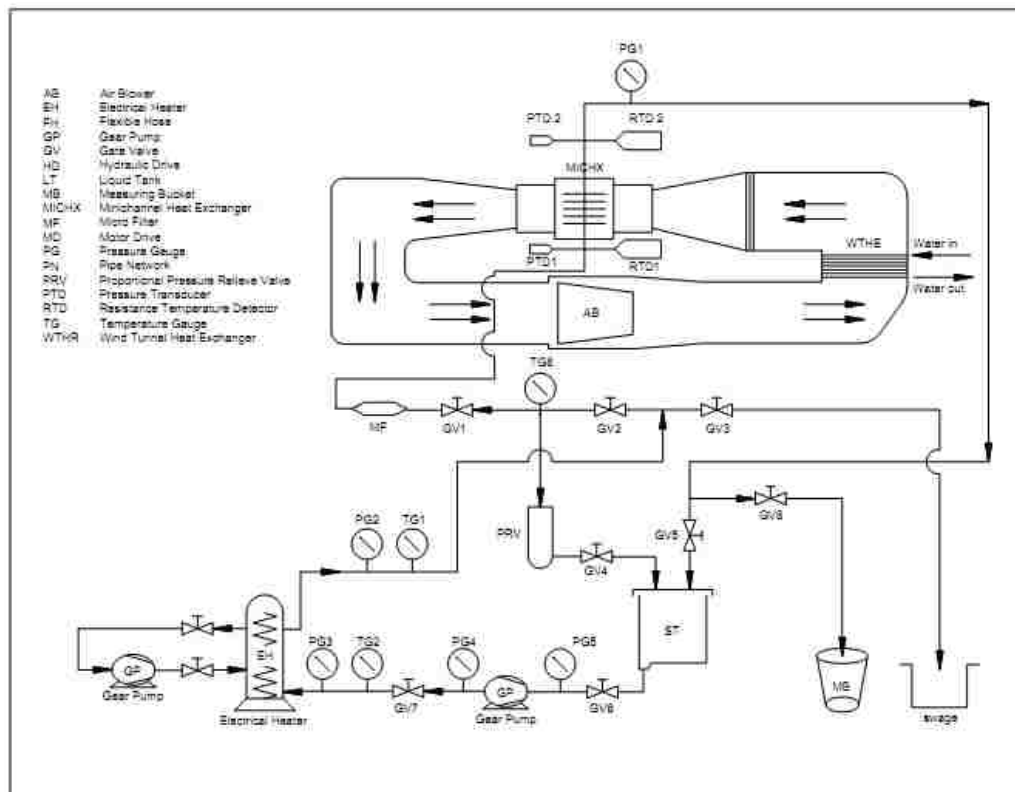
Figure 4.1 Schematic diagram of the experimental setup
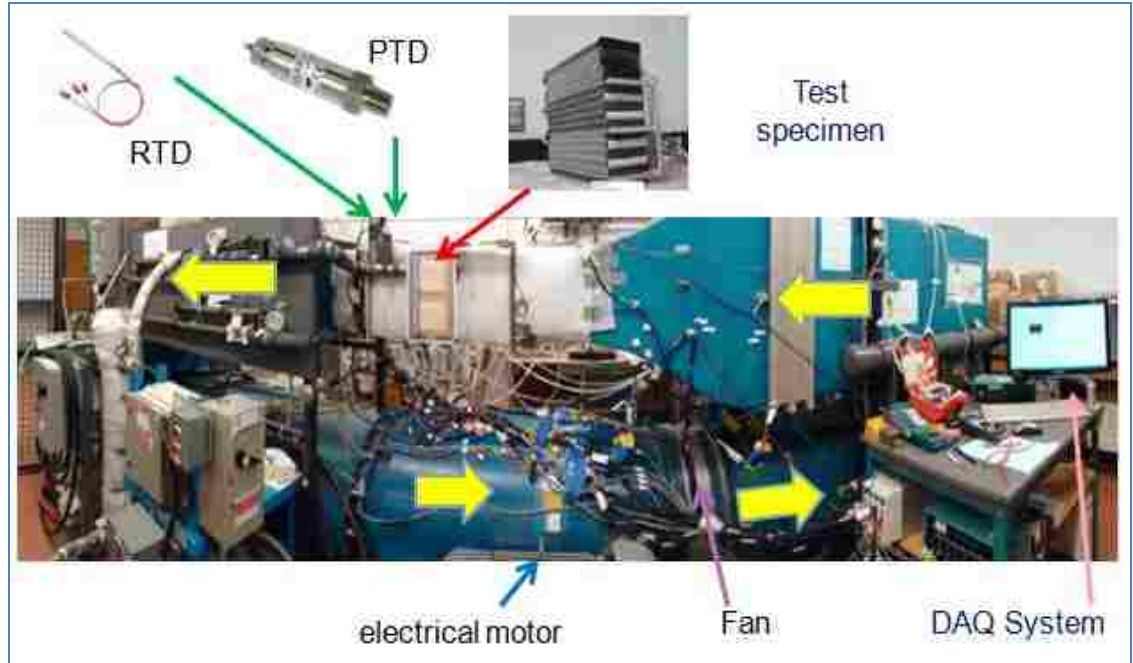
Figure 4.2 The experimental setup

4.1 Air Handling System

4.1.1 The Closed Loop Thermal Wind Tunnel

The largest component in the experimental setup is the closed loop thermally insulated wind tunnel (thermal wind tunnel). It consists mainly of a built-in heat exchanger and a test section. The wind tunnel is 544 cm long, 75 cm wide and 164 cm high and has a contraction ratio of 6.25 with a wall thickness of 1cm. The air is forced to flow inside the wind tunnel by means of a blower which is driven by an electrical motor. The arrows in Fig. 4.1 show the direction of the air inside the wind tunnel. It is capable of providing 30 m/s free stream velocity without the test specimen, whereas a velocity of 18 m/s with the test specimen installed in the test chamber. A built-in heat exchanger is mounted inside the wind tunnel to maintain the inlet-air temperature to the required temperature. The test chamber is installed in the middle upper part of the wind tunnel. The wavy-finned serpentine cross-flow minichannel heat exchanger is located inside the test chamber. Two

T-type thermocouple grids are installed at the upstream and downstream of the test chamber. Those thermocouples measure accurately the inlet and outlet temperatures of the air across the test chamber.

4.1.2 The Test Chamber

The test chamber is a cubic shape cross section of 305 mm X 305 mm dimensions and has a length of 610 mm along the flow direction as illustrated in Fig. 4.2. It is made of 6.5 mm thick plexiglass with a thermal conductivity of $0.19\frac{W}{m.°C}$. The test chamber is also well insulated to ensure a negligible heat transfer between the test chamber and its surroundings. It is made to fit the wind tunnel, and ensure disturbance of the flow does not occur while passing through the test chamber in order to minimize uncertainties. To measure the air inlet velocity, a 12 inch Pitot static tube was installed in the middle inlet of the test chamber.

4.1.3 Air Temperature Measurements

Two grids of 9 and 25 thermocouples as shown in Figures (4.3) and (4.4) are installed at the upstream and downstream of the test chamber, respectively, to measure the inlet and outlet air temperatures across the test chamber. Each grid plane is installed at a distance of 14 times the semi axial length away from the inner and outer boundaries of the test chamber. They accurately measure the temperatures of the air upstream ($T_{a,i}$) and downstream ($T_{a,o}$) the test chamber. While running an experiment, a sufficient time is needed for the air side temperatures to be stabilized. Then a DAQ system is used to collect and record all the temperatures. It is found that the air temperature is more uniform at the upstream than it is at the downstream.

The air side specifications of the minichannel heat exchanger are given in Table 4.1.

Table 4.1 Airside specifications of the MICHX

Frontal area	0.304m × 0.304m
Minimum free flow area	70.9×10^{-3} m
Air flow length	100×10^{-3} m
Hydraulic diameter	3.49×10^{-3} m
Fin type	Deep Wavy
Fin density	12 fins per inch
Fin height	16×10^{-3} m
Fin thickness	0.1×10^{-3} m
Total fin area	7.88 m^2
Total heat transfer area-airside	8.13 m^2
Contraction ratio	0.818
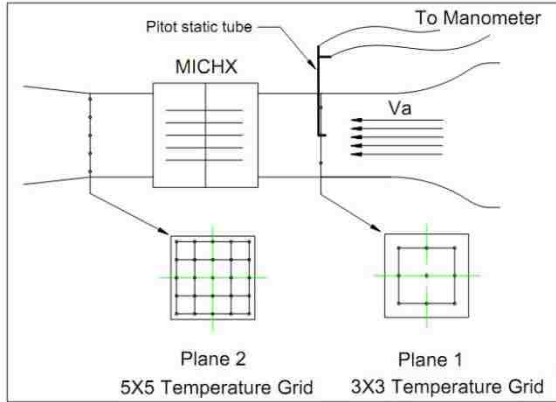
Figure 4.3 Thermocouples arrangement at the inlet and outlet of the MICHX
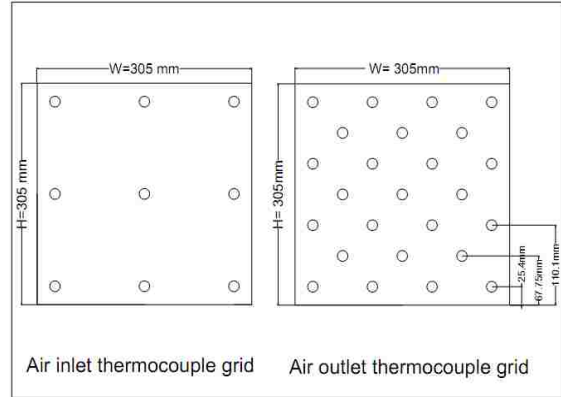
Figure 4.4 Thermocouple grids

4.2 Liquid Handling System

The liquid handling system consists of major operational components, as well as flow measurements, monitoring and safety devices. The major operational components are:

- Electric heater

- Gear pump

- Reservoir tank

4.2.1   Inline Immersion Heater with PDI Controller

The inline circulation immersion heater has a PDI controller and made by Wattco with model # of MFLI606X2818. The heater consists of a 6×1 KW element to produce up to 6 KW of heat with dimensions of 1.5" (38.1 mm) inlet and outlet. It also has a 4" (150 lb. flanged) and a stainless steel vessel. This heater is capable of sustaining a pressure of 6.8 Mpa and a temperature of 150°C. The heater has a $4.6\frac{W}{cm^2}$ watt density which falls within the medium range. An inbuilt thermocouple placed at the center of the flange feeds the data to the PID controller that controls the heater operation. The PID controller model

number is # SD6C-HJAAAARG. It provides a better control of the temperature than an on-off controller since the on-off controller only sets the heater as fully on or fully off.

Figure 4.5 Inline immersion heater with a PDI controller (Durex Industrial)

4.2.2 Recirculation Gear Pump

A gear pump is generally used when a constant volume flow rate is required regardless of the upstream pressure change. The gear pump used in this study has the capacity of producing 17.4 GPM and 150 psi. It is operated through a controlled electric motor with a 5.6 kW and 60 Hz frequency that is able to produce the desired liquid flow rate throughout the system. The operating temperature range of the pump is (-54 to 12)℃. The make and the model of the pump are Omega and FPUGR205 − RCB, respectively. The pump has a power of 3.6 hp at a maximum pressure. It can handle all non-corrosive liquids up to 21,630 cSt. The maximum viscosity the pump can handle is 750 cP.

Figure 4.6 Frequency controlled gear pump

4.2.3   Reservoir Tank

The reservoir tank is a storage tank placed at the gear pump suction. It is usually filled with liquid to avoid any cavitation at the entrance of the pump. The liquid is forced flow from the tank throughout the system and then return to the tank again. The tank has a cylindrical shape with a capacity of 23 gallons (87 liters) and dimensions of: Height=60 cm, Diameter = 43cm and thickness= 0.4 cm. The tank is well insulated by 2 inches glass wool. The tank can sustain a temperature of up to 100℃.

4.2.4 Resistance Temperature Detector (RTD)

The resistance temperature detector (RTD) is a highly precise temperature detector that works based on the Wheatstone bridge theory. It has a wide temperature range of (-100℃~400℃) for Thin film type and a temperature range of (-200℃~850℃) for wire-wound type. Compared to the thermocouples, RTDs possess greater accuracy. In the current experiment, two RTDs, pt100 and PM1/10-1/4xxx that are capable of reading up to 5 volts are used. They are located at the entrance of the inlet header and at the exit of

the outlet header to measure the temperatures of DI-water at the inlet and outlet of the heat exchanger core.

Figure 4.7 Resistance temperature detector (RTD)

4.2.5 Differential Pressure Transducer (PTD)

A pressure transducer is an instrument used to precisely measure the pressure of the fluid. Two PTDs, PX 309 and 005G5V, are used at the entrance of the inlet header and at the exit of the outlet header to measure the pressure of DI-water at the inlet and outlet of the heat exchanger core. The PTDs have an accuracy of $\pm0.25\%$ FS (full scale) with overvoltage protection and reverse polarity.

Figure 4.8 Pressure transducer (PTD)

4.2.6 Oil-filled Pressure and Temperature Gauges

The oil-filled temperature and pressure gauges are used in this research to monitor the temperature and pressure at critical points such as the pressure at the outlet of the pump and the temperature at the outlet of the immerse heater.

Figure 4.9 Oil-filled pressure gauge   Figure 4.10 Oil-filled temperature gauge

4.2.7 Flow Meters

Two types of flow meters are used in the experimental setup: impeller flow meter (IFM) and digital flow meter (DFM). They are used to record and monitor the fluid flow rate,

temperature, and pressure. The make and model of the IFM are Omega and FPR304, respectively, which is capable of monitoring 0.5-40GPM and is located at the outlet of the MICHS core. The make and model of the DFM is Proteus and FLUID-VISION 4000. The RTD mechanism uses a semi-conductor transducer to measure the temperature in terms of an electric voltage. It provides an output voltage range of 0-5 VDC at the inlet and 0-10 VDC or 4-20 mA at the outlet, respectively. This device works at temperature range between -40℃ and 140℃. For DFM actuation, a 24 VDC$\pm$ 10% and a 200mA supply are needed. The accuracy of both IFM and DFM are $\pm$0.5% FS and $\pm$ 1% FM, respectively.

Figure 4.11 Digital flow meter   Figure 4.12 Impeller flow meter

4.2.8 Micro Filter

A micro filter is a filter with a micron mesh element to protect the MICHX and the digital flow meter from blockage. It is mounted before the digital flow meter at the inlet tubing. Two types of micro elements are available (230 µm, and 420µm). For this study, a 230 µm filter element was used. Any blockage in the micro filter results in a pressure rise

⏎

at the pump outlet, therefore, the filter was installed so that it can be easily removed and cleaned.

Figure 4.13 Filter element   Figure 4.14 Cross section of the micro filter
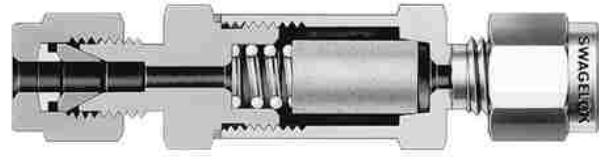
4.2.9 Safety Valve

A valve is installed at the inlet line for safety in case the filter or the MICHX are clogged and the pressure rises unexpectedly. The safety valve prevents any damages to the system.

Figure 4.15 Safety valve

- Calibration

A calibration procedure should be applied at the same experimental conditions. Preceding any experiment, the inlet and outlet RTDs, PTDs, and thermocouples on both air and DI-water sides were calibrated using the thermocouple and RTD calibrators. These

experiment results were recorded and entered into the National Instrument data acquisition system.

4.3 Data Acquisition System (DAQ)

The data acquisition system (DAQ) is the main and highly accurate part of the system that records all the data needed to perform the analysis. The main components of the DAQ system are:

4.3.1 Data Acquisition System Software (LabView)

The Laboratory Virtual Instrumentation Engineering Workbench (LabView version 8), which is produced by National Instruments, is used in the current system. It collects all the data at a sampling rate of 100 kHz. It is supported by a National Instrument data acquisition card, NI-PCI-6052E multi-function I/O Board that is connected to the PC.

4.3.2 SCXI Signal Conditioning

The devices in the DAQ system that collect electrical signals from the measuring devices are called signal conditioning. An SCXI signal conditioning consists of multichannel signal conditioning modules placed in one or more rugged chassis. The signals come from thermocouples (TCs), RTDs, PTDs, and flow meters and are processed by the LabView software to present the final data.

4.3.3 Terminal Block Model SCXI-1300/1303

The terminal block has 32 available channels and is connected to the modules through screws which in turn are connected to the chassis. The terminal block can conveniently connect input signals such as RTDs, PTDs, thermocouples, and flow meters.

Figure 4.16 Terminal Block model SCXI -1300/1303

4.3.4 Module SCXI-1102

The Module SCXI- 1102 sets signals as legible by the 16-bit data acquisition card   (NI 6052E). More than 300 analog signals are collected from RTDs, PTDs, and TCs from different voltage and current sources that are required to process the data.

4.3.5 SCXI-1000

The SCXI-1000 is a chassis that holds the terminal block as well as the modules and supply the power to them.

4.3.6 Data Acquisition Card

The data acquisition card is a switchless, jumperless data acquisition (DAQ) card. It is connected to the PC and transfers the data from the DAQ to the PC. The system has 128 channels for acquiring data. It is able to monitor, read, and record 96 individual parameters through 96 channels at a rate of 100 Hz.

4.3.7 Flow Kinetics (FKT)

The Flow Kinetics device used in the experimental set up measures the pressure, relative humidity, density, and the temperature of the air side. The make and model of the device

is Flow Kinetics TM-LLC /FKT-3DP1A-0.4-5-1. Pressure measurements include: an absolute pressure (P_{abs}) and three differential pressures (P1, P2, P3) concurrently for the airside inside the wind tunnel. The sample rate in the present study is 1 kHz for accuracy and consistency.

Figure 4.17 Flow Kinetics device (FKT)

4.4 Minichannel Heat Exchanger MICHX

The serpentine slab minichannel heat exchanger is constructed of 15 multiport aluminum serpentine slabs in three circles as illustrated in Figures 4.18 and 4.19. Each slab is 2 mm thick and has 68 circular channels with inner hydraulic diameters of 1 mm. The frontal area of the MICHX is 304mm X 304 mm. The MICHX is capable of sustaining 15 MPa working pressure. The de-ionized water (DI water) coming from the inlet header is distributed into three inlet manifolds and passed through the three circuits. After

participating in the heat transfer, it leaves the heat exchanger core through three outlet manifolds and an outlet header.
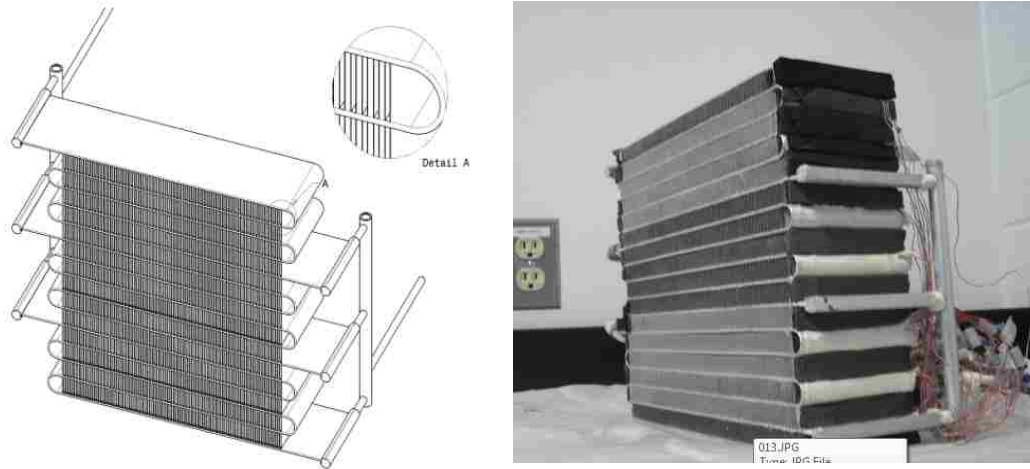
Figure 4.18 Minichannel heat exchanger, front and side view
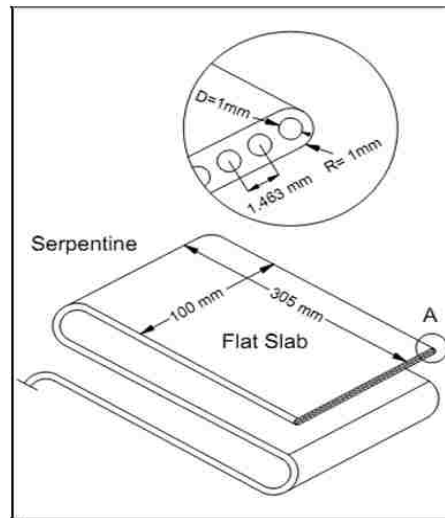
Figure 4.19 Minichannel serpentine flat slabs

The specifications of the liquid side of the MICHX are given in Table 4.2.

Table 4.2 Specifications on the liquid side of the MICHX

Hydraulic diameter	0.01 m
Minichannel slab height	0.02 m
Number of header(inlet &outlet)	2
Number of flow passes	3
Number of slabs in a circuit	5
Total number of slabs	15
Number of channels per slab	68
Total heat transfer area-waterside	974.7×10^{-3} m^2

4.5 Experimental Methods and Operating Conditions

In this study, the thermal performance and flow behavior of the working fluid, Di-ionized water and air, in a prototype multiport mini-channel heat exchanger were investigated for air heating. The DI-water was passed through the prototype multiport minichannel heat exchanger at a constant temperature of 70°C $\pm$ 0.5°C. Three essential variables including DI-water mass flow rate ($\dot{m}_w$), air inlet temperature (T_a), and air velocity (V_a) are used to study the fluid flow and heat transfer behavior. Mass flow rate was changed from 1.35 kg/s to 2.15 kg/s that corresponded to Re_w of 255 to 465. Air inlet temperature varied

from 25°C ±0.5°C to 38°C ±0.5°C at 5 steps (26°C, 29°C, 32°C, 35°C, 38°C). The air velocity passing through the heat exchanger core diverted from 6m/s to 18 m/s at 4 steps (6m/s ,10,m/s 14m/s,18m/s) that corresponded to Re_a of 1650 to 5317 for each DI-water mass flow rate.

Table 4.3 The operating conditions

Inlet DI-water temperature °C	Inlet air temperature °C	Air Velocity m/s	DI-Water mass flow rate Kg/s
70	26	6, 10, 14, 18	0.022, 0.029, 0.035
70	29	6, 10, 14, 18	0.022, 0.029, 0.035
70	32	6, 10, 14, 18	0.022, 0.029, 0.035
70	35	6, 10, 14, 18	0.022, 0.029, 0.035
70	38	6, 10, 14, 18	0.022, 0.029, 0.035

CHAPTER V

ANALYSIS OF RESULTS

5.1   De-Ionised Water Properties

5.1.1   Density

De-ionised water is just what it sounds like, water that has the ions removed. The reason that in this experiment deionised water is used is that ions cause interference while an experiment is running. They can switch place with other ions. Water with ions in it is also quite a lot more electrically conductive than water without ions.

The variation in density of DI-water with temperature is shown in Figure 5.1. The change in the water density is less than 2 percent for the temperature range of the case study Ma (2007). There is not much changes in other properties of DI-water such as specific heat c_p, dynamic viscosity μ, and conductivity k.
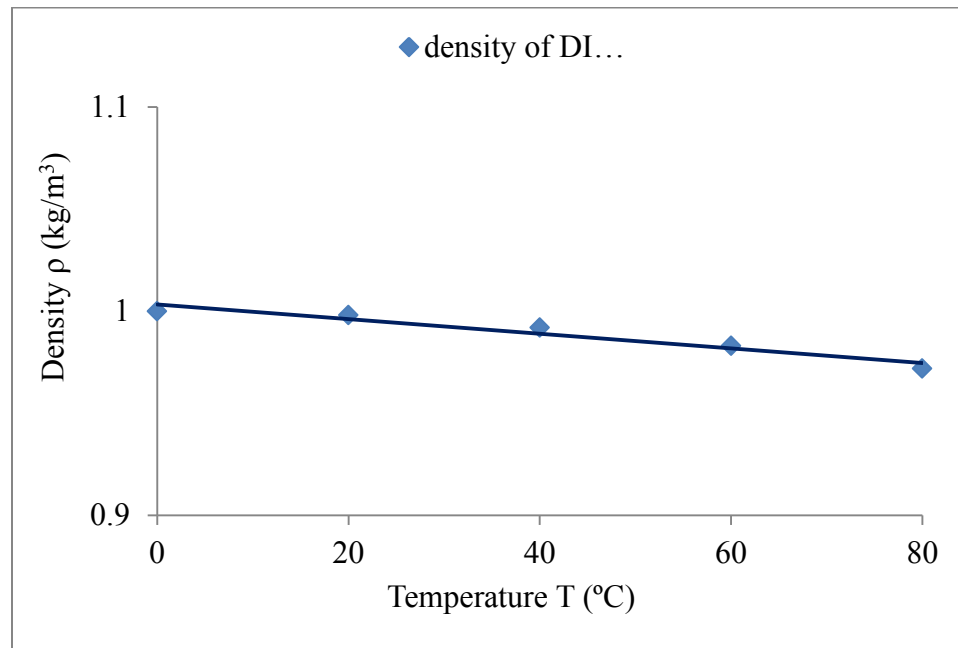
Figure 5.1 The effect of temperature on the density of water

5.2 Deionised Water Properties

5.2.1 System Heat Balance (HB)

According to ASME PTC-1991, it is set that all the data collected in the defined operating condition is accepted in the range of ±15%. As shown in Figure 5.2, our current experimental data is between $\pm 7\%$ which indicates that the heat loss to the surroundings is negligible due to proper heat insulation of the test section. The validation of these data confirms its suitability to be used for heat transfer calculations.
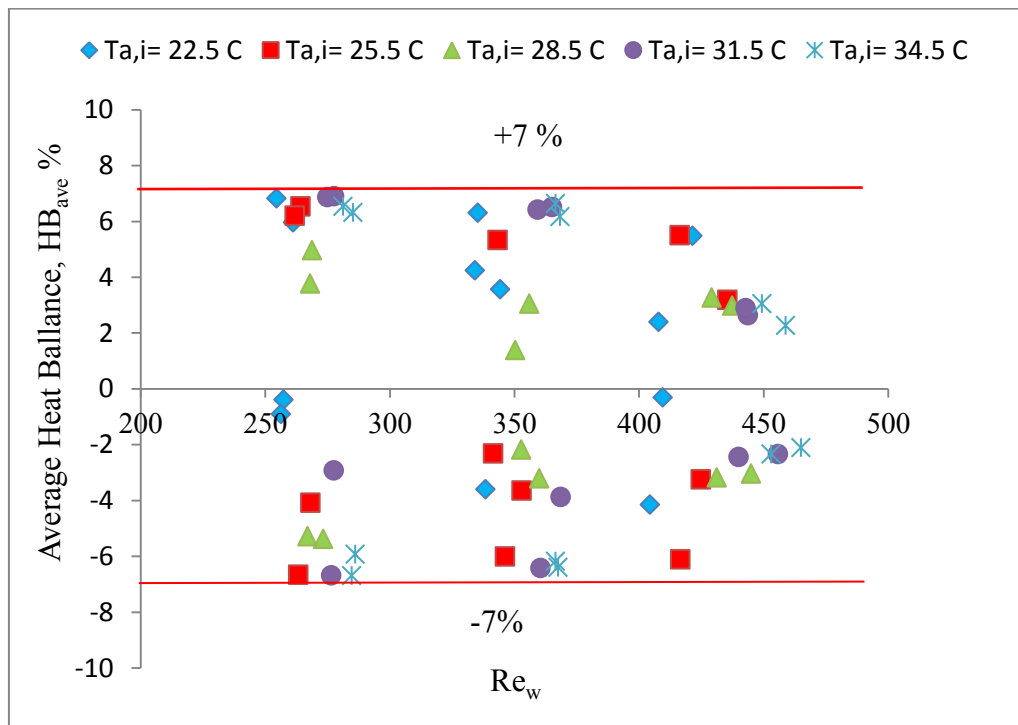
Figure 5.2 Heat balance vs. water Reynolds number

5.2.2 Effects of Re_w on $T_{a,i}$ and $T_{a,o}$ of DI-Water

The effect of Re_w on the water temperature drop (ΔT_w) in the heat exchanger is illustrated in Figure 5.3. The inlet-outlet temperature differences are higher at lower Re and lower at higher Re. Thus by increasing the Re_w, the ΔT_w will decrease. The trend shows that for a specific high Re_w the temperature drop will be insignificant. It is also shown that the Re_a has a minimum influence on the temperature drop.
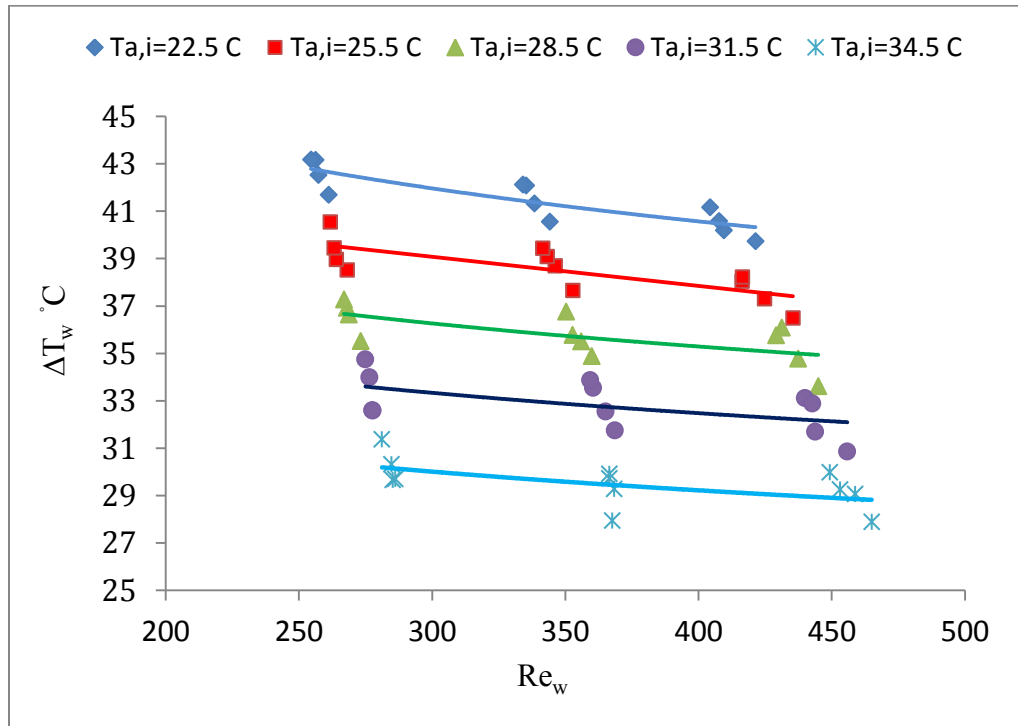
Figure 5.3 Effects of water side Reynolds number on the temperature drop

5.2.3 Effect of Re_w on Normalized Heat Transfer

The normalized heat transfer (Q^*) has an immense role in analysing the heat transfer characteristics. It is defined as

$$Q^* = \frac{\dot{Q}}{A_F(T_{w,i} - T_{a,i})} \tag{5-1}$$

Where, Q* is the normalized heat transfer rate, A_f is the frontal area of the heat exchanger, $T_{w,i}$ and $T_{a,i}$ are the water and air inlet temperatures, respectively. The effect of Re_w on Q* is plotted in Figure 5.4 It is revealed that Q* is dependent on Re_w and increases with the increase of Re_w. The following correlation demonstrates a power law relation.

$$Q* = 0.012 \, Re_w^{0.894} \tag{5-2}$$
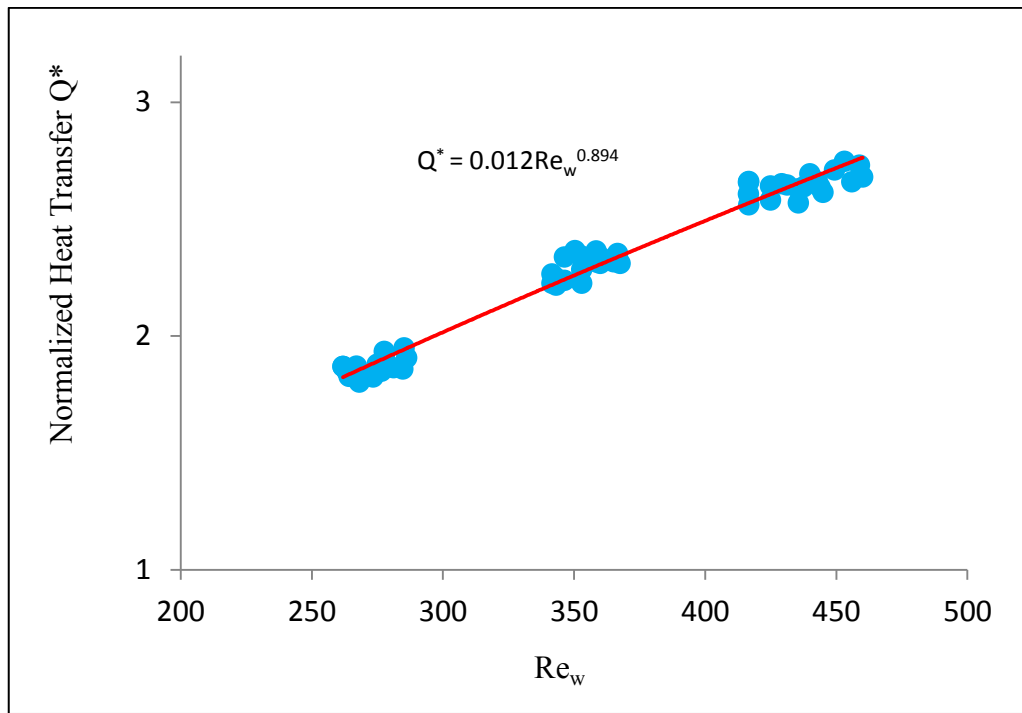
Figure 5.4 The effect of water-side Reynolds number on normalized heat transfer (Q^*)

5.2.4 Effect of Re_a on Air and Water Heat Transfer Rate
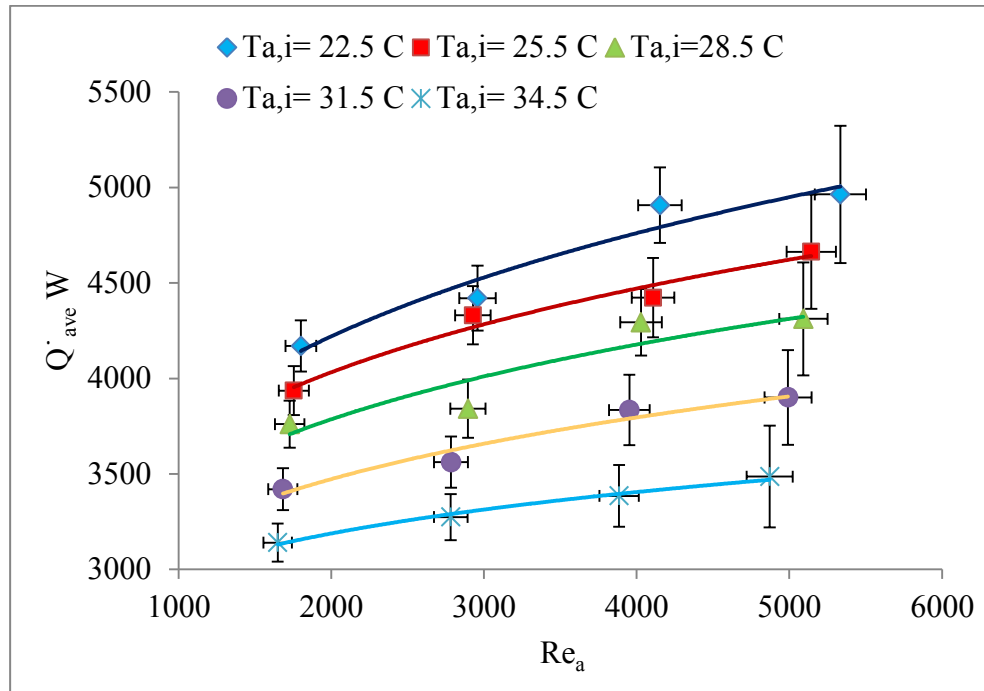
Figure 5.5 The effect of Re_a on the average heat transfer rate
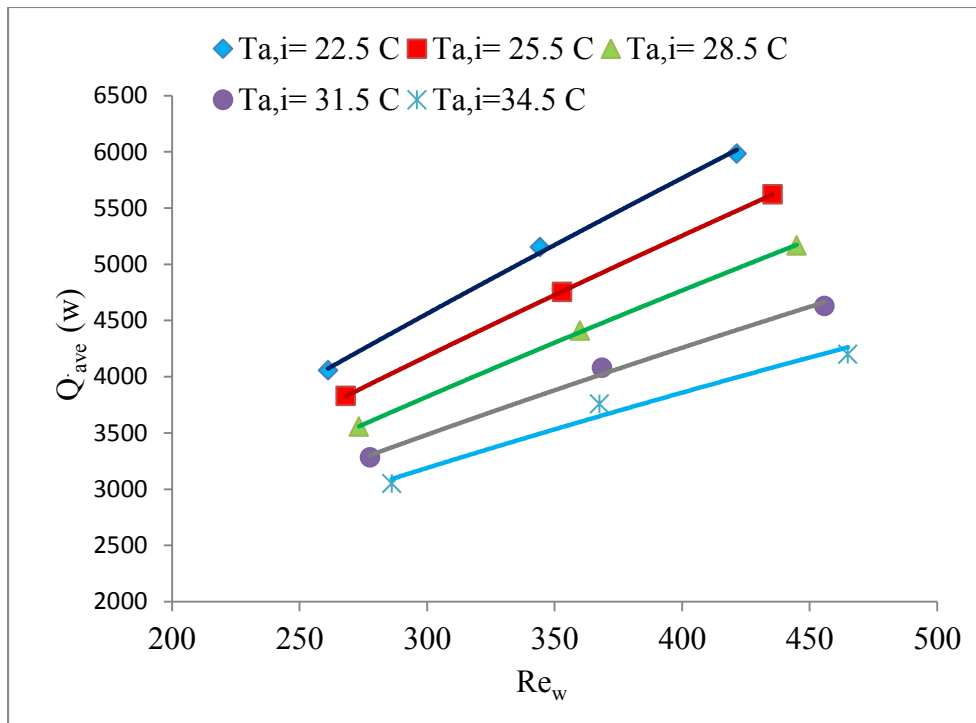
Figure 5.6 The effect of Re_w on the average heat transfer rate

5.2.5 <u>Effect of Re_a on LMTD</u>

Log Mean Temperature Difference (LMTD) is used to determine the temperature motivating force for heat transfer in flow systems, most remarkably in heat exchangers. The size and the heat transfer area could be found using LMTD method. LMTD is a normalized parameter that can be used to compare two different heat exchangers. The large the LMTD, the more heat is transferred. Figure 5.7 shows the effect of Re_w on LMTD for different temperatures of water. The power law was the best curve fit. It is found from the figure that the highest LMTD belongs to the lowest $T_{a,i}$ for a constant Re_w. The illustration also shows that the LMTD is elevated as Re_w is enlarged.
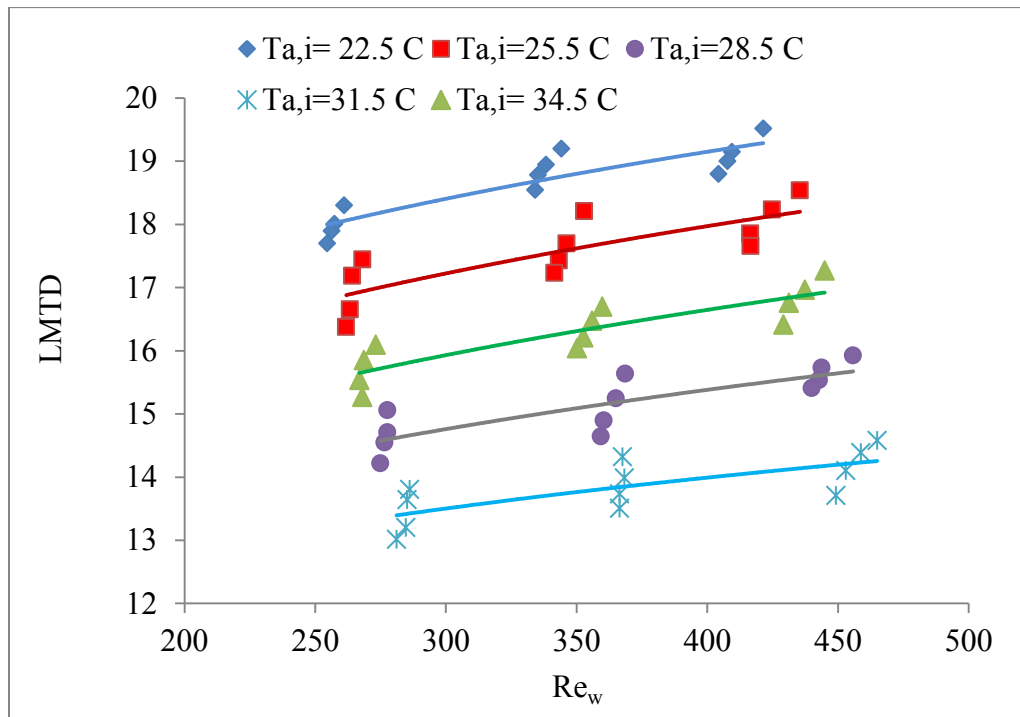
Figure 5.7 The effect of Re_a on LMTD

5.2.6 Effect of Re_w on LMTD

There are two dimensionless temperature quantities used in heat exchangers which are named as LMTD-dimensionless and ΔT-dimensionless. The dimensionless ΔT is expressed in Equation (5-3) as the ratio of the temperature change in the water side to the maximum temperature difference between the two fluids in heat exchangers.

$$\Delta T_{dimentionless} = \frac{T_{w,i} - T_{w,o}}{T_{w,i} - T_{a,i}} \tag{5-3}$$

The LMTD-dimensionless is described in equation (5-4) as the ratio of LMTD to the maximum temperature difference, water and air inlet temperatures.

$$LMTD_{dimentionless} = \frac{LMTD}{T_{w,i} - T_{a,i}} \tag{5-4}$$

Figure 5.8 illustrates the relation between Re_w, LMTD-dimensionless, and ΔT-dimensionless. It demonstrates that by increasing Re_w, LMTD-dimensionless will be reduced, and on the contrary the $\Delta T_{dimensionless}$ will be increased as expected. The plot includes all the air temperatures and velocities. The slope of both curves flattens as Re_w increases.
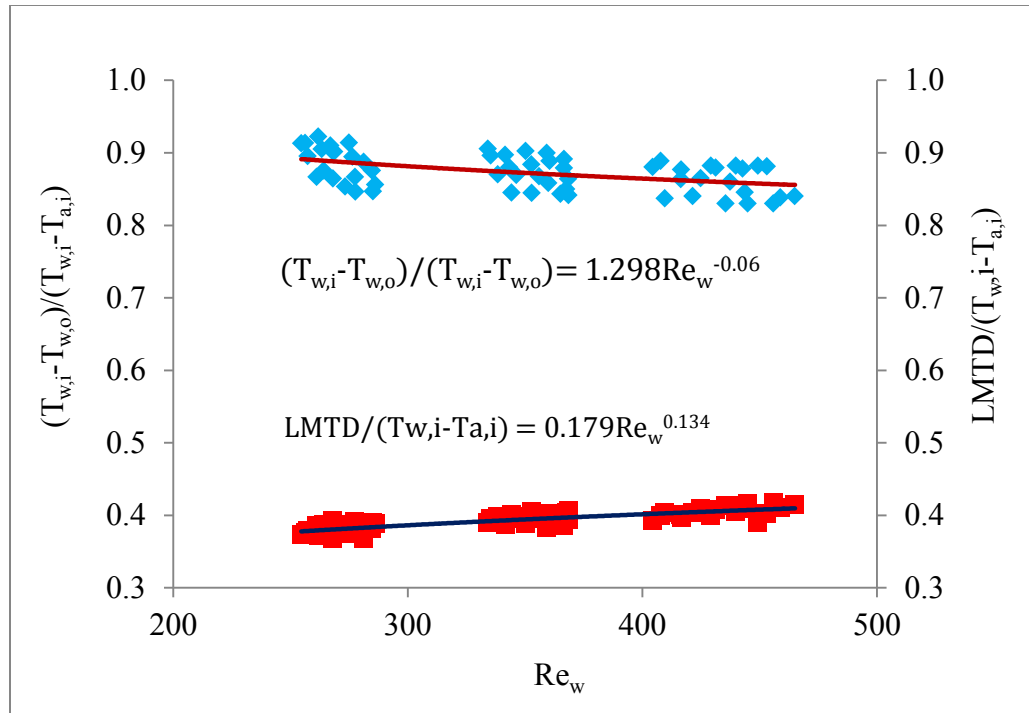
Figure 5.8 The effect of Re_w on $T_{non-dimensional}$

5.2.7 Effect of Re_w on Nu_w

The water side and air side Nusselt number (Nu_w) verses Re_w for the 5 different air temperatures and velocities are illustrated in Figure 5.9. The correlation is a power law curve-fit with a positive exponent. The slope of the trend is gentler as Re increases. A correlation established for Nu_w on Re_w is given below,

$$Nu_w = 1.87\ Re_w^{0.15} \qquad\qquad (5\text{-}5)$$
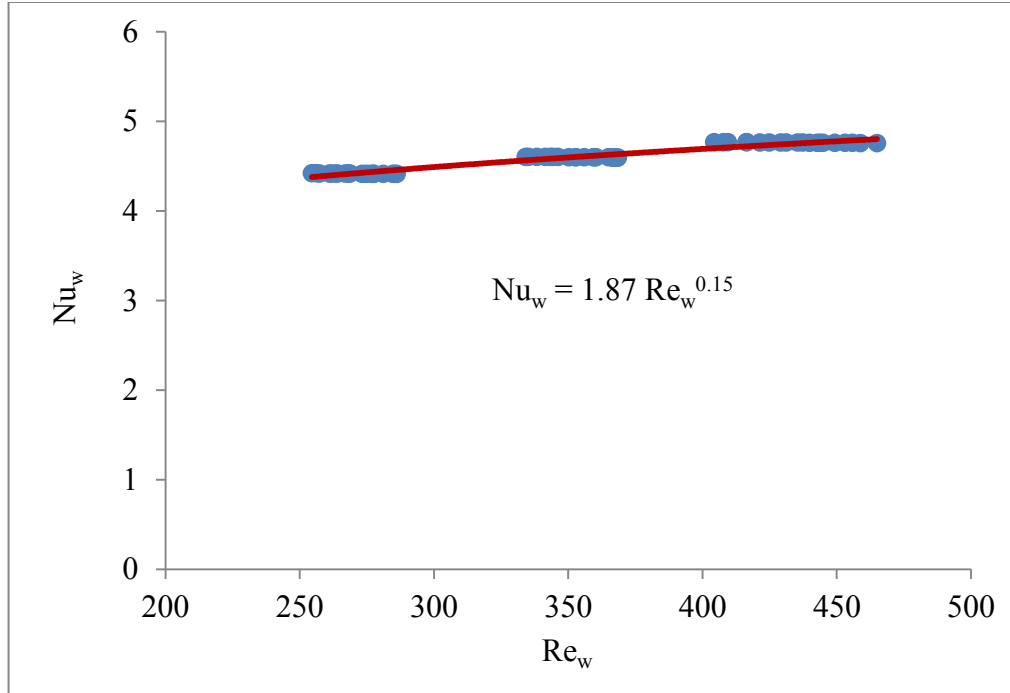
Figure 5.9 The effect of Re_w on Nu_w

5.2.8 Effect of Re_w on Nu_w, and Pr_w

The relationship between the non-dimensional parameters; water-side Reynolds number, and Prandtl number on water-side Nusselt number, has been investigated. The effect of Re_w, Pr_w on Nu_w is plotted in Figure 5.10. The investigation shows that Nu_w will increase with the increase of Re_w and Pr_w. The dependency of Nu on Re, and Pr followed the power law relation. The water-side heat transfer general correlation is obtained in the form of Nusselt number as a function of water-side Reynolds number and Prandtl number shown as,

$$Nu_w = 1.2\ Re_w^{0.17}\ Pr_w^{0.33} \tag{5-6}$$

Khan et al. (2010) performed an investigation on ethylene glycol-water mixture for a similar MICHX to characterize the heat transfer and fluid flow behaviour. They found a correlation of $Nu_g = 0.152\ Re_g^{0.49}\ Pr^{0.33}$ for the developing fluid. The current results

compare reasonably well with their findings. The differences between the results are due to the difference in liquid properties of DI- water and ethylene glycol-water, number of slabs which was 2, whereas for this study it is 15 slabs in three circuits, and also the range of Reynolds number of water which was 400-1900 compared to the current study of 257 to 411.

The Nusselt number should be 3.66 for the laminar developed flow in circular shape geometry under constant surface temperature boundary condition. In this investigation, Nu_w was calculated to be between 4.41 and 4.76 at constant property condition. This discrepancy is attributed to the developing flow regime in channels and the deviation from the ideal case of constant surface temperature.
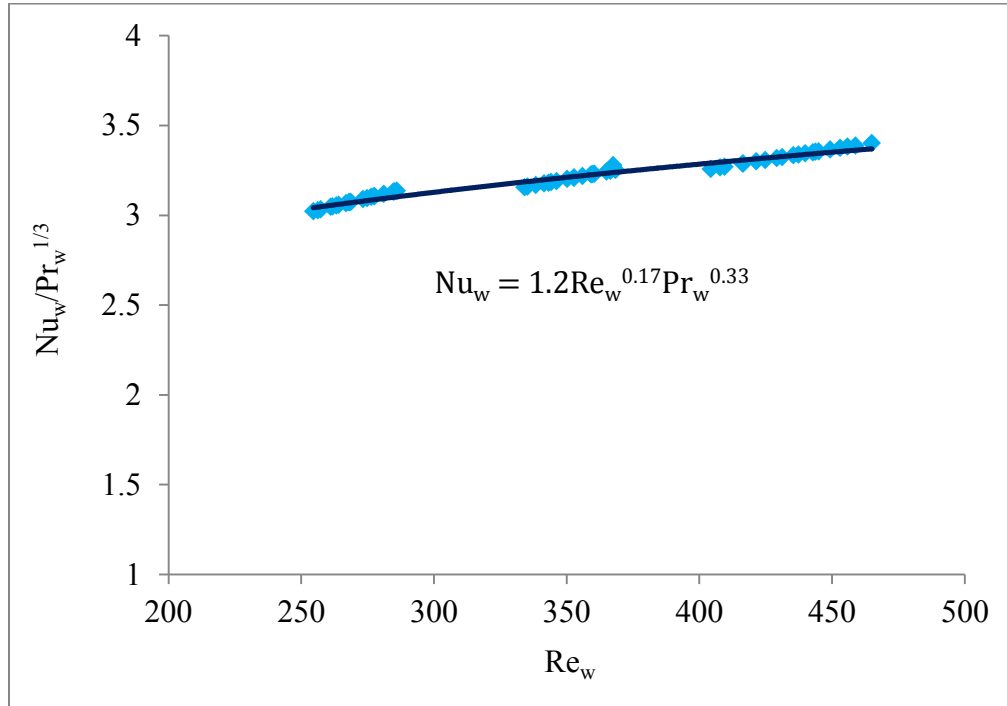
Figure 5.10 The effect of Re_w and Pr_w on Nu_w
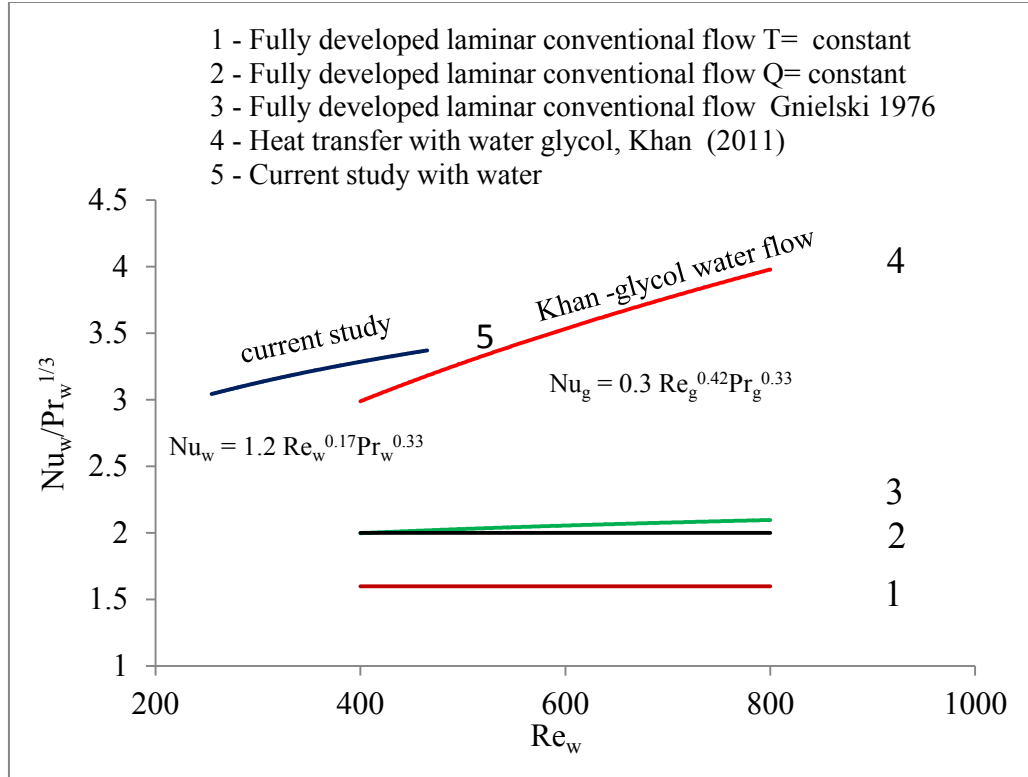
Figure 5.11 A comparison of the current correlation (Re_a, Nu_a, Pr_a)

5.2.9 Effect of Re_a on Nu_a, and Pr_a

The effect of Re_a and Pr_a on Nu_a has been investigated and the result is demonstrated in Figure 5.12. The best curve fit practiced as power law relation. As Re_a and Pr_a increase, Nu_a will increase. Since air is not a high viscous fluid, therefore its Prandtl number, which is a function of viscosity and conductivity, doesn't have a lot of variation and can be considered as a constant. At the bulk temperature, the correlation is found as,

$$Nu_a = 0.315\, Re_a^{0.373}\, Pr_a^{0.33}, \text{ for } 1750 > Re_a > 5750,\ 0.71 > Pr_a > 0.72 \qquad (5\text{-}7)$$

or $$Nu_a = 0.281\, Re_a^{0.373} \qquad\quad , \text{ for } 1750 > Re_a > 5750,\ 0.71 > Pr_a > 0.72 \qquad (5\text{-}8)$$

The Nu_a-Re_a-Pr_a correlation in equation (5-7) for the current study is compared to the correlation developed by Dasgupta (2011) for air cooling using the same MICHX in a Reynolds number range of $283 <\leq Re_a < 1384$ as,

$$Nu_a = 0.529 \, Re_a{}^{0.275} \, Pr_a{}^{0.33}, \text{ for } 283 > Rea > 1384, \, 0.71 > Pr_a > 0.72 \qquad (5\text{-}9)$$

Figure 5.12 shows that the heat transfer performance of the current study for the air heating followed the trend of air cooling established by Dasgupta (2011) with a slightly higher value for the heating mode.
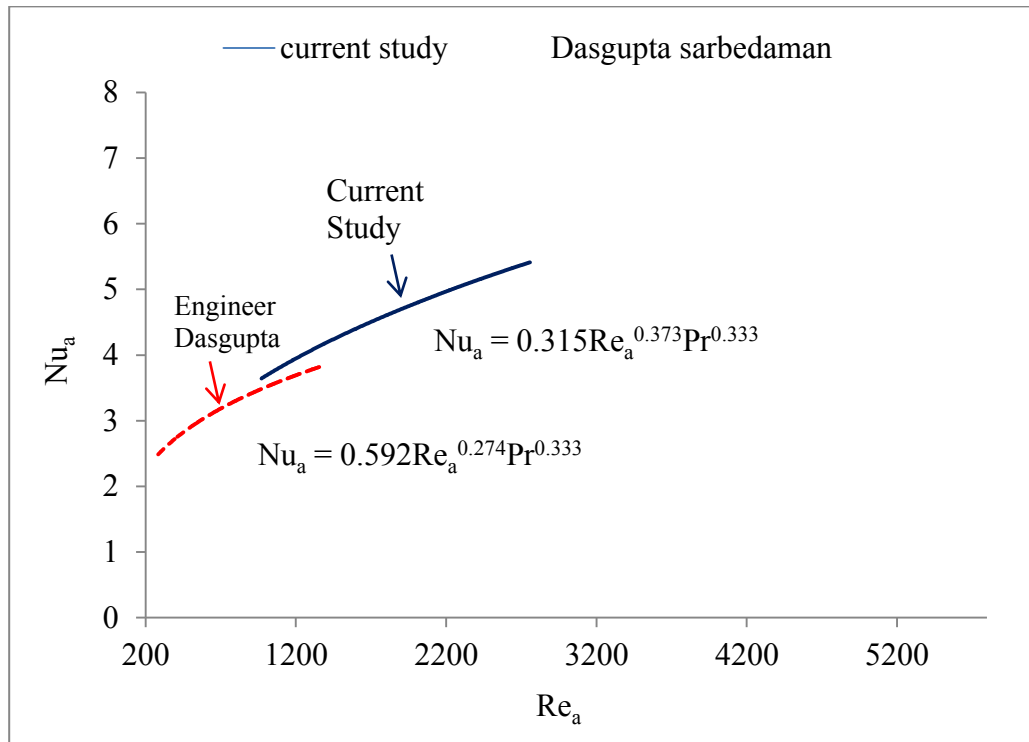
Figure 5.12 A comparison of the current correlation (Re_a, Nu_a, Pr_a)

5.2.10 Air-side heat transfer coefficient (h_a)

Air side heat transfer coefficient (h_a) can be calculated by an iteration method. Figure 5.13 shows the effect of Re_a on h_a, while keeping the water side Reynolds number Re_w constant. It is obvious from the curve that h_a increases with the increase in Re_a, however the effect of Re_a on h_a is less compared to the effect of Re_w on h_a. An instant change of Re_a from 1800 to 5300 affects h_a to change from 29.6 to 40.7, while varying Re_w from 257 to 411 for a constant Re_a=5300, h_a varies from 40.7 to 59.5. Thus convection heat

transfer in mini-channel heat exchangers, Re_w has a dominating role in heat transfer occurrences.
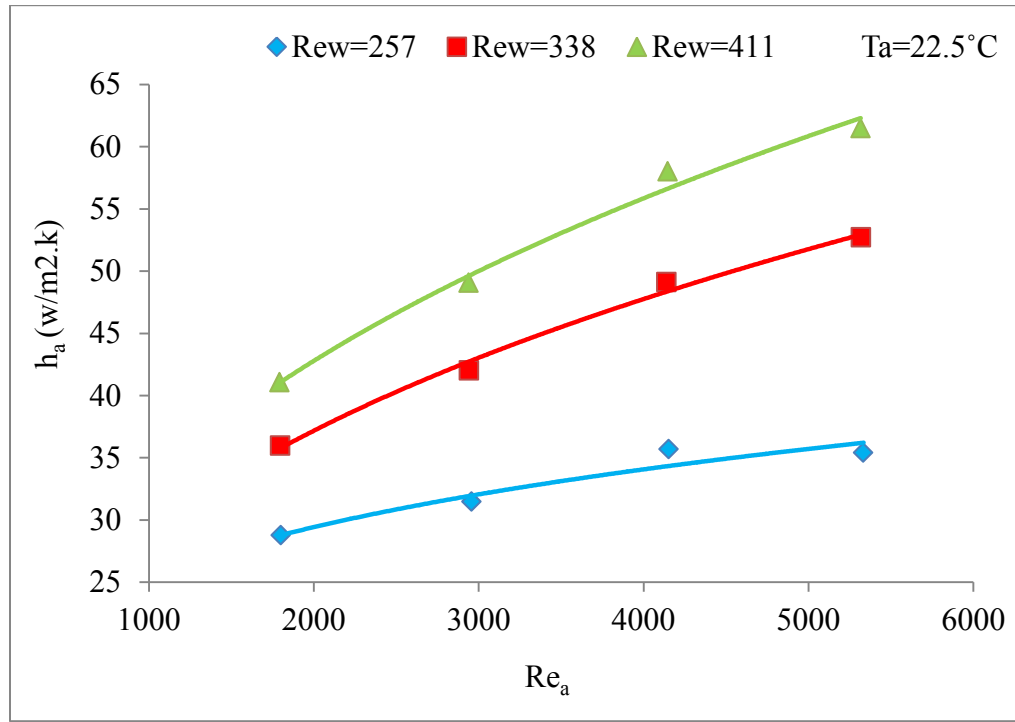
Figure 5.13 The effect of Re_a on h_a

5.2.11 Air-side Nusselt number (Nu$_a$)

The effect of the Re_a on Nu_a is plotted in Figure 5.14 for constant air inlet temperature and different Re_w. The air-side Nusselt number is varied from 4.3 to 6.3 while Re_a changes from 1800 to 5300. The variation of Re_w from 257 to 411 changes Nu_a from 6.3 to 7.6. This effect difference of Re_a and Re_w on Nu_a is similar to the effect on h_a. Therefore, the velocity of air has very smaller effect on Nu_a than Re_w.
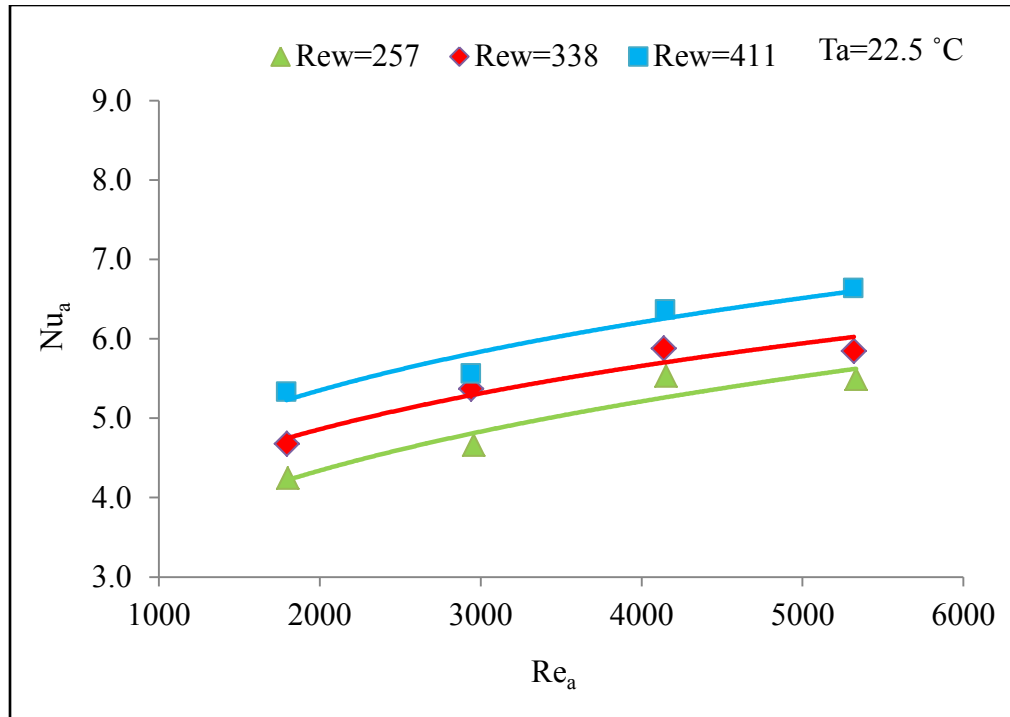
Figure 5.14 The effect of the Re_a on the Nu_a

5.3 Serpentine Effect

The Dean number is a dimensionless number in fluid mechanics which takes place in the study of flow in curved pipes and channels. It represents the ratio of the viscous force acting on a fluid flowing in a curved pipe to the centrifugal force. In the current study the fluid passes through the serpentine path of the heat exchanger core which is a curved pipe. The study of Dean number is vital in analyzing the fluid flow behavior. De can be calculated from equation 3.16. Dean number of higher than 11.6, indicate that the curvature has a significant effect on the fluid flow characteristics. In the current study, Dean number was found to be from 182 to 315 which means that the friction factor in the straight part of the channel and the serpentine is different. In other words, the result shows that there is a secondary flow in the serpentine which disturbs the boundary layer in the curvature. At the exit of the bend, the boundary layer starts developing. This

process intensifies the heat transfer rate. De is plotted against Nu_w and Pr_w in Figure 5.15. The correlation for De established on Nu_w and Pr_w is shown as,

$$Nu_w = 1.258\, De^{0.17}\, Pr_w^{\,0.33} \tag{5-10}$$

It predicts the serpentine effect on the enhancement of the heat transfer.
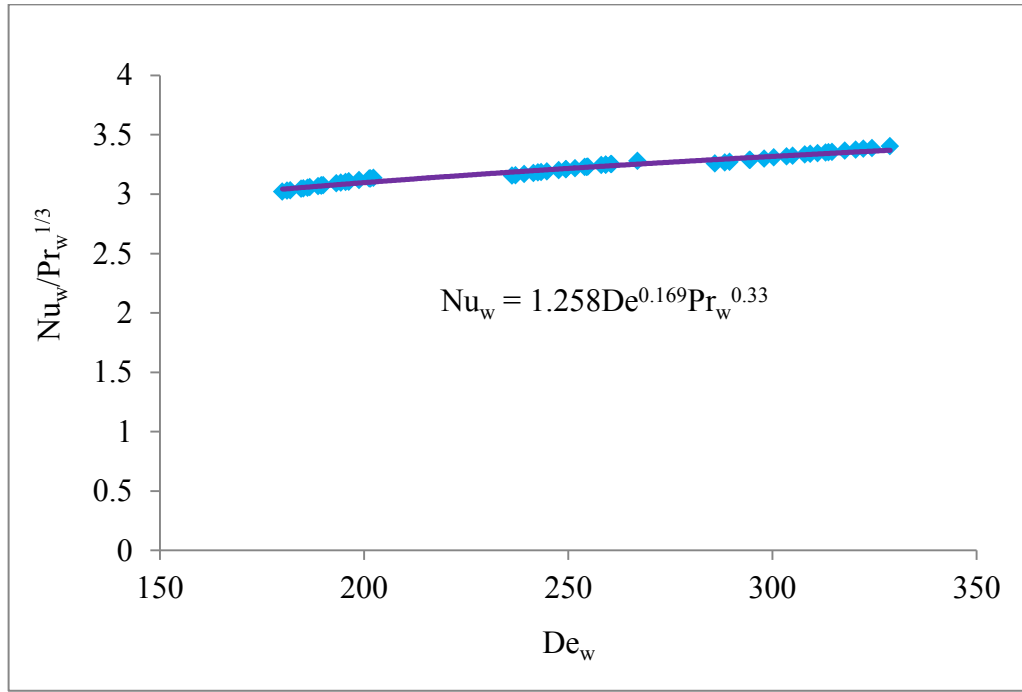
Figure 5.15 The effect of water-side Dean number on $Nu_w/Pr_w^{1/3}$

5.4 Viscous dissipation

Brinkman number, Br, is defined as the ratio of the heat production caused by the viscous forces to the heat transferred through the wall. It basically measures the viscous dissipation. Figure 5.16 presents the relation between the mass flux and Br. Brinkman number increases as mass flux increases by power law relation. It is calculated from equation (5.11). Br depends on the dynamic viscosity which is depends highly on temperature, so at low temperature the viscosity increases and more viscous dissipation occurs. Results from the study shows that Br lies between 5E-9 < Br < 1.334E-8. A

practical correlation at a constant temperature boundary condition has been established as,

$$Br_w = 9E\text{-}14G_w^{1.82} \tag{5.11}$$
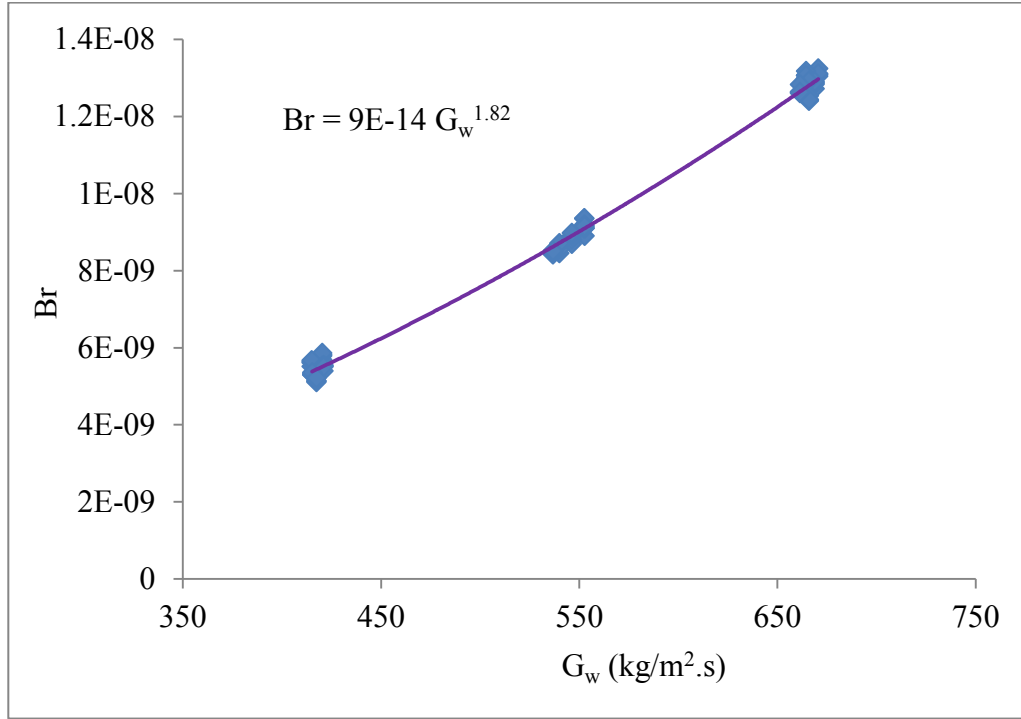
Figure 5.16 The effect of water-side mass flux on Brinkman number

5.5 Eckert number (Ec)

Eckert number is a non-dimensional number utilized in fluid dynamics. It states the relationship between kinetic energy and enthalpy of a flow and is employed to characterize dissipation through viscosity. The relation between Eckert, Brinkman, and Prandtl numbers is expressed as $Br_w = Ec_w . Pr_w . Ec$. Eckert number is plotted vs. mass flux (G_w) in Figure 5.17 and Nu_w versus Ec in Figures 5.18 and 5.19. Ec_w is calculated from the equation $Ec = V^2/c_p \; (T_b\text{-}T_{wall})$. The Br_w and Ec are both used to estimate the heat

transfer characteristics and viscous dissipation. In the recent study, Eckert number was found within $1.6E\text{-}9 < Ec_w < 3.9E\text{-}9$.

However, it is really small in scale but cannot be ignored owing to its influence on the viscous dissipation. Due to Ec being the ratio of kinetic energy of the fluid to the differential enthalpy at the boundary layer, it means that the kinetic energy is small compared to the enthalpy difference. While the kinetic energy increases with the increase of velocity or inertia, Ec increases which indicates that the viscous dissipation exists at a higher velocity and cannot be ignored. On the other hand, from Ec number equation, when T_{wall} increases, it results in an increase in T_b. The increase in T_{wall} leads to a decrease the viscosity, which in turns enhances the movement of the fluid molecules and results in a higher velocity, as well as an increase in Ec. The correlation established for the relation is found as,

$$Nu_w = 26.24 \ Ec_w^{\ 0.088} \tag{5-12}$$
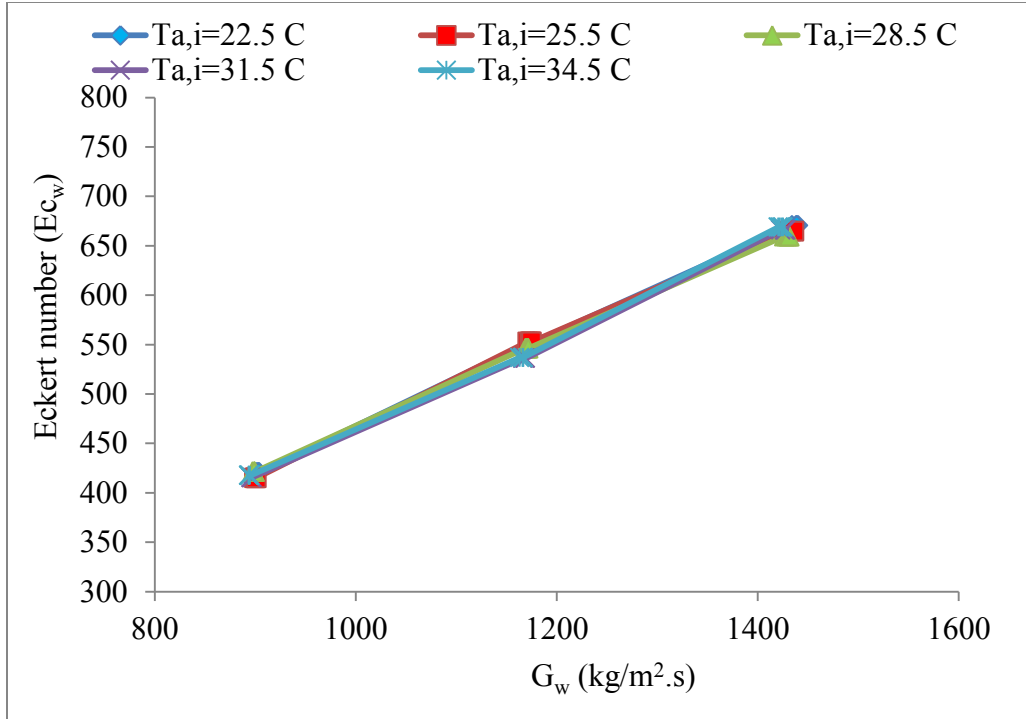
Figure 5.17 The effect of mass flux on Eckert number for the water side
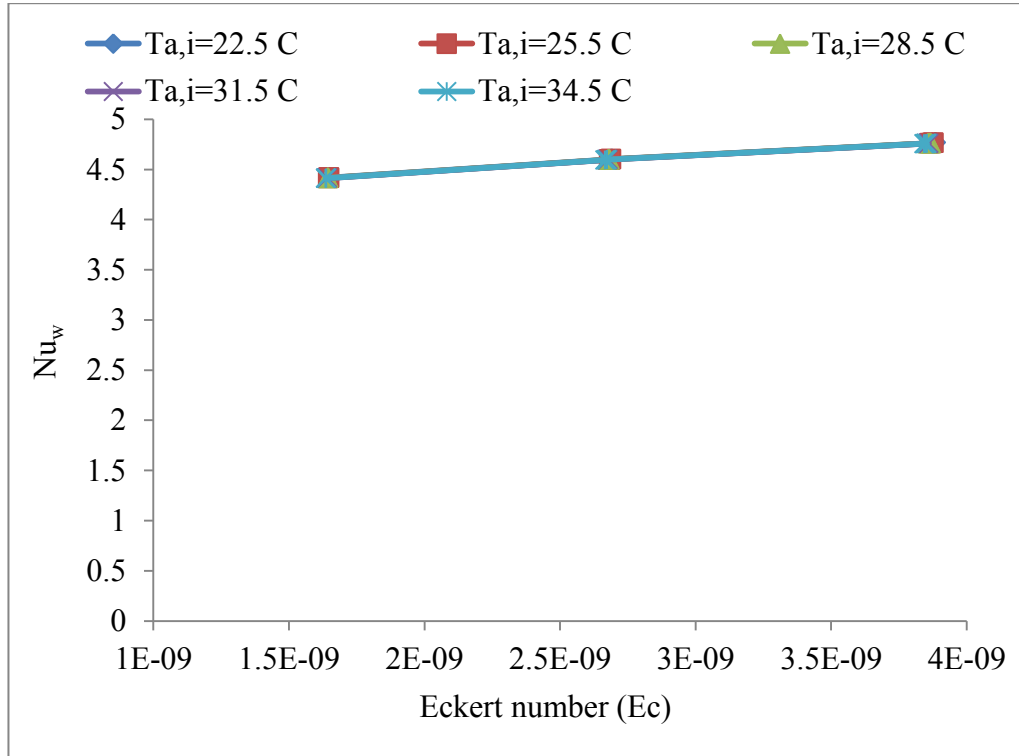
Figure 5.18 The effect of waterside Eckert number on Nu_w
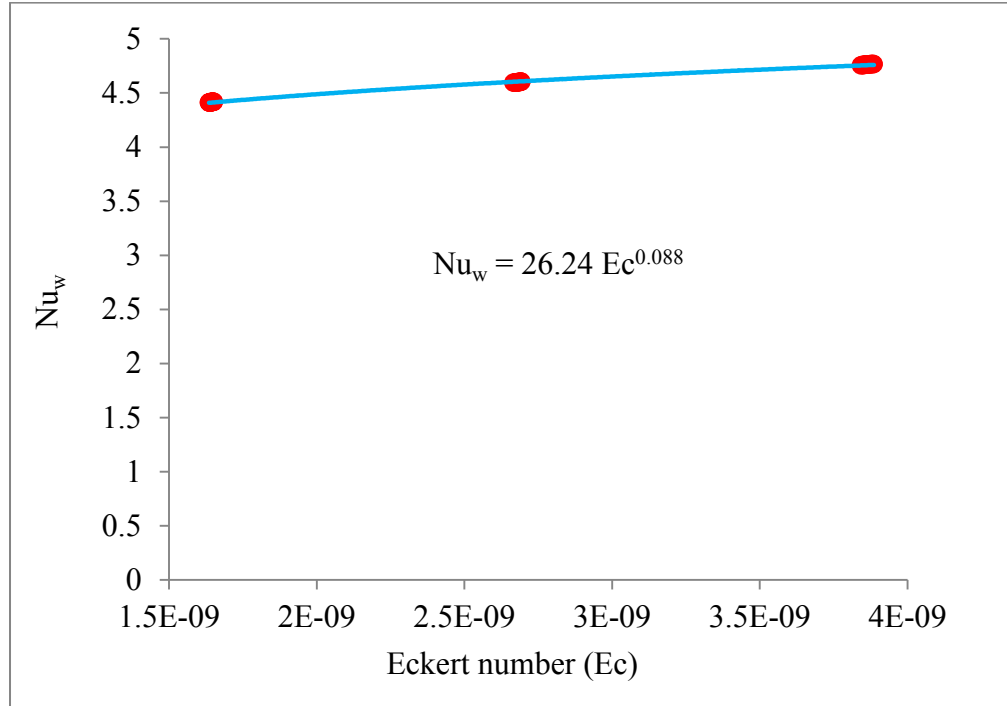
Figure 5.19 The effect of water-side Eckert number on Nu_w

5.6 Heat Exchanger Performance

There are two important factors in evaluating a heat exchanger performance; effectiveness (ε) and NTU.

5.6.1 Effectiveness (ε)

The effectiveness of the recent MICHX has been calculated from equation 3-42. Figure 5.20 demonstrates the effects of varying Re_a on effectiveness. It is revealed that ε increases by increasing Re_a in a power law curve. The slope of the curves from the figure indicates that the heat exchanger is at its high effectiveness and the change of ε with Re_a is monotonous. It also shows that effectiveness is higher at a higher air inlet temperature. For the current study as Re_a varies from 1750 to 5300 for a defined air inlet temperature

between 22.5 C and 34.5 C, effectiveness change is found to be from 0.82% to 0.97%. Consequently the effect of Re_a and $T_{a,i}$ on effectiveness is diminutive.
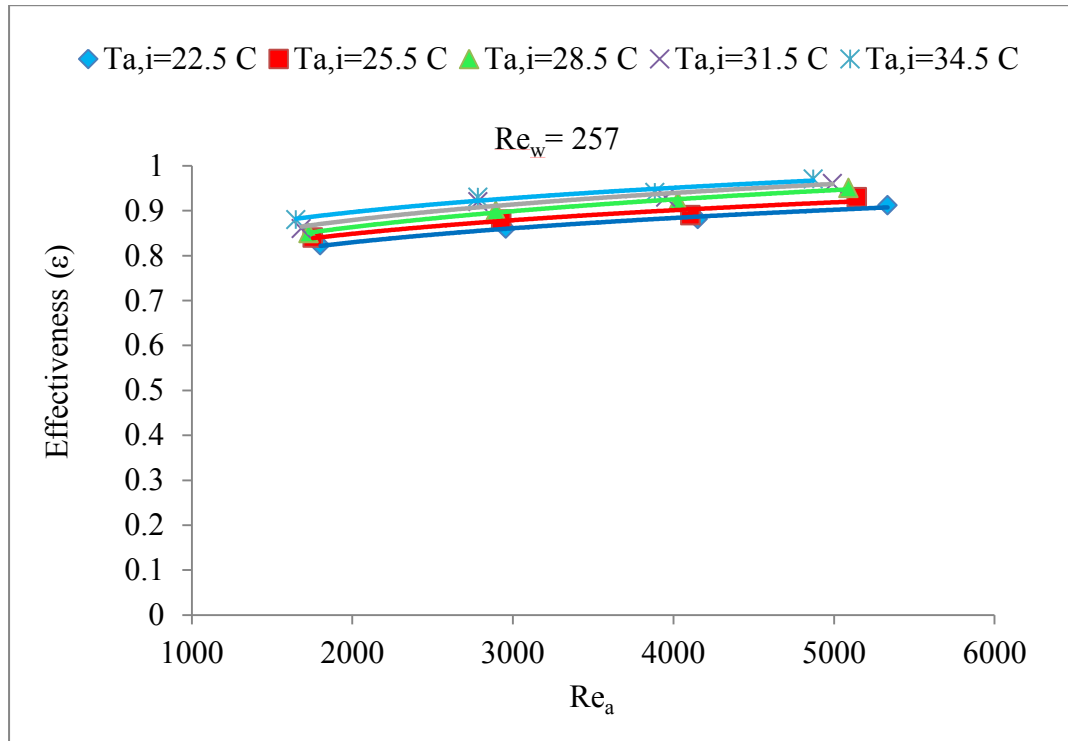
Figure 5.20 The effect of air-side Reynolds number on effectiveness

Figure 5.21 demonstrates the relation between ε and Re_w. Water Reynolds number was changed from 257 to 411. It is shown that ε increases with the increase in Re_w in a power law basis. Effectiveness is higher at lower Re_w. The reason is that at low Re_w, water flows at a low velocity, the dwelling time for water in the channels is higher which means more heat transfer and that leads to higher ε. The correlation found is,

$$\varepsilon = 4.11 \ Re_w^{-0.26} \tag{5-13}$$

As discussed previously, Re_w possess a higher effect than Re_a and $T_{a,i}$. Thus, in optimizing a heat exchanger design, Re_w is considered as the more influential factor.

These results agree with the study of Khan et al. (2010) using a similar heat exchanger but with two slabs where a similar correlation was obtained.
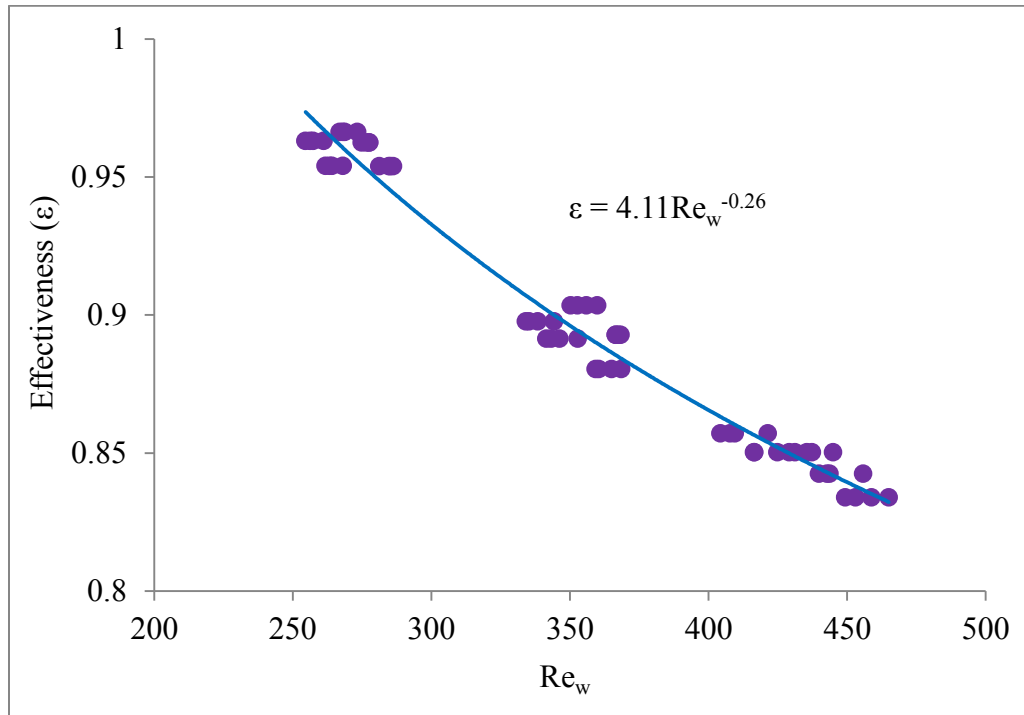
Figure 5.21 The effect of air-side Reynolds number on effectiveness

5.6.2   Number of Transfer Units (NTU)

The Number of Transfer Units (NTU) method is used to compute the rate of heat transfer in heat exchangers when there is a lack of information to determine the Log-Mean Temperature Difference (LMTD). In a heat exchanger analysis, if the fluid inlet and outlet temperatures are indicated or can be easily calculated from the energy balance equation, the LMTD method can be used. NTU is plotted against Re_a in Figure 5.22. It is evaluated from equation (3-43). From the three figures, one can conclude that NTU increases by increasing Re_a and decreases when higher Re_w is used. It also clarified that Re_w has a dominant effect on NTU.
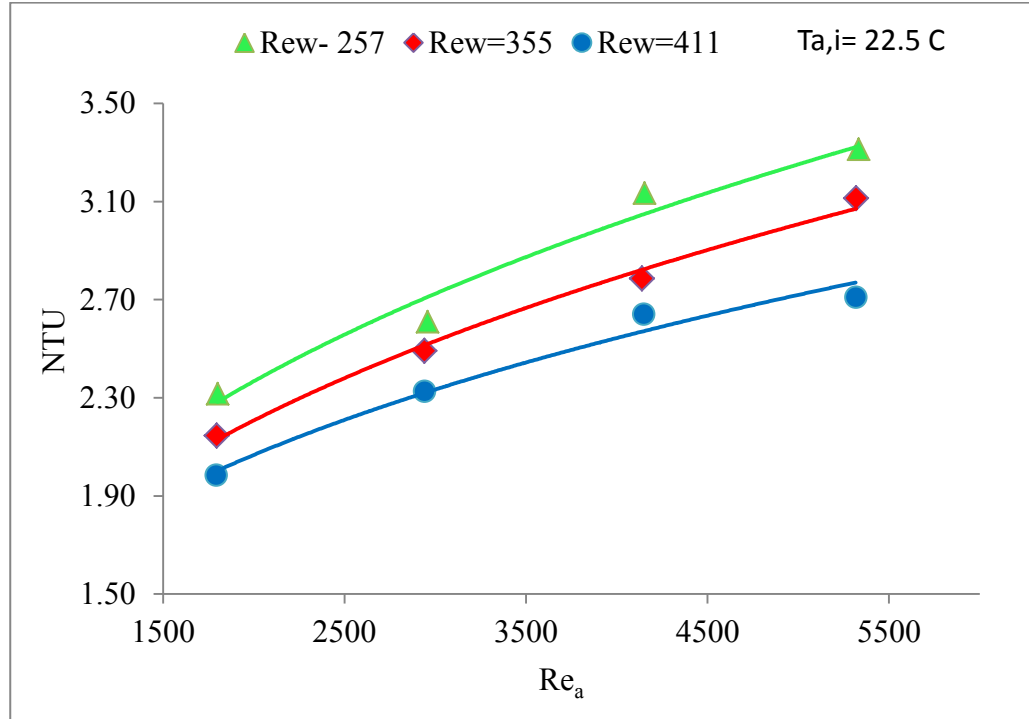
Figure 5.22 The effect of Re_w on NTU

The effect of Re_w on NTU for 5 different air inlet temperatures is illustrated in Figure 5.23 and Figure 5.24. The correlation found from the best fitted power law curve can be shown as,

$$NTU = 17.56 \, Re_w^{-0.33} \tag{5-14}$$
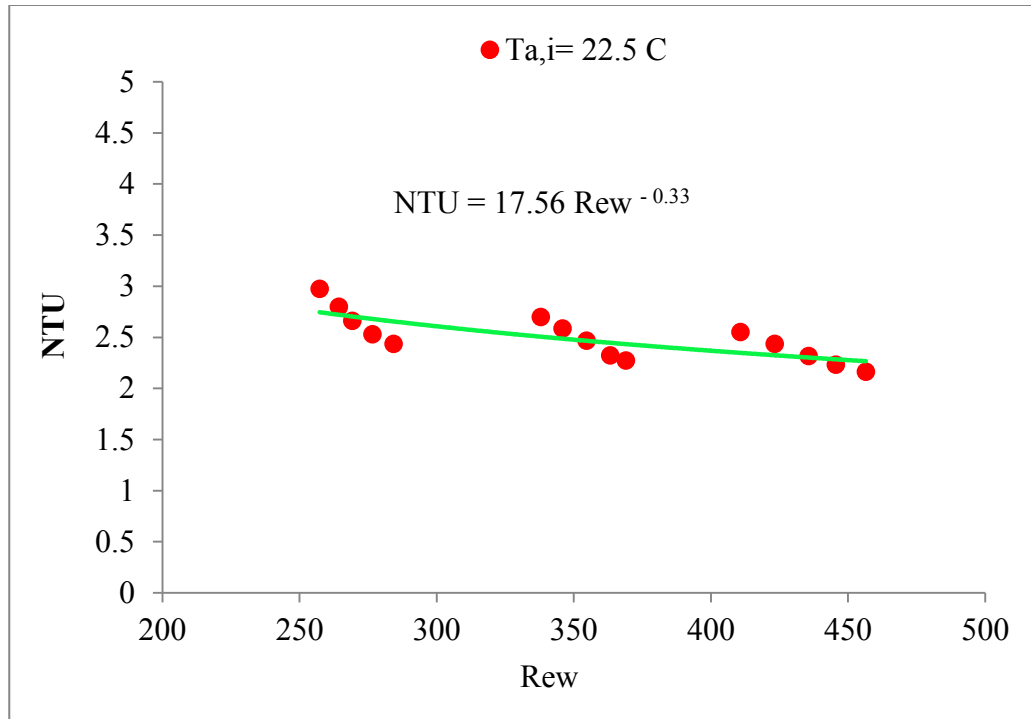
Figure 5.23 The effect of Re_w on NTU ($T_{a,i}$=22.5ºC)

$$NTU = 17.56\ Re_w^{-0.33}$$
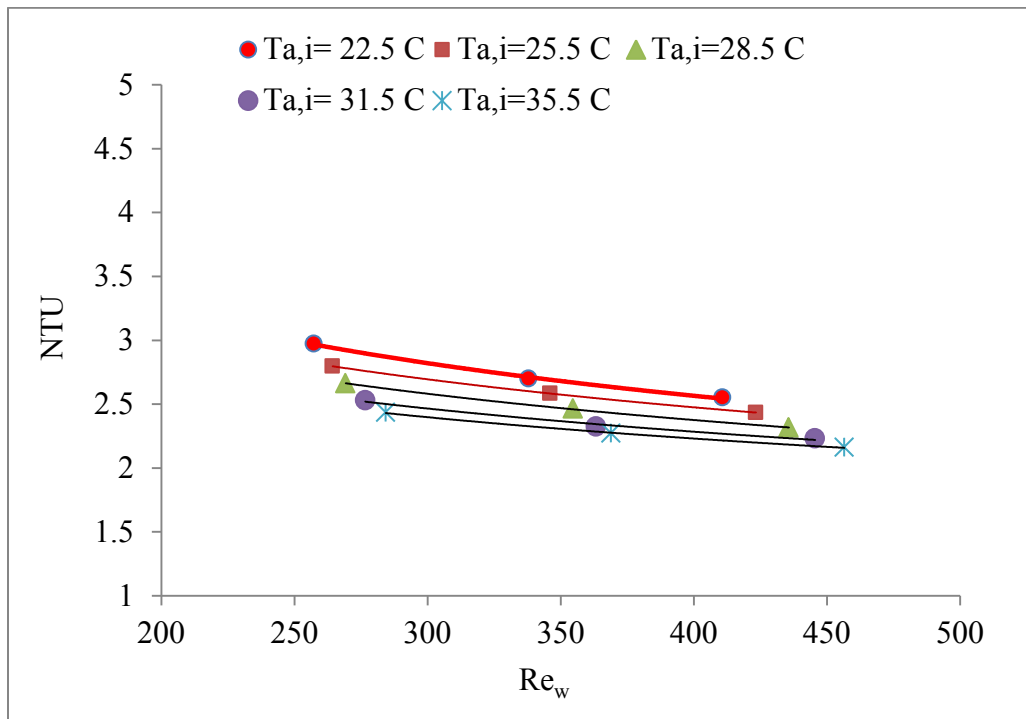
Figure 5.24 The effect of Re_w on NTU for different $T_{a,i}$

5.6.3   The Heat Capacity Rate Ratio (C*) Effect

The effect of the capacity rate ratio (C*) on ε and NTU is plotted in Figure 5.25, where generally ε increases with the increase in NTU. The increase in NTU values starts around 1.5 that corresponds to an effectiveness value close to 0.8. The correlations for both curves are as follows,

$$\varepsilon = 0.66 \, C^{*-0.12} \tag{5-15}$$

$$NTU = 1.18 \, C^{*-0.32} \tag{5-16}$$

NTU > 3 is not economically justifiable. The NTU values for this type of heat exchanger lie within the economical range which is 2 < NTU < 3.1. The plot also shows that both ε and NTU decrease when increasing C*, knowing that the range of C* varies between 0 < C* < 1. Effectiveness reaches its maximum value of 1 at C*=0 and a minimum value when C*=1. In this investigation, C* was found within 0.05 < C* < 0.23 which is lower than 1.

The ε-NTU relation is illustrated in Figure 5.26 where a power law curve fit initiates to be best curve fit.

$$\varepsilon = 0.63 NTU^{0.37} \tag{5-17}$$
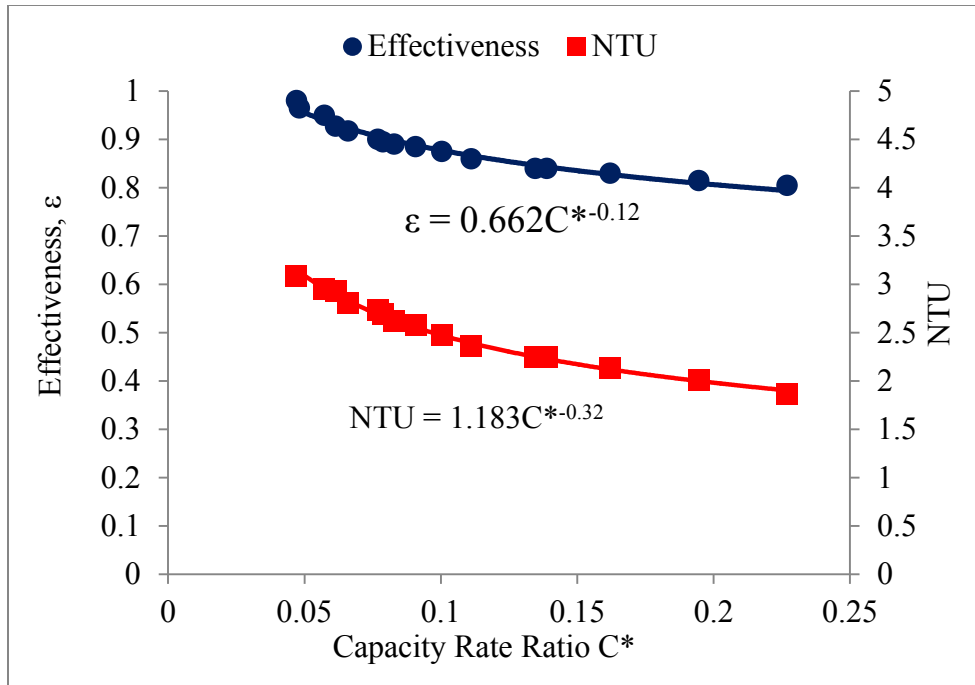
Figure 5.25 The effect of C* on ε and NTU
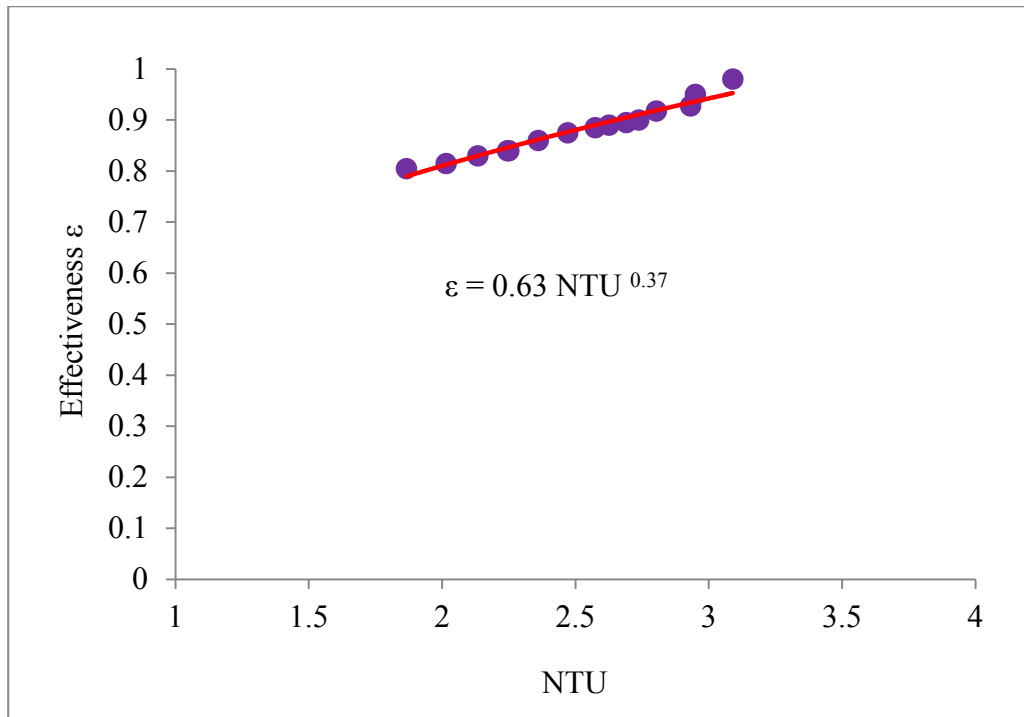
Figure 5.26 The effect of NTU on effectiveness

5.6.4 Overall Heat Transfer Coefficient (UA)

The overall heat transfer coefficient (UA) shows how well the heat scatters in heat exchangers and represents the reciprocal of the total thermal resistance (R_{total}). It can be directly calculated from equation (3.40). The relationship between water Reynolds number and the overall heat transfer units (UA) is illustrated in Figure 5.27, UA increases with the increase in Re_w for a specific air inlet temperature as well as with the increase of $T_{a,i}$ for a particular value of Re_a.

In the current study, UA values varied from 240 <UA< 350. The correlation of UA- Re_w is obtained as,

$$UA = -0.001\ Re_w^2 + 1.609\ Re_w - 81.72 \tag{5-18}$$
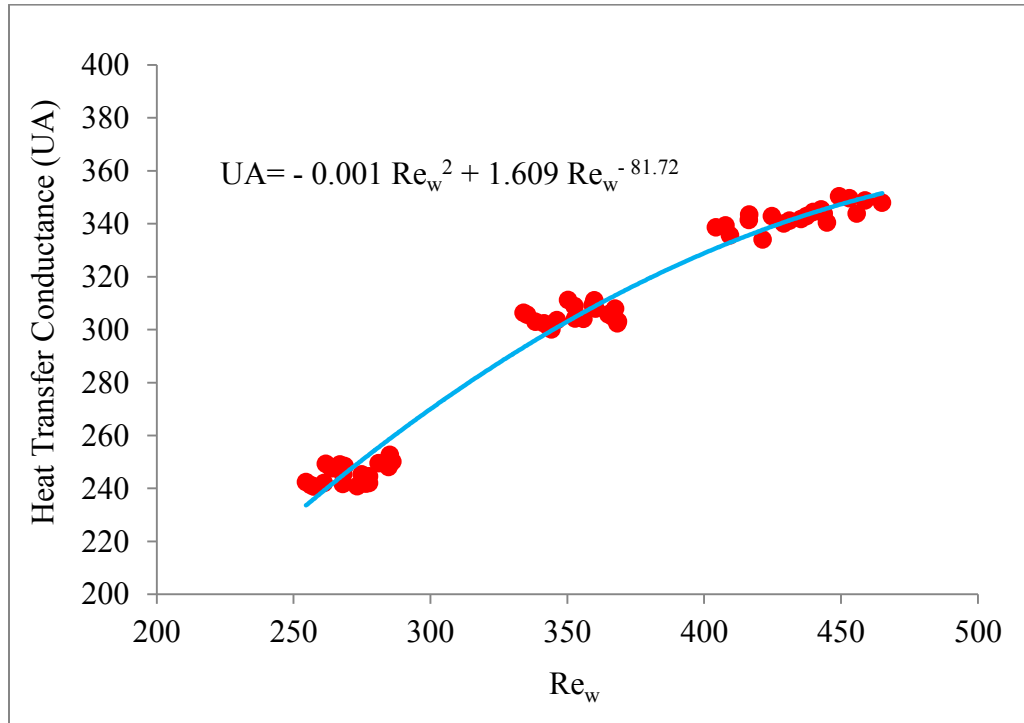
Figure 5.27 The effect of Re_w on heat transfer coefficient (UA)

5.7 <u>Axial Conduction Number (M)</u>

A new non-dimensional number quantifying the axial conduction part in the walls is the axial conduction number (M). Heat transfer by conduction in the walls of mini–micro-channels is quite multidimensional, which can become strongly non-uniform for low Reynolds numbers. Most of the heat flux is transferred to the fluid flow at the entrance of the mini–micro-channels, Maranzana (2004). As a conclusion, the axial conduction in the walls of a mini–micro heat exchanger yields a loss of efficiency. An optimal wall conductivity that maximizes this efficiency exists, Maranzana (2004). Axial conduction number can be calculated from equation (3.19). Figure 5.28 illustrates Re_w vs. the axial conduction number. It indicates that at lower Re_w, the axial conduction number is higher which results in higher axial heat conduction. It also shows that by increasing $T_{a,i}$ for a constant Re_w, as M increases, the axial heat conduction increases as well. Axial heat conduction is significant when M get higher than M > 0.01. For the current study, the axial conduction number varied between 0.002 < M < 0.0033, which shows that the axial heat conduction doesn't have an influence on the heat transfer in the MICHX. Moreover, the trend shows that even for lower velocity, consequently lower Re_w in MICHX, the axial heat conduction could not be taken into consideration because the M <<0.01.
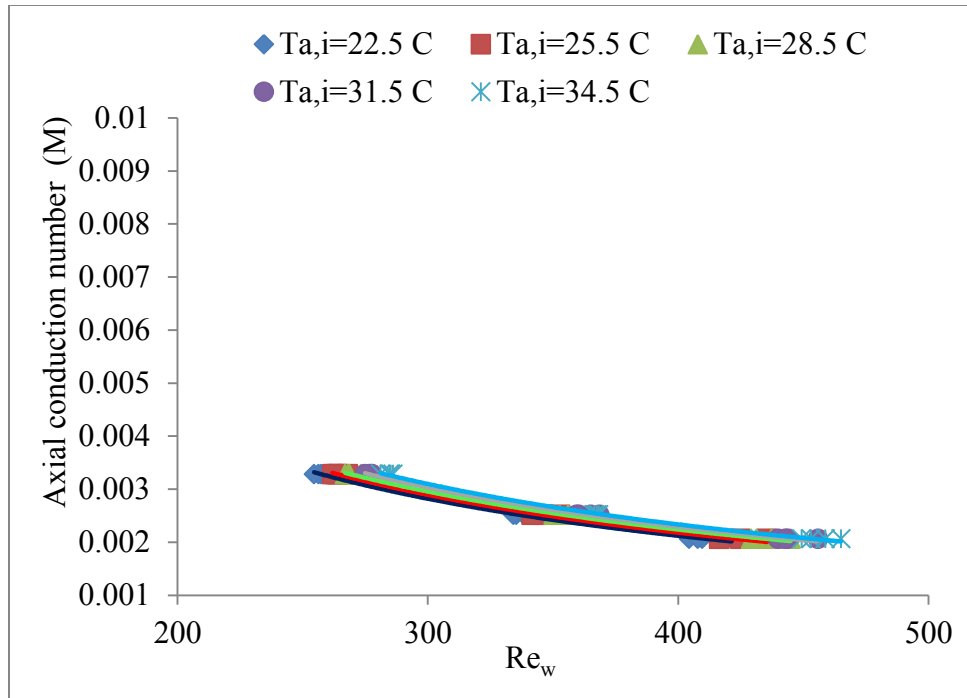
Figure 5.28 The effect of Re_w on M
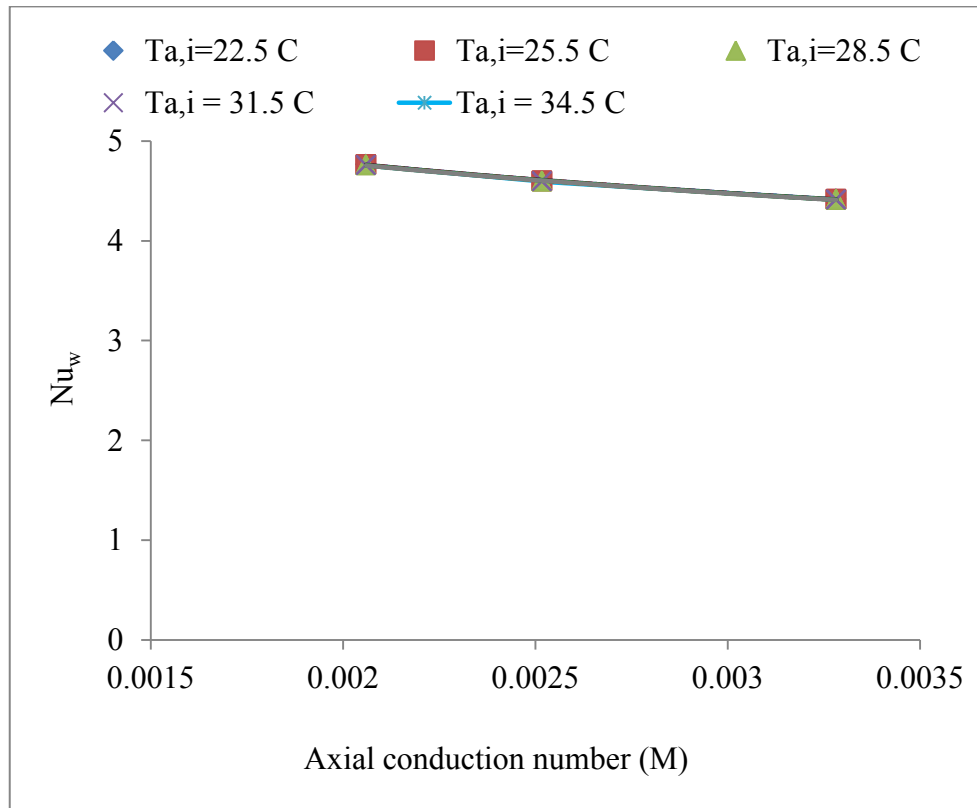
Figure 5.29 The effect of axial conduction number (M) on Nu_w

5.8 Distribution of ΔT_s along the Channel Length

The distribution of temperature drop along the channel length for the water flow is illustrated in Fig. 5.30. The liquid temperature drops significantly in the first three slabs which indicate that most of the heat transfer occurs there. The heat transfer rate in the last two slabs is found to be less significant. According to this finding, eliminating the last two slabs from the MICHX will lead to:

- Reduce the size of the heat exchanger and save space.

- Decrease the pressure drop across the heat exchanger which decreases the required power.

- Reduced material and fabrication cost.
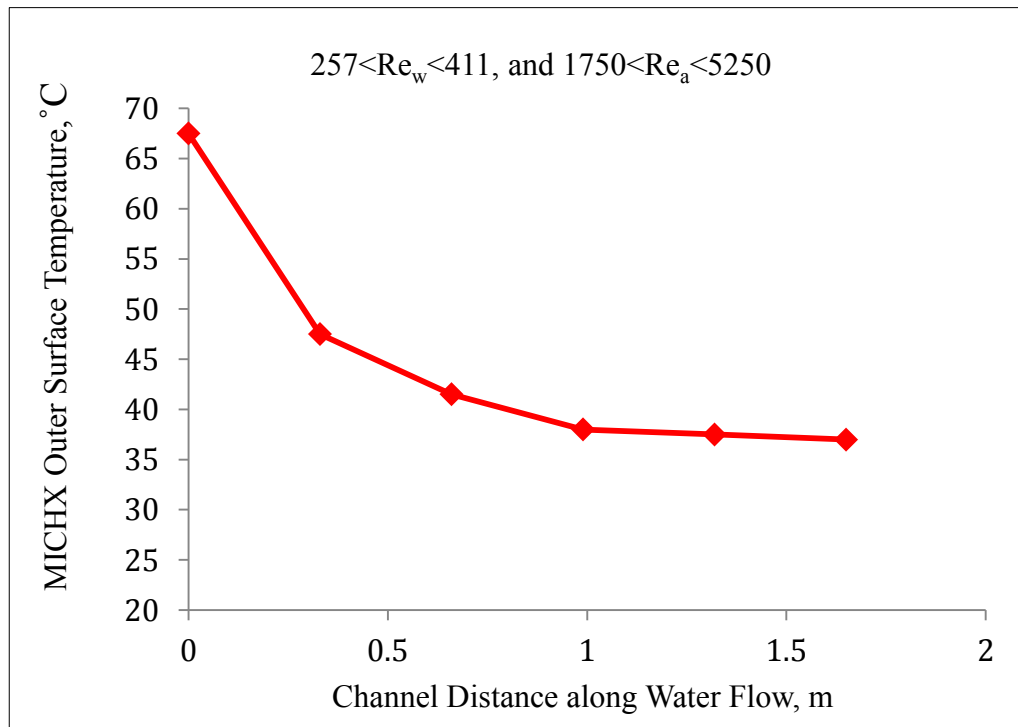
Figure 5.30 Temperature drop vs. channel length

CHAPTER VI

CONCLUSIONS AND RECOMMENDATIONS

6.1 Summary and Conclusion

A thermal performance study is carried out to characterize the heat transfer in cross-flow MICHX with DI-water and air as the working fluids. This study investigates the effects of dimensionless parameters such as: Reynolds number (Re), and Nusselt number (Nu) for both fluids upon heat flow behaviour. The key parameters, such as heat transfer rates, *NTU*, Effectiveness, overall thermal resistance, axial heat conduction, and viscous dissipation are investigated. Empirical relationships are created between the heat transfer and key fluid-flow dimensionless parameters. Sixty distinct operating conditions are maintained in order to obtain these key Parameters. DI-water inlet temperature has been maintained constant at 75˚C all through the study, while air temperatures were varied at 22.5, 25.5, 28.5, 31.5, and 34.5˚C. Three different DI water mass flow rates 0.022 Kg/s, 0.029 Kg/s, and 0.035 Kg/s were examined. For each mass flow rate, four air velocities: 6, 10, 14, and 18 m/s were applied. The following observations have been found from the current study:

1. The heat Balance (HB %) indicates the difference in rate of the heat released by DI-water and the heat gained by air to be less than 7%, which means that the MICHX has a negligible heat loss to the surrounding.

2. The results for Nu_a correlation found from the current study for air heating are compared to Dasgupta's results for air cooling. It is found that the heat transfer performance for air cooling and heating followed the same trend and slightly more enhanced for heating mode.

The correlations found in this study are:

$$Nu_a = 0.315 \, Re_a^{0.373} \, Pr_a^{0.33}, \qquad \text{for } 1750 < Re_a < 5250, \; 0.71 \leq Pr \leq 0.72$$

or

$$Nu_a = 0.281 \, Re_a^{0.373}, \qquad \text{for } 1750 < Re_a < 5250$$

The Pr for air is 0.71 which is incorporated into the constant 0.281.

3. The current study results for Nu_w correlation and air heating using DI-water are compared to Khan's results for 50% glycol-water mixture. Although the current predicted somewhat higher Nu_w, however, it agrees reasonably well with the result found by Khan et al. (2004).

The correlations found in this investigation are:

$$Nu_w = 1.2 Re_w \, 0.17 Pr_w 0.33, \qquad \text{for } 255 < Re_w < 411$$

4. The Reynolds number found to be the key factor affecting the heat transfer mechanism. The heat transfer rate increases with the increase of Re_a and Re_w in a power law relationship. The increase in Q when increasing Re_w is found larger compared to the increase in Q with the increase of Re_a.

5. Liquid heat transfer important factors such as; Nusselt number, heat transfer rate, convective heat transfer coefficient, normalized heat transfer rate, and LMTD are highly dependent on DI-water Reynolds number. The parameters increase with the increase in water Reynolds number in accordance to a power-law correlation.

6. The Dean number (De) in the channel curvature is higher than 11.6 which indicate an existence of a secondary flow in the bend. Thus, the serpentine plays a key role in developing a new velocity profile and boundary layer at the inlet of the proceeding

slab which enhances the heat transfer. This effect is more prominent in the first three slabs compared to the last two slabs.

7. The Brinkman number is an important dimensionless number related to viscosity. The range of Br is found as 5.0E-9 < Br < 1.3E-8. This number is small in amount; it indicates that DI-water contribution to viscous dissipation is negligible.

8. Effectiveness (ε) and NTU increase with the increase in Rea in MICHX. However, they decrease with the increase in Rew, and heat capacity rate ratio (C*). Both factors make a power-law relationship with Rew, and C* as,

$$\varepsilon = 4.2 \, \text{Re}_w^{0.26}$$

$$\text{NTU} = 16.79 \, \text{Re}_w^{0.326}$$

$$\varepsilon = 1.27 \, C^{*-0.3}$$

$$\text{NTU} = 0.64 \, C^{*-0.158}$$

9. The NTU values varied from 2.25 < NTU < 2.75 and effectiveness varied from 82% < ε < 97%. Therefore, MICHX was operating nearly at its maximum thermal size.

10. Scale down multiport MICHX has superior capability to transfer heat between DI-water and air due to the slab serpentine geometry. The flat heat transfer surface on both sides of each slab provide a better contact with the air stream as it eliminates the wake region formation at the back of the tubes in inline conventional heat exchangers. Adding to that, the flat surface makes the temperature distribution uniform on the air side resulting in a superior heat transfer rate for air heating and cooling.

6.2 Recommendations

The findings of the recent investigation in the field of heat transfer and fluid flow can contribute to future research in multiport cross flow MICHXs. Many challenges have been faced to collect the imperative information from the recent study; however substantial observation is still remained to be considered. The observation can be enhanced by using a wider range of operating conditions and conducting more experiments. Extended recommendations can also include:

1. Investigation of changing different heat exchanger core geometries and sizes, various fins size and shapes to check their effect on heat transfer and fluid flow characteristics.

2. Optimization of the channel diameter and its effect on the fluid flow and heat transfer characteristics.

3. Axial heat conduction in the wall and the liquid, particularly at low Nu and Re numbers, can be further examined.

4. The use of a thermal imaging device to study the heat and temperature distribution along the channels, in the serpentines, and on the air-side for the MICHX. Since the use of this device will provide the temperature distribution along the channel which is assumed constant for the current study. This will result in a better insight of the heat transfer and fluid flow.

6. Increase the capability of the system to include different operating conditions such as: fluid temperatures, flow rates, and more variation of air velocities to cover a wide range of applications.

APPENDICES

APPENDIX A

Uncertainty Analysis

Several fluid flow and heat transfer parameters have been discussed in the previous chapters. This appendix presents an evaluation method of the uncertainty associated with these parameters. Uncertainties can be generated for several independent and dependent parameters which influence the final correlations and analysis. Any error consists of two components, bias and precision and the final evaluation of the bias and the precision errors is taken through the Root Sum Square method, RSS. It is worthy to mention that there are two types of parameters; independent and dependent. The independent parameters are those that are directly recorded by the data acquisition system, DAQ, or measured during the experiments. Some examples of the independent parameters are the dimensions of the heat exchanger or the channels and the measurements recorded by the data acquisition system DAQ such as: temperatures, pressures, time, mass flow rates, etc. However, the dependent parameters are those which depend on the independent parameters and can be obtained through calculation such as: Reynolds number, Nusselt number, Prandtl number, heat transfer rate, etc.

Bias

The Bias error can be estimated as follows,

$$B_i = \pm \sqrt{B_{i,1}^2 + B_{i,2}^2 + \cdots + B_{i,k}^2} \qquad \text{i=1, 2, 3}$$

Where, i refer to the error source groups i.e. calibration error, i=1, data acquisition error, i=2, and data reduction error, i=3, Figliola and Beasley (1995). The bias and precision errors can be calculated using the Root Sum Square (RSS) method.

$$B = \pm\sqrt{B_1^2 + B_2^2 + B_3^2}$$

Precision

The precision error can be evaluated using the following formula,

$$P_i = \pm\sqrt{P_{i,1}^2 + P_{i,2}^2 + \cdots + P_{i,k}^2} \qquad \text{i=1, 2, 3}$$

The reduction of this formula will results in the following,

$$P = \pm\sqrt{P_1^2 + P_2^2 + P_3^2}$$

Repeatability

The repeatability error for an apparatus can be calculated as,

$$U_R = \pm\sqrt{R_1^2 + R_2^2 + \cdots + R_n^2}$$

The combination error of those three can be found in the proceeding formula,

$$U_x = \pm\sqrt{B^2 + P^2 + R^2}$$

A.1 Uncertainty of the Parameters

A.1.1 Uncertainty of the Independent Parameters

The uncertainty analysis in the independent parameters include the bias and precision errors defined as,

$$U_x = \pm\sqrt{B^2 + (t_{v,95}P)^2} \qquad (95\%)$$

Where, $t_{v,95}P$ is the precision error at 95% confidence and v is the degree of freedom. v can be calculated using the welch-satterthwaite equation,

$$v = \frac{\left(\sum_{i=1}^{3}\sum_{j=1}^{k} P_{ij}^2\right)^2}{\sum_{i=1}^{3}\sum_{j=1}^{k} \left(\frac{P_{ij}^4}{v_{ij}}\right)}$$

Where, i is a source error group and j is an elemental error within each source group, $v_{ij}=N_{ij}-1$.

A.1.2   Uncertainty of the Dependent Parameters

The following formula demonstrates the correlation between the dependents and the independents parameters.

$$Y = f(X_1 + X_2 + X_3 + \cdots + X_n)$$

Y refers to the dependent parameter and X_n refers to the independent parameters. The errors are computed using the RSS method. Therefore, the absolute uncertainty of Y can be estimated as follows,

$$U_Y = \sqrt{\left(\frac{\partial Y}{\partial x_1}U_{x_1}\right)^2 + \left(\frac{\partial Y}{\partial x_2}U_{x_2}\right)^2 + \left(\frac{\partial Y}{\partial x_3}U_{x_3}\right)^2 + \cdots + \left(\frac{\partial Y}{\partial x_n}U_{x_n}\right)^2}$$

The relative uncertainty of Y can be found as,

$$\frac{U_Y}{Y} = \frac{\sqrt{\left(\frac{\partial Y}{\partial x_1}U_{x_1}\right)^2 + \left(\frac{\partial Y}{\partial x_2}U_{x_2}\right)^2 + \left(\frac{\partial Y}{\partial x_3}U_{x_3}\right)^2 + \cdots + \left(\frac{\partial Y}{\partial x_n}U_{x_n}\right)^2}}{f(X_1 + X_2 + X_3 + \cdots + X_n)}$$

The absolute uncertainty of a parameter can be shown as,

$$Y \pm U_y = Y \pm \sqrt{\left(\frac{\partial Y}{\partial x_1}U_{x_1}\right)^2 + \left(\frac{\partial Y}{\partial x_2}U_{x_2}\right)^2 + \left(\frac{\partial Y}{\partial x_3}U_{x_3}\right)^2 + \cdots + \left(\frac{\partial Y}{\partial x_n}U_{x_n}\right)^2}$$

A.2 Uncertainty of the Airside Hydraulic Diameter

The hydraulic diameter is a function of other parameters and is defined as,

$$D_{h,a} = f\left(L_a, A_{fr,a}, A_a\right) = \frac{4L_a A_{fr,a}}{A_a}$$

$$D_{h,a} = \frac{4\,(0.1)(0.7092)}{(8.1282)} = 0.00394\ m$$

Absolute Uncertainty of Airside Hydraulic Diameter

$$U_{D_{h,a}} = \pm\sqrt{\left(\frac{\partial D_{h,a}}{\partial L}U_L\right)^2 + \left(\frac{\partial D_{h,a}}{\partial A_{min,a}}U_{A_{min,a}}\right)^2 + \left(\frac{\partial D_{h,a}}{\partial A_a}U_{A_a}\right)^2}$$

$$U_{D_{h,a}} = \pm \sqrt{\left(\frac{A_{min}}{A_a}U_L\right)^2 + \left(\frac{L_a}{A_a}U_{A_{min,a}}\right)^2 + \left(-\frac{L_aA_{min,a}}{A_a^2}U_{A_a}\right)^2}$$

$$U_{D_{h,a}} = \pm \sqrt{\left(\frac{0.07092}{8.1282}(0.0001)\right)^2 + \left(\frac{0.1}{8.1282}(0.00023)\right)^2 + \left(-\frac{(0.1)(0.07092)}{8.1282^2}(0.00021)\right)^2}$$

$$U_{D_{h,a}} = \pm 0.000003031 \, m$$

The relative uncertainty of the hydraulic diameter is presented as, $\quad U_{D_{h,a}} = \pm \frac{U_{D_{h,a}}}{D_{h,a}}X100$

$$= \pm \frac{0.000003031}{0.00349}X100 = \pm 0.087\%$$

A.3 Uncertainty of Key Dimensional Parameters

The uncertainty for the key dimensional parameters are presented in Table A.1

Table A.1 Uncertainty of key parameters

Description	Mean Value	Uncertainty (%)
Air-side heat transfer length, L_a	0.1 m	± 0.15
Air-side total frontal area, $A_{fr,a}$	$0.09290 \, m^2$	± 0.37
Air-side minimum free flow area, $A_{min,a}$	$0.07092 \, m^2$	± 0.33
Air-side heat transfer area, A_a	$8.12821 \, m^2$	± 0.0026
Water-side heat transfer area, A_w	$0.001 \, m^2$	± 3.49
MICHX hydraulic diameter, $D_{h,w}$	0.987 m	± 3.48
Single slab length, L_{slab}	0.304 m	± 0.15

A.4 Uncertainty for one Operating Condition

($V_a = 10$ m/s, $T_{a,i} = 28.5$ °C, $T_{w,i} = 70$ °C, $\dot{m}_w = 0.029$ kg/s)

Table A.2 Different parameters at T_b for one operating condition

Parameter	Mean Value
Air inlet temperature, $T_{a,i}$	28.5 °C
Air outlet temperature, $T_{a,o}$	34.15 °C
Air mass flow rate, $\dot{m}_a$	$1.096 \frac{kg}{s}$
Air velocity, V_a	$10 \frac{m}{s}$
Air-side pressure drop, ΔP	60.00 Pa
Air Density, ρ_a	$1.1597 \frac{kg}{m^3}$
Air specific heat, $C_{p,a}$	$1006.51 \frac{J}{kg.°C}$
Air-side Reynolds number, Re_a	2880
Air-side Nusselt number, Nu_a	5.860
Air-side Prandtl number, Pr_a	0.713
Air-side Heat transfer rate, $\dot{Q}_a$	6232 W
Water-side Heat transfer rate, $\dot{Q}_w$	4364 W
Air-side overall Heat transfer rate, $\dot{Q}_{Overall,a}$	5298 W
De-water inlet temperature, $T_{w,i}$	70.52 °C
De-water outlet temperature, $T_{w,o}$	34.52 °C
DI-water mass flow rate, $\dot{m}_w$	$0.029 \frac{kg}{s}$
DI-water Reynolds number, Re_w	356

A.4.1 Uncertainty for Air Inlet Temperature

The mean temperature $(\bar{T}_m)$ and the standard deviation (σ) for 108,000 data, obtained from the nine thermocouples that are distributed uniformly at the cross section of the air inlet, are found as,

$$\bar{T}_m = \frac{1}{n}\sum_{n=1}^{n=108000} T_{mn}$$

$$\sigma = \sqrt{\frac{1}{n-1}\sum_{n=1}^{n=108000}(T_{mn} - \bar{T}_m)^2}$$

The mean temperature of the air inlet can be calculated from the average of the 9 thermocouples as,

$$\langle \bar{t} \rangle = \frac{1}{m}\sum_{m=1}^{m} \bar{T}_m$$

Where, m=9. The air inlet mean temperature is taken as,

$$\langle \bar{T}_{a,i} \rangle = 31.45°C$$

The calibration and data reduction errors are ignored as the sources of errors. Followed is the information for the data acquisition system errors.

σ: The standard deviation of each thermocouple at the inlet and outlet

$\bar{T}_m$: Mean of the samples for a specific thermocouple

v: Degree of freedom

$\langle \bar{T} \rangle$: The mean of each thermocouple reading at the inlet and outlet

Data Acquisition System Errors:

Based on the instrumental error defined by Figiola and Beasley (1995), the value of J is determined as follows,

For the instrumental error, J=2

For the signal conditioning stage, J=3

For the spatial variation error, J=8

For the temporal variation errors, J=9

The instrument errors and accuracy are found from the manufacturer's catalogues.

1- Considering the thermocouples (instrumental error) with $i = 2$ and $J = 2$

Resolution $= \pm 1°C$

Accuracy $= \pm\ 0.01\ °C$

So the bias uncertainty is shown as,

$$B_{22} = \sqrt{\left(\tfrac{1}{2}(0.01)\right)^2 + (1)^2} = \pm 1°C \quad 95\%$$

$$P_{22} = 0$$

2- Signal conditioning stage (instrumental error) with $i = 2$ and $j = 3$

Accuracy $= \pm 0.06\ °C$

Resolution $= \pm\ 0.038\ °C$

Offset error $= \pm\ 0.025\ °C$

System noise error $= \pm\ 0.0125\ °C$

The bias uncertainty is shown as,

$$B_{23} = \sqrt{\left(\frac{1}{2}(0.038)\right)^2 + (0.06)^2 + (0.025)^2 + (0.0125)^2} = \pm 0.142°C \quad 95\%$$

$$P_{23} = 0$$

3- Considering the spatial variation error with $i = 2$ and $j = 8$

These errors are caused by the non-uniformity of the air inlet temperature. The standard deviation and precision index of the air inlet mean temperature is as follows,

$$\sigma = \sqrt{\frac{\sum_{m=1}^{9} (\bar{T}_m - \langle T \rangle)^2}{m-1}}$$

$$\sigma = 1.724 \, ^\circ\mathrm{C}$$

$$P_{28} = \frac{\sigma}{\sqrt{m}}$$

$$P_{28} = \frac{1.274}{\sqrt{9}} = 0.424 \, ^\circ\mathrm{C}$$

ν_{28} (The degree of freedom) = 9-1= 8

Assuming B_{28}=0

4- Considering the temporal variation error with i = 2 and j = 9

The temporal variation error originated from taking measurement at various time.

$$\sigma = \sqrt{\frac{\sum_{m=1}^{9}\sum_{n=1}^{108000}(T_{mn}-\bar{T}_m)^2}{m-(N-1)}}$$

$$= \sqrt{\frac{1}{m}\sum_{m=1}^{9}(\sigma_m)^2}$$

$$= \sqrt{\frac{1}{9} X \, 0.172556} = 0.138455$$

$$P_{29} = \frac{\sigma}{\sqrt{9x108000}} = \frac{0.138455}{\sqrt{972000}} = 0.00014 \, ^\circ\mathrm{C}$$

V_{29} (The degree of freedom) = M (N-1) =9 × 107999= 971991

$$B_{29} = 0$$

5- Bias error

$$B_1 = B_3 = 0$$

$$\mathrm{B} = B_2 = \sqrt{B_{22}^2 + B_{23}^2 + B_{28}^2 + B_{29}^2} = \pm\sqrt{(1)^2 + (0.142)^2 + (0)^2 + (0)^2} = \pm1.01 \, ^\circ\mathrm{C}$$

Precision index,

$$P_1 = P_3 = 0$$

$$P = P_2 = \sqrt{P_{22}^2 + P_{23}^2 + P_{28}^2 + P_{29}^2}$$

$$= \pm\sqrt{(0)^2 + (0)^2 + (0.5745)^2 + (0.00014)^2}$$

$$= \pm 0.424°C$$

The degree of freedom from Welch-Satterthwaite method is,

$$\nu = \frac{(\sum_{i=1}^{3} \sum_{j=1}^{k} P_{ij}^2)^2}{\sum_{i=1}^{3} \sum_{j=1}^{k} \left(\frac{P_{ij}^4}{\nu_{ij}}\right)} = \frac{(P_{28}^2 + P_{29}^2)^2}{\frac{P_{28}^2}{\nu_{28}} + \frac{P_{29}^2}{\nu_{29}}}$$

i, is the error source group and j, is the elemental error.

$$\nu = \frac{\left((0.424)^2 + (0.00014)^2\right)^2}{\frac{(0.424)^4}{8} + \frac{(0.00014)^4}{971991}} = 8$$

$$U_{T_{a,i}} = \sqrt{B^2 + (t_{8,95}P)^2}$$

The absolute uncertainty for air inlet temperature is presented as,

$$U_{T_{a,i}} = \sqrt{(1.01)^2 + (2.306 \times 0.5745)^2} = 95\%$$

With $t_{24,95}=2.306$

Relative uncertainty $= \frac{U_{T_{a,i}}}{T_{a,i}} \times 100 = \frac{1.3346}{28.5} \times 100 = \pm 4.93\%$

A.4.2 Uncertainty of the Air Outlet Temperature

The mean temperature $(\bar{T}_m)$ and the standard deviation (σ_m) for 108,000 readings for any of the twenty thermocouples distributed uniformly at the cross section of the air outlet in the specified run are found as follows,

$$\langle \bar{T} \rangle = \frac{1}{m} \sum_{m=1}^{m} \bar{T}_m$$

Where, m=25. Air outlet mean temperature is $\langle \bar{T}_{a,0} \rangle = 34.15°C$

Data Acquisition System Errors

1- Thermocouples (instrument error) with i = 2 and j = 2

Resolution $= \pm 1°C$

Accuracy $= \pm 0.01°C$

So, the bias uncertainty is shown as,

$B_{22} = \pm 1°C$ 95%

$P_{22} = 0$

2- Signal conditioning (instrumental error) with i = 2 and j = 3

The bias limit is,

$B_{23} = \pm 0.142°C$ 95%

$P_{23} = 0$

3- The spatial variation error with i = 2 and j = 8

$$\sigma = \sqrt{\frac{\sum_{m=1}^{25}(\bar{T}_m - \langle T \rangle)^2}{m-1}} = 2.94 \,°C$$

$\sigma = 2.94 \,°C$

$$P_{28} = \frac{\sigma}{\sqrt{m}}$$

$$P_{28} = \frac{2.94039}{\sqrt{25}} = 0.588 \,°C$$

v_{28} (The degree of freedom) = 25-1=24

Assuming, $B_{28}=0$

The temporal variation error with i = 2 and j = 25

The temporal variation error originated from taking measurements at various times.

$$\sigma = \sqrt{\frac{\sum_{m=1}^{25} \sum_{n=1}^{108000}(T_{mn} - \bar{T}_m)^2}{m-(N-1)}} = \sqrt{\frac{1}{m}\sum_{m=1}^{25}(\sigma_m)^2} = 2.880 \,°C$$

$$P_{29} = \frac{\sigma}{\sqrt{25 x 108000}} = \frac{2.880}{\sqrt{2700000}} = 0.001752 \text{ °C}$$

v_{29} (The degree of freedom) = M (N-1) = $25 \times 107999 = 2699975$

$B_{29} = 0$

5- Bias error

$$B_1 = B_3 = 0$$

$$\text{B} = B_2 = \sqrt{B_{22}^2 + B_{23}^2 + B_{28}^2 + B_{29}^2} = \pm\sqrt{(1)^2 + (0.142)^2 + (0)^2 + (0)^2} = \pm 1.01 \text{°C}$$

Precision index

$$\text{P}_1 = \text{P}_3 = 0$$

$$\text{P} = P_2 = \sqrt{P_{22}^2 + P_{23}^2 + P_{28}^2 + P_{29}^2}$$

$$= \pm\sqrt{(0)^2 + (0)^2 + (0.588)^2 + (0.001752)^2}$$

$$= \pm 0.588 \text{°C}$$

The degree of freedom from Welch-Satterthwaite method is shown as,

$$\text{V} = \frac{(\sum_{i=1}^{3} \sum_{j=1}^{k} P_{ij}^2)^2}{\sum_{i=1}^{3} \sum_{j=1}^{k} \left(\frac{P_{ij}^4}{v_{ij}}\right)} = \frac{(P_{28}^2 + P_{29}^2)^2}{\frac{P_{28}^2}{v_{28}} + \frac{P_{29}^2}{v_{29}}}$$

Where, i is the source error group and j is the elemental error.

$$\text{v} = \frac{((0.588)^2 + (0.001752)^2)^2}{\frac{(0.588)^4}{8} + \frac{(0.001752)^4}{971991}} = 24$$

$$U_{T_{a,i}} = \sqrt{B^2 + \left(t_{8,95}P\right)^2}$$

Absolute uncertainty for air inlet temperature is obtained as,

$$U_{T_{a,0}} = \sqrt{(1.01)^2 + (2.064 X 0.5745)^2} = 1.57 \quad 95\%$$

With $t_{24,95} = 2.064$

Relative uncertainty $= \dfrac{U_{T_{a,0}}}{T_{a,0}} \times 100 = \dfrac{1.56}{28.5} \times 100 = \pm 5.50~\%$

A.4.3 Uncertainty of the Air-Side Pressure Drop

$\Delta P = \pm 71.20$ Pa

Data Acquisition System Errors

The pressure transducer (instrumental error) with i = 2 and j = 2

Bias limit

Omega pressure transducer - PX277

Accuracy$= \pm 0.1\%$ of full scale

$e_1 = \pm \dfrac{0.1}{100} \times 5 \times 249.1\text{Pa} = \pm 1.25$ Pa

Thermal effect $= \pm 0.2\% \dfrac{FS}{\degree C}$

$e_2 = \pm 3.71$ Pa

Bias limit:

$$B_{22} = \pm \sqrt{e_1^2 + e_2^2}$$

$$= \pm \sqrt{(1.25)^2 + (3.71)^2} = \pm 3.91 \text{ Pa}$$

Precision index, P_{22}=0

Signal conditioning (instrumental error) with i = 2 and j = 3

Accuracy $= \pm\ 0.0003$ Pa

Resolution $= \pm 0.0002$ Pa

Offset error $= \pm\ 0.0001$ Pa

System noise error $= \pm\ 0.0011$ Pa

Uncertainty due to bias errors are obtained as,

$$B_{23} = \sqrt{\left(\frac{1}{2}(0.0002)\right)^2 + (0.0003)^2 + (0.0001)^2 + (0.0011)^2} = \pm 0.0008 \, Pa \ \ 95\%$$

$$P_{23} = 0$$

Signal conditioning (instrumental error) with i = 2 and j = 9

Bias limit, B_{29}=0

Number of data points = 108000

Degree of freedom, v= N-1 = 108000-1=107999

Mean differential pressure, $\overline{\Delta P}$ = 389.357Pa

Standard deviation, $\sigma_{\Delta P}$ = 0.30655749

$$P_{28} = \frac{\sigma}{\sqrt{m}}$$

Precision index, $P_{29} = \frac{\sigma_{\Delta P}}{\sqrt{N}}$

$$= \frac{0.30655749}{\sqrt{108000}} = \pm 0.00093 \, \text{Pa}$$

Bias limit $B = \pm\sqrt{B_{22}^2 + B_{23}^2}$

$$= \pm\sqrt{(3.91)^2 + (0.0008)^2} = \pm 3.91$$

Precision index, P= P_{29}= $\pm$ Pa

Absolute uncertainty is

$$U_{\Delta P} = \sqrt{B^2 + \left(t_{8,95}P\right)^2}$$

$$t_{107999,0.95} = \pm 1.960$$

$$U_{\Delta P} = \pm\sqrt{(3.91)^2 + (1.960 \times 0.00093)^2} = 3.91$$

Relative uncertainty is= $\frac{U_{\Delta P}}{\Delta P} \times 100 = \frac{3.91}{71.2} \times 100 = \pm 5.491 \, \%$

A.4.4 Uncertainty of Air Velocity

For calculating uncertainty, air velocity value is taken as 10 m/s. Therefore, the precision error is not involved however, the bias error is considered. From the FKT manual, the resolution is equal to 0.01 m/s and the accuracy is ± 0.05 m/s

The absolute uncertainty can be calculated as,

$$U_v = \pm \sqrt{(0.005)^2 + (0.05)^2} = \pm 0.05 \; m/s$$

The relative uncertainty is found as,

$$\frac{U_v}{v} \times 100 = \pm \frac{0.05}{10} \times 100 = \pm 5\%$$

A.4.5 Uncertainties of the Thermo Physical Properties of Air

From the average of the air inlet and outlet temperatures, the thermo physical properties can be found as,

$$T_b = \frac{T_{a,i} + T_{a,o}}{2} = \frac{28.5 + 34.15}{2} = 31.325 \; °C$$

$$\rho_a = 1.1597 \; \frac{kg}{m^3}$$

$$\mu_a = 1.87 \times 10^{-5} \; \frac{kg}{m.s}$$

$$C_{p,a} = 1006.51 \; \frac{J}{kg.°C}$$

$$K_a = 0.02643 \; \frac{W}{m.°C}$$

a- Uncertainty estimation for density (ρ_a)

$$U_{\rho,a} = \pm \frac{\rho_{a,i} - \rho_{a,o}}{T_{a,o} - T_{a,i}} = \pm \frac{1.1706 - 1.1490}{34.15 - 28.5} = \pm 0.00382 \; \frac{kg}{m^3}$$

b- The uncertainty estimation for dynamic viscosity (μ_a) can be found as follows,

$$U_{\mu,a} = \pm \frac{\mu_{a,o} - \mu_{a,i}}{T_{a,o} - T_{a,i}}$$

$$U_{\mu,a} = \pm \frac{1.8875 - 1.8609) \times 10^{-5}}{34.15 - 28.5}$$

$$= \pm 0.0047 \times 10^{-5} \frac{kg}{m.s}$$

c-The uncertainty estimation for the specific heat $(c_{p,a})$ is found as,

$$U_{c_{p,a}} = \pm \frac{c_{p_{a,o}} - c_{p_{a,i}}}{T_{a,i} - T_{a,o}}$$

$$U_{c_{p,a}} = \pm \frac{1006.639 - 1006.4}{34.15 - 28.5}$$

$$U_{c_{p,a}} = \pm 0.0423 \frac{J}{kg°C}$$

d- The uncertainty estimation for thermal conductivity (k_a)

$$U_{k,a} = \pm \frac{k_{a,o} - k_{a,i}}{T_{a,o} - T_{a,i}}$$

$$U_{c_{p,a}} = \pm \frac{0.02664 - 0.02622}{34.15 - 28.5}$$

$$U_{c_{p,a}} = \pm 0.000074 \frac{w}{m. °C}$$

A.4.6   Uncertainty of the Air Mass Flow Rate

The uncertainty for the air mass flow rate can be found as,

$$\dot{m}_a = F(A_f, V_a, \rho_a) = A_{fr} . V_a . \rho_a$$

$$\dot{m}_a = (0.0929)(10.17)(1.1597)$$

$$= 1.095 \frac{Kg}{s}$$

The absolute uncertainty for the air-side mass flow rate is obtained as,

$$U_{\dot{m}_a} = \pm \sqrt{\left(\frac{\partial \dot{m}}{\partial A_{fr}} U_{A_{fr}}\right)^2 + \left(\frac{\partial \dot{m}}{\partial V_a} U_{V_a}\right)^2 + \left(\frac{\partial \dot{m}}{\partial \rho} U_\rho\right)^2}$$

$$U_{\dot{m}_a} = \pm \sqrt{\left(\rho_a . V_a . U_{A_{fr}}\right)^2 + \left(\rho_a . A_{fr} . U_{V_a}\right)^2 + \left(A_{fr} . V_a . U_{\rho,a}\right)^2}$$

$$U_{\dot{m}_a} = \pm \sqrt{\begin{array}{c}[(1.1597)(10.17)(0.000345)]^2 \\ +[(0.0929)(1.1597)(0.05)]^2 + [(0.0929)(10.17)(0.00382)]^2\end{array}}$$

$$U_{\dot{m}_a} = 0.0076 \frac{kg}{s}$$

The relative uncertainty is found as,

$$\frac{U_{\dot{m}_a}}{\dot{m}_a} \times 100 = \pm \frac{0.0076}{1.096} \times 100 = \pm 0.693\%$$

A.4.7   Uncertainty of the Airside Reynolds Number

Reynolds number: $Re_a = \frac{\rho_a V_a D_{h,a}}{\mu_a} = 2880$

Absolute uncertainty:

$$U_{Re_a} = \pm \sqrt{\left(\frac{\partial Re_a}{\partial \rho_a} U_{\rho_a}\right)^2 + \left(\frac{\partial Re_a}{\partial V_a} U_{V_a}\right)^2 + \left(\frac{\partial Re_a}{\partial D_{h,a}} U_{D_{h,a}}\right)^2 + \left(\frac{\partial Re_a}{\partial \mu_a} U_{\mu_a}\right)^2}$$

$$\frac{\partial Re_a}{\partial \rho_a} = \frac{V_a D_{h,a}}{\mu_a} = \frac{(10.17)(0.00349)}{1.87 \mathrm{X} 10^{-5}} = 1898$$

$$\frac{\partial Re_a}{\partial V_a} = \frac{\rho_a D_{h,a}}{\mu_a} = \frac{(1.1597)(0.00349)}{1.87 \mathrm{X} 10^{-5}} = 216.4$$

$$\frac{\partial Re_a}{\partial D_h} = \frac{\rho_a V_a}{\mu_a} = \frac{(1.1597)(10.17)}{1.87 \mathrm{X} 10^{-5}} = 6.30 \mathrm{X} 10^5$$

$$\frac{\partial Re_a}{\partial \mu_a} = -\frac{\rho_a V_a D_{h,a}}{\mu_a{}^2} = -\frac{(1.1597)(10.17)(0.00349)}{(1.87 \mathrm{X} 10^{-5})^2} = -1177 \times 10^5$$

$$U_{\rho_a} = \pm 0.00382 \frac{kg}{m^3}$$

$$U_{V_a} = \pm 0.05 \frac{m}{s}$$

$U_{D_{h,a}} = \pm 0.3 \times 10^{-5}\ m$

$U_{\mu_a} = \pm 0.0047 \times 10^{-5}\ \frac{kg}{m.s}$

$U_{Re_a} = \pm 87.27$

The relative uncertainty for the airside Reynolds number is,

$$\frac{U_{Re_a}}{Re_a} \times 100 = \pm \frac{87.27}{2880} \times 100 = \pm 3.03\%$$

A.4.8   Uncertainty of the Airside Heat Transfer Rate

Airside heat transfer rate equation is as follows,

$$\dot{Q}_a = \dot{m}_a c_{p,a}\left(T_{a,i} - T_{a,o}\right) = 6232.1\ \text{watt}$$

$$U_{\dot{Q}_a} = \pm \sqrt{\left(\frac{\partial \dot{Q}_a}{\partial \dot{m}_a} U_{\dot{m}_a}\right)^2 + \left(\frac{\partial \dot{Q}_a}{\partial c_{p,a}} U_{c_{p,a}}\right)^2 + \left(\frac{\partial \dot{Q}_a}{\partial \Delta T_a} U_{\Delta T_a}\right)^2}$$

$$\frac{\partial \dot{Q}_a}{\partial \dot{m}_a} = c_{p,a}\Delta T_a = 1006.639 \times 5.65 = 5687.51$$

$$\frac{\partial \dot{Q}_a}{\partial c_{p,a}} = \dot{m}_a \Delta T_a = 1.096 \times 5.65 = 6.19$$

$$\frac{\partial \dot{Q}_a}{\partial \Delta T_a} = \dot{m}_a C p_a = 1.096 \times 1006.639 = 1103.27$$

$U_{\dot{m}_a} = 0.0076\ \frac{kg}{s}$

$U_{c_{p,a}} = \pm 0.0423\ \frac{J}{Kg\,°C}$

$U_{\Delta T_a} = \pm 0.44°C$

$$U_{\dot{Q}_a} = \pm \sqrt{(5687.51 \times 0.0076)^2 + (6.19 \times 0.0423)^2 + (1103.27 \times 0.44)^2}$$

$= \pm 487.36\ \text{W}$

The relative uncertainty for the airside heat transfer rate is,

$$\frac{U_{\dot{Q}_a}}{\dot{Q}_a} \times 100 = \pm \frac{487.36}{6232.1} \times 100 = \pm 7.82\%$$

A.4.9 Uncertainty of Airside Prandtl Number

Airside Prandtl number equation is $Pr_a = \frac{\mu_a c_{pa}}{k_a}$

$Pr_a = 0.713$

$$U_{Pr_a} = \pm \sqrt{\left(\frac{\partial Pr_a}{\partial \mu_a} U_{\mu_a}\right)^2 + \left(\frac{\partial Pr_a}{\partial c_{p,a}} U_{c_{p,a}}\right)^2 + \left(\frac{\partial Pr_a}{\partial k_a} U_{k_a}\right)^2}$$

$$\frac{\partial Pr_a}{\partial \mu_a} = \frac{c_{p,a}}{k_a} = 38082.1$$

$$\frac{\partial Pr_a}{\partial c_{p,a}} = \frac{\mu_a}{k_a} = 70.75 \times 10^{-5}$$

$$\frac{\partial Pr_a}{\partial k_a} = -\frac{\mu_a c_{pa}}{k_a^2} = -26.94$$

$$U_{\mu_a} = \pm 0.0047 \times 10^{-5} \frac{kg}{m.s}$$

$$U_{c_{p_a}} = \pm 0.0423 \frac{J}{kg.°C}$$

$$U_{k_a} = \pm 7.4 \times 10^{-5} \frac{W}{m.°C}$$

$$U_{Pr_a} = \pm \sqrt{\begin{array}{c}(38082.1\text{X}0.0047\text{X}10^{-5})^2 + (70.75\text{X}10^{-5}\text{X}0.0423)^2 \\ +(-26.94\text{X}7.4\text{X }10^{-5})^2\end{array}} = \pm 0.002$$

The relative uncertainty for the airside Prandtl number is found as,

$$\frac{U_{Pr_a}}{Pr_a} \times 100 = \frac{0.002}{0.713} \times 100 = \pm 0.28\ \%$$

A.4.10 Uncertainty of the Water Inlet Temperature

The mean de-ionized water inlet temperature, $T_{w,i} = 70°C$

Data Acquisition System Errors

RTD Sensor (instrumental error) with $i = 2$ and $j = 2$

Bias limit:

For Omega Resistance Temperature Detector –Pt100

Accuracy = ±0.012°C

Bias limit, B_{22}=0.012°C

Precision index, P22 = 0

Signal conditioning (instrumental error) with i = 2 and j = 3

Accuracy = ±0.06°C

Resolution = ±0.038°C

Offset error = ±0.025°C

System noise error = ±0.125°C

Uncertainty caused by bias is found as,

Bias limit,

$$B_{23} = \sqrt{\left(\frac{1}{2}(0.038)\right)^2 + (0.06)^2 + (0.025)^2 + (0.0125)^2} = \pm0.142°C \quad 95\%$$

$P_{23}= 0$

Signal conditioning (instrumental error) with i = 2 and j = 9

Bias limit, B_{29}=0

No. of data points, N = 108000

Degree of freedom, ν= N-1= 107999

Standard deviation, $St_{w,i}$ = 0.028°C

Precision Index, $P = P_{29} = \frac{St_{w,i}}{\sqrt{N}} = \frac{0.028}{\sqrt{108000}} = \pm\ 0.00008\ °C$

Degrees of freedom, ν= N-1= 107999

Bias limit, B=$\sqrt{B_{22}^2 + B_{23}^2}$=$\sqrt{(0.012)^2 + (0.142)^2}$= $\pm\ 0.142\ °C$ 95%

The absolute uncertainty is found as,

$$U_{T_{w,i}} = \sqrt{B^2 + \left(t_{8,95}P\right)^2}$$

$$t_{107999,0.95} = 1.960 \quad T > 1000$$

$$U_{T_{w,i}} = \pm\sqrt{(0.142)^2 + (1.96 \times 0.00008)^2} = \pm\ 0.142\ °C$$

The relative uncertainty is found as,

$$\frac{U_{T_{w,i}}}{T_{w,i}} \times 100 = \pm\frac{0.142}{70} \times 100 = \pm 0.2\%$$

A.4.11 Uncertainty of the Water Outlet Temperature

The mean de-ionised water outlet temperature is $T_{w,o}$= 34.52 °C

Data Acquisition System Errors

Sensor RTD stage (instrument error) with i = 2 and j = 2

Bias limit:

For Omega resistance temperature detector –Pt100

Accuracy = ±0.012°C

Bias limit, B_{22}= 0.012°C

Precision index, P_{22} = 0

Signal conditioning (instrumental error) with i = 2 and j = 3

Accuracy = ±0.06°C

Resolution = ±0.038°C

Offset error = ±0.025°C

System noise error = ±0.125 °C

Uncertainty caused by bias,

$$B_{23} = \sqrt{\left(\frac{1}{2}(0.038)\right)^2 + (0.06)^2 + (0.025)^2 + (0.0125)^2} = \pm 0.142°C \quad 95\%$$

$P_{23} = 0$

Signal conditioning (instrumental error) with i = 2 and j = 9

Bias limit, B29=0

No. of data points, N = 108000

Degree of freedom, v=107999

Bias limit, $B = \sqrt{(0.012)^2 + (0.142)^2} = \pm 0.143 \; °C \quad 95\%$

Precision index, P = P29 = $\pm$0.0002 °C

The absolute uncertainty is found as,

$$U_{T_{w,o}} = \sqrt{B^2 + \left(t_{8,95}P\right)^2}$$

$t_{v,0.95} = 1.960 \quad T > 1000$

$$U_{T_{w,o}} = \pm\sqrt{(0.143)^2 + (1.96 \times 0.0002)^2} = \pm \; 0.143 \; °C$$

The relative uncertainty is found as,

$$\frac{U_{T_{w,o}}}{T_{w,o}} \times 100 = \pm \frac{0.143}{34.52} = \times 100 = \pm 0.41\%$$

A.4.12 Uncertainties of the DI-Water Properties

The thermo physical properties of DI-Water can be found using the bulk temperature of the fluid inlet and outlet as,

$$T_b = \frac{T_{w,i} + T_{w,o}}{2} = \frac{70.52 + 34.52}{2} = 52.52°C$$

$$\rho_w = 997.05 \frac{kg}{m^3}$$

$$\mu_w = 0.00051 \frac{kg}{m.s}$$

$$c_{p,w} = 4165.86 \ \frac{J}{kg.°C}$$

$$k_w = 0.64666 \ \frac{W}{m.°C}$$

a-The uncertainty estimation for density (ρ_w):

$$U_{\rho w} = \pm \frac{\rho_{w,i} - \rho_{w,o}}{T_{a,o} - T_{a,i}}$$

$$U_{\rho w} = \pm \frac{996.349 - 977.5}{70.52 - 34.52} = \pm 0.5235 \ \frac{kg}{m^3}$$

b-The uncertainty estimation for the dynamic viscosity (μ_a):

$$U_{\mu w} = \pm \frac{\mu_{w,i} - \mu_{w,o}}{T_{a,o} - T_{a,i}}$$

$$U_{\mu w} = \pm \frac{0.000707 - 0.000391}{70.52 - 34.52} = \pm 0.0000087 \ \frac{kg}{m.s}$$

c-The uncertainty estimation for the specific heat ($c_{p,a}$):

$$U_{c_{p,a}} = \pm \frac{c_{p w,i} - c_{p w,o}}{T_{a,o} - T_{a,i}}$$

$$U_{c_{p,a}} = \pm \frac{4168.6 - 4166.91}{70.52 - 34.52} = \pm 0.0469 \ \frac{J}{kg.°C}$$

d-The uncertainty estimation for the thermal conductivity (k_w):

$$U_{k_w} = \pm \frac{k_{w,i} - k_{w,o}}{T_{a,o} - T_{a,i}}$$

$$U_{k_w} = \pm \frac{0.6255 - 0.6631}{70.52 - 34.52} = \pm 0.001 \ \frac{W}{m.°C}$$

A.4.13 Uncertainty of the DI-Water Mass Flow Rate

The uncertainty of the DI-water mass flow rate,

$$\dot{m}_w = \frac{m_w}{t}, \quad m_w = 3.71 kg, \ t = 127.75s$$

$= 0.029$ kg/s

The absolute uncertainty for the DI-water mass flow rate is as follows,

$$U_{\dot{m}_w} = \pm \sqrt{\left(\frac{\partial \dot{m}_w}{\partial m_w} U_{m_w}\right)^2 + \left(\frac{\partial \dot{m}_w}{\partial t_w} U_{t_w}\right)^2}$$

$$\frac{\partial \dot{m}_w}{\partial m_w} = \frac{1}{t} = \frac{1}{127.75} = 0.0078$$

$$\frac{\partial \dot{m}_w}{\partial t_w} = \frac{m_w}{t^2} = \frac{3.71}{(127.75)^2} = 0.00022$$

$$U_{m_w} = \pm 0.09021 \text{kg}$$

$$U_{t_w} = \pm 0.051 \text{s}$$

$$U_{\dot{m}_w} = \pm \sqrt{(0.0078 \times 0.09021)^2 + (0.00022 \times 0.051)^2} = 0.0007 \text{ kg/s}$$

The relative uncertainty can be found as,

$$\frac{U_{\dot{m}_w}}{m_w} \times 100 = \frac{0.0007}{0.029} \times 100 = \pm 2.41 \text{ \%}$$

A.4.14 <u>Uncertainty of the Water Side Heat Transfer Rate</u>

De-ionized water-side heat transfer rate can be found as,

$$\dot{Q}_w = \dot{m}_w c_{p,w}(T_{w,i} - T_{w,o}) = 4364 \text{ W}$$

The absolute uncertainty for the de-ionized water heat transfer rate is found as,

$$U_{Q_w} = \pm \sqrt{\left(\frac{\partial \dot{Q}_w}{\partial \dot{m}_w} U_{\dot{m}_w}\right)^2 + \left(\frac{\partial \dot{Q}_w}{\partial c_{p,w}} U_{c_{p,w}}\right)^2 + \left(\frac{\partial \dot{Q}_w}{\partial \Delta T_w} U_{\Delta T_w}\right)^2}$$

$$\frac{\partial \dot{Q}_w}{\partial \dot{m}_w} = c_{p,w} \Delta T_w = 4165.86 \times 127.75 = 532188.6$$

$$\frac{\partial \dot{Q}_w}{\partial c_{p,w}} = \dot{m}_w \Delta T_w = 0.0292 \times 127.75 = 3.7303$$

$$\frac{\partial \dot{Q}_w}{\partial \Delta T_w} = \dot{m}_w \Delta T_w = 0.0292 \times 4165.86 = 121.64$$

$$U_{\dot{m}_w} = 0.0007 \text{ kg/s}$$

$$U_{c_{p,w}} = \pm 0.0469 \frac{J}{kg°C}$$

$U_{\Delta T_w} = \pm\ 0.2°C$

$U_{Q_w} = \pm 373.32$

The relative uncertainty for the DI-water Reynolds number is obtained as,

$$\frac{U_{\dot{Q}_w}}{\dot{Q}_w} \times 100 = \pm \frac{273.32}{4364} \times 100 = \pm 8.5\%$$

A.4.15 Uncertainty of the DI-Water Reynolds Number

Reynolds number $Re_w = \dfrac{\dot{m}_w}{51\pi\mu_w D_{h,w}}$

$Re_w = 356$

The absolute uncertainty for the DI-water is as follows,

$$U_{Re_w} = \pm \sqrt{\left(\frac{\partial Re_w}{\partial \dot{m}_w} U_{\dot{m}_w}\right)^2 + \left(\frac{\partial Re_w}{\partial \mu_w} U_{\mu_w}\right)^2 + \left(\frac{\partial Re_w}{\partial D_{h,w}} U_{D_{h,w}}\right)^2}$$

$$\frac{\partial Re_w}{\partial \dot{m}_w} = \frac{1}{51\pi\mu_w D_{h,w}} = \frac{1}{51\pi(0.00051)(0.001)} = 12237.98$$

$$\frac{\partial Re_w}{\partial \mu_w} = \frac{\dot{m}_w}{51\pi\mu_w{}^2 D_{h,w}} = \frac{0.02918}{51\pi(0.00051)^2(0.001)} = 700204.5$$

$$\frac{\partial Re_w}{\partial D_{h,w}} = \frac{\dot{m}_w}{51\pi\mu_w D_{h,w}{}^2} = \frac{0.02918}{51\pi 0.00051(0.001)^2} = 357104.3$$

$U_{\dot{m}_w} = \pm 0.0007\ \dfrac{kg}{s}$

$U_{\mu_w} = \pm\ 0.0000087\ \dfrac{kg}{m.s}$

$U_{D_{h,w}} = \pm 0.0000348\ m$

$$U_{Re_w} = \pm \sqrt{\begin{array}{c}(12237.98 \times 0.0007)^2 + (700204.5 \times 0.0000087)^2 \\ +(357104.3 \times 0.0000348)^2\end{array}}$$

$U_{Re_w} = \pm 16.27$

The relative uncertainty for the DI-water side Reynolds number is obtained as,

$$\frac{U_{Re_w}}{Re_w} \times 100 = \frac{16.27}{356} \times 100 = \pm 4.57\ \%$$

A.4.16 <u>Uncertainty of the Water Side Prandtl Number</u>

Prandtl number $Pr_w = \frac{\mu_w\ c_{p,w}}{k_w}$

$Pr_w = 3.2868$

$$U_{Pr_w} = \pm \sqrt{\left(\frac{\partial Pr_w}{\partial \mu_w} U_{\mu_w}\right)^2 + \left(\frac{\partial Pr_w}{\partial c_{p,w}} U_{c_{p,w}}\right)^2 + \left(\frac{\partial Pr_w}{\partial k_w} U_{k_w}\right)^2}$$

$$\frac{\partial Pr_w}{\partial \mu_w} = \frac{c_{p,w}}{k_w} = \frac{4165.86}{0.64666} = 6442.1$$

$$\frac{\partial Pr_w}{\partial c_{p,w}} = \frac{\mu_w}{k_w} \frac{0.00051}{0.64666} = 0.00079$$

$$\frac{\partial Pr_w}{\partial k_w} = -\frac{\mu_w\ c_{p,w}}{k_w^{\ 2}} = -\frac{(0.00051)(4165.86)}{(0.64666)^2} = -5.08$$

$$U_{\mu_w} = \pm\ 0.0000087\ \frac{kg}{m.s}$$

$$U_{c_{p,w}} = \pm 0.0469\ \frac{J}{kg.^{\circ}C}$$

$$U_{k_w} = \pm\ 0.001 \frac{W}{m.^{\circ}C}$$

$$U_{Pr_w} = \pm \sqrt{(6442.1 \text{X} 0.0000087)^2 + (0.00079 \text{X} 0.0469)^2 + (-5.08 \text{X} 0.001)^2}$$

$$= \pm 0.056$$

The relative uncertainty for the DI-water Reynolds number can be estimated as,

$$\frac{U_{Pr_w}}{Pr_w} \times 100 = \frac{0.056}{3.2868} \times 100 = \pm 1.7\ \%$$

A.4.17 <u>Uncertainty of the DI-Water Peclet Number</u>

Peclet number can be found as,

$Pe_w = Re_w\ .\ Pr_w = 1170.05$

The absolute uncertainty for Pe_w is estimated as,

$$U_{Pe_w} = \pm \sqrt{\left(\frac{\partial Pe_w}{\partial Re_w} U_{Re_w}\right)^2 + \left(\frac{\partial Pe_w}{\partial Pr_w} U_{Pr_w}\right)^2}$$

$$\frac{\partial Pe_w}{\partial Re_w} = Pr_w = 3.286$$

$$\frac{\partial Pe_w}{\partial Pr_w} = Re_w = 356$$

$$U_{Re_w} = \pm 10.58$$

$$U_{Pr_w} = \pm 0.056$$

$$U_{Pe_w} = \pm \sqrt{(3.286 X 10.58)^2 + (356 X 0.056)^2} = \pm 40.07$$

The relative uncertainty for the airside Reynolds number

$$\frac{U_{Pe_w}}{Pe_w} \times 100 = \pm \frac{40.07}{1170} \times 100 = \pm 3.42 \%$$

The following Gnielinski correlation is used to evaluate the de-ionised water side $\frac{Pe_w.D_{MC}}{L_{MC}}$

A.4.18 <u>Uncertainty of the Water-Side Nusselt Number (Nu$_w$)</u>

$$Nu_w = [3.66^3 + 1.61^3(\frac{Pe_w.D_{MC}}{L_{MC}})]^{\frac{1}{3}} = 4.598$$

The absolute uncertainty for Nu$_w$ is estimated as,

$$U_{Nu_w} = \pm \sqrt{\left(\frac{\partial Nu_w}{\partial Pe_w} U_{Pe_w}\right)^2 + \left(\frac{\partial Nu_w}{\partial D_{MI}} U_{D_{MI}}\right)^2 + \left(\frac{\partial Nu_w}{\partial L_{MI}} U_{L_{MI}}\right)^2}$$

$$\frac{\partial Nu_w}{\partial Pe_w} = \frac{1.61^3}{3}\left[3.66^3 + 1.61^3\left(\frac{Pe_w.D_{MI}}{L_{MI}}\right)\right]^{-\frac{2}{3}}\left(\frac{D_{MI}}{L_{MI}}\right)$$

$$= \frac{1.61^3}{3}\left[3.66^3 + 1.61^3\left(\frac{1170.497 X 0.001}{,304}\right)\right]^{-\frac{2}{3}}\left(\frac{0.001}{0.304}\right)$$

$$= 1.391 x \, 0.0618 \, x 0.003289 = 0.000282$$

$$\frac{\partial Nu_w}{\partial D_{MI}} = \frac{1.61^3}{3}\left[3.66^3 + 1.61^3\left(\frac{Pe_w.D_{MI}}{L_{MI}}\right)\right]^{-\frac{2}{3}}\left(\frac{Pe_w}{L_{MI}}\right)$$

$$= 1.391 \, x \, 0.0618 \, x \, 3848.8157 = 330.858$$

$$\frac{\partial \text{Nu}_w}{\partial \text{L}_{\text{MI}}} = \frac{1.61^3}{3}\left[3.66^3 + 1.61^3 \left(\frac{\text{Pe}_w. \text{D}_{\text{MI}}}{L_{MI}}\right)\right]^{-\frac{2}{3}} \left(\frac{\text{Pe}_w. \text{D}_{\text{MI}}}{L_{MI}^2}\right)$$

$$= 1.391 \text{ x } 0.0618 \text{ x } 12.66 = 1.088$$

Therefore, $Nu_w = \pm 0.41$ W/m^2.°C

The relative uncertainty for the de-ionised water Nusselt number is estimated as,

$$\frac{\text{U Nu}_w}{\text{Nu}_w} \times 100 = \pm \frac{0.41}{4.598} \times 100 = \pm 8.91 \text{ \%}$$

A.4.19 <u>Uncertainty of the Water Heat Transfer Coefficient</u>

The de-ionized water side heat transfer coefficient (h_w) is a function of water-side Nusselt number (Nu_w), thermal conductivity (k_w) and hydraulic diameter ($D_{h,MC}$) as,

$$h_w = \frac{Nu_w.k_w}{D_{h,w}} = 2973.39$$

The absolute uncertainty for h_w is estimated as,

$$\text{U}_{h_w} = \pm \sqrt{\left(\frac{\partial h_w}{\partial \text{Nu}_w}\text{U}_{\text{Nu}_w}\right)^2 + \left(\frac{\partial h_w}{\partial k_w}\text{U}_{k_w}\right)^2 + \left(\frac{\partial h_w}{\partial \text{D}_{h,w}}\text{U}_{\text{D}_{h,w}}\right)^2}$$

$$\frac{\partial h_w}{\partial \text{Nu}_w} = \frac{k_w}{D_{h,w}} = \frac{0.6466}{0.001} = 646.6$$

$$\frac{\partial h_w}{\partial k_w} = \frac{\text{Nu}_w}{D_{h,w}} = \frac{4,598}{0.001} = 4598$$

$$\frac{\partial h_w}{\partial \text{D}_{h,w}} = -\frac{\text{Nu}_w.k_w}{D_{h,w}^2} = -\frac{4.598 X 0.6466}{0.001^2} = -2973066$$

Therefore, $\text{U}_{h_w} = \pm 200.49 \frac{\text{w}}{\text{m}^2.°C}$

The relative uncertainty for the de-ionised water Nusselt number is estimated as,

$$\frac{\text{U h}_w}{h_w} \times 100 = \pm \frac{200.49}{2973.39} \times 100 = \pm 6.74 \text{ \%}$$

A.4.20 <u>Uncertainty of the DI-Water Side Thermal Resistance</u>

The liquid side thermal resistance can be expressed as,

$$Re_w = \frac{1}{h_w A_w} = 0.000345$$

Therefore, the absolute uncertainty for the liquid side thermal resistance is estimated as,

$$U_{Re_w} = \pm\sqrt{\left(\frac{\partial R_w}{\partial h_w} U_{h_w}\right)^2 + \left(\frac{\partial R_w}{\partial A_w} U_{A_w}\right)^2}$$

$$\frac{\partial Re_w}{\partial h_w} = -\frac{1}{h_w^2 A_w} = \frac{1}{(0.9746)(2973.39)^2} = 0.00000012$$

$$\frac{\partial Re_w}{\partial A_w} = -\frac{1}{A_w^2 h_w} = \frac{1}{(2973.39)(0.9746)^2} = 0.000354$$

Therefore,

$$U_{Re_w} = \pm\sqrt{(1.2 \times 10^{-7} \times 4.6)^2 + (0.000354 \times 0.034)^2} = \pm 0.000016 \frac{°C}{w}$$

The relative uncertainty for the de-ionised water Nusselt number is estimated as,

$$\frac{U_{Re_w}}{Re_w} \times 100 = \pm\frac{0.000016}{0.000345} \times 100 = \pm 4.64\%$$

A.4.21 Uncertainty of LMTD

The log mean temperature difference (LMTD) is a function of ΔT_1 and ΔT_2 as,

$\Delta T_1 = T_{a,o} - T_{w,i} = 34.15 - 70 = -35.85$

$\Delta T_2 = T_{a,i} - T_{w,o} = 28.5 - 34.52 = -6.02$

The uncertainty for ΔT_1 is calculated as,

$$U_{\Delta T_1} = \pm\sqrt{\left(\frac{\partial \Delta T_1}{\partial T_{a,o}} U_{T_{a,o}}\right)^2 + \left(\frac{\partial \Delta T_1}{\partial T_{w,i}} U_{T_{w,i}}\right)^2}$$

Where,

$$\frac{\partial \Delta T_1}{\partial T_{a,o}} = 1$$

$$\frac{\partial \Delta T_1}{\partial T_{w,i}} = 1$$

$U_{T_{a,o}} = 1.56\ °C \qquad U_{T_{w,i}} = 0.142°C$

$$U_{\Delta T_1} = \pm\sqrt{(1\times 1.56)^2 + (1\times 0.142)^2} = \pm 1.57°C$$

The uncertainty for ΔT_1 is estimated as,

$$U_{\Delta T_2} = \pm\sqrt{\left(\frac{\partial_{\Delta T_2}}{\partial_{T_{a,i}}}U_{T_{a,i}}\right)^2 + \left(\frac{\partial_{\Delta T_2}}{\partial_{T_{w,o}}}U_{T_{w,o}}\right)^2}$$

Where,

$$\frac{\partial_{\Delta T_2}}{\partial_{T_{a,i}}} = 1$$

$$\frac{\partial_{\Delta T_2}}{\partial_{T_{w,o}}} = 1$$

$U_{T_{a,i}} = 1.33°C \qquad U_{T_{w,o}} = 0.142\ °C$

$$U_{\Delta T_2} = \pm\sqrt{(1 \times 1.33)^2 + (1 \times 0.142)^2} = \pm 1.34°C$$

$$\Delta T_{LM} = \frac{\Delta T_1 - \Delta T_2}{\ln\frac{\Delta T_1}{\Delta T_2}} = \frac{-35.85 + 6.02}{\ln\frac{-35.85}{-6.02}} = -16.72$$

$$U_{\Delta T_{LM}} = \pm\sqrt{\left(\frac{\partial_{\Delta T_{LM}}}{\partial_{T_1}}U_{T_1}\right)^2 + \left(\frac{\partial_{\Delta T_{LM}}}{\partial_{T_2}}U_{T_2}\right)^2}$$

Where,

$$\frac{\partial_{\Delta T_{LM}}}{\partial_{T_1}} = \frac{\ln\frac{\Delta T_1}{\Delta T_2} - (1-\frac{\Delta T_2}{\Delta T_1})}{\left(\ln\frac{\Delta T_1}{\Delta T_2}\right)^2} = \frac{\ln\frac{35.85}{6.02} - (1-\frac{6.02}{35.85})}{\left(\ln\frac{6.02}{35.85}\right)^2} = 0.299$$

$$\frac{\partial_{\Delta T_{LM}}}{\partial_{T_2}} = \frac{\ln\frac{\Delta T_1}{\Delta T_2} - (1-\frac{\Delta T_2}{\Delta T_1})}{\left(\ln\frac{\Delta T_1}{\Delta T_2}\right)^2} = \frac{\ln\frac{35.85}{6.02} - (\frac{35.85}{6.02}-1)}{\left(\ln\frac{6.02}{35.85}\right)^2} = -0.996$$

Therefore,

$$U_{\Delta T_{LM}} = \pm\sqrt{(0.299\times 1.57)^2 + (-0.996\times 1.34)^2} = \pm 1.37°C$$

The relative uncertainty for the de-ionised water Nusselt number is estimated as,

$$\frac{U_{\Delta T_{LM}}}{\Delta T_{LM}} \times 100 = \pm\frac{1.37}{16.72}\times 100 = \pm 8.19\ \%$$

A.4.22 Uncertainty of the Average Heat Transfer Rate

The average heat transfer rate is used to evaluate the other heat transfer parameters such as Nusselt number, NTU, effectiveness, Colburn factor, etc. The average heat transfer rate is obtained as,

$$\dot{Q}_{avg,a} = \frac{\dot{Q}_a + \dot{Q}_w}{2} = \frac{6232.1 + 4364}{2} = 5298.05 \text{W}$$

The absolute uncertainty of the average heat transfer rate is estimated as,

$$U_{\dot{Q}_{Overall}} = \pm \sqrt{\left(\frac{\partial \dot{Q}_{oa}}{\partial \dot{Q}_a} U_{Q_a}\right)^2 + \left(\frac{\partial \dot{Q}_{oa}}{\partial \dot{Q}_w} U_{Q_w}\right)^2}$$

$$\frac{\partial \dot{Q}_{Overall}}{\partial \dot{Q}_a} = \frac{1}{2} = 0.5$$

$$\frac{\partial \dot{Q}_{Overall}}{\partial \dot{Q}_w} = \frac{1}{2} = 0.5$$

$$U_{\dot{Q}_{overall}} = \pm\sqrt{(0.5 \times 487.36)^2 + (0.5 \times 373.32)^2} = \pm 306.95 \text{ W}$$

The relative uncertainty for the average heat transfer rate is estimated as,

$$\frac{U_{Overall}}{\dot{Q}_{Overalla}} \times 100 = \pm \frac{306.95}{5298.05} \times 100 = \pm 5.79\%$$

A.4.23 Uncertainty of the Total Thermal Resistance

The total thermal resistance can be shown for a cross flow heat exchanger as,

$$R_{total} = \frac{1}{UA} = \frac{F\Delta T_{lm,cf}}{\dot{Q}_{oa}} = 0.00312 = 0.00312$$

Where, the value of F is the correction factor that is found to be 0.98 throughout the experiment.

Therefore, the absolute uncertainty of the total thermal resistance is found as,

$$U_{R_{total}} = \pm \sqrt{\left(\frac{\partial R_{total}}{\partial \Delta T_{lm,cf}} U_{\Delta T_{lm,cf}}\right)^2 + \left(\frac{\partial R_{total}}{\partial \dot{Q}_{oa}} U_{\dot{Q}_{oa}}\right)^2}$$

$$\frac{\partial R_{total}}{\partial \Delta T_{lm,cf}} = \frac{F}{\dot{Q}_{oa}} = \frac{0.98}{6232.1} = 0.00016$$

$$\frac{\partial R_{total}}{\partial \dot{Q}_{oa}} = \frac{0.98 \Delta T_{lm,cf}}{\dot{Q}_{oa}^2} = \frac{098 X 16.72}{6232.1^2} = 0.00000042$$

$$U_{R_{Total}} = 0.00025 \; \frac{°C}{W}$$

The relative uncertainty for the de-ionised water Nusselt number is estimated as,

$$\frac{U_{R_{Total}}}{R_{Total}} \times 100 = \pm \frac{0.00025}{0.00312} \times 100 = \pm 8.01 \; \%$$

A.4.24 Uncertainty of Effectiveness

Effectiveness (ε) is shown as,

$$\varepsilon = \frac{\dot{Q}_{Overall,a}}{\dot{Q}_{max}}$$

$$= \frac{\dot{Q}_{Overall,a}}{(\dot{m}C_p)_{min} \Delta T_{max}}$$

$$\varepsilon = \frac{\dot{Q}_{oa}}{(\dot{m}C_p)_w (T_{a,i} - T_{w,i})} = 0.87$$

The absolute uncertainty for effectiveness is found as,

$$U_\varepsilon = \pm \sqrt{\left(\frac{\partial \varepsilon}{\partial \dot{Q}_{oa}} U_{\dot{Q}_{oa}}\right)^2 + + \left(\frac{\partial \varepsilon}{\partial \dot{m}_w} U_{\dot{m}_w}\right)^2 \left(\frac{\partial \varepsilon}{\partial c_{p,w}} U_{c_{p,w}}\right)^2 + \left(\frac{\partial \varepsilon}{\partial t_{a,i}} U_{t_{a,i}}\right)^2 + \left(\frac{\partial \varepsilon}{\partial t_{w,i}} U_{t_{w,i}}\right)^2}$$

$$\frac{\partial \varepsilon}{\partial \dot{Q}_{oa}} = \frac{1}{(\dot{m}C_p)_w (T_{a,i} - T_{w,i})}$$

$$\frac{\partial \varepsilon}{\partial \dot{m}_w} = \frac{\dot{Q}_{oa}}{(\dot{m}C_p)_w (T_{a,i} - T_{w,i})}$$

$$\frac{\partial_{\varepsilon}}{\partial_{c_{p_w}}} = \frac{\dot{Q}_{oa}}{\dot{m}_w c_{p,w}^2 (T_{a,i} - T_{w,i})}$$

$$\frac{\partial_{\varepsilon}}{\partial_{t_{a,i}}} = \frac{\dot{Q}_{oa}}{\dot{m}_w c_{p,w} \ (T_{a,i} - T_{w,i})^2}$$

$$\frac{\partial_{\varepsilon}}{\partial_{t_{w,i}}} = \frac{\dot{Q}_{oa}}{\dot{m}_w c_{p,w} \ (T_{a,i} - T_{w,i})^2}$$

$U_{\varepsilon} = \pm 0.041$

The relative uncertainty for effectiveness is found as,

$$\frac{U_{\varepsilon}}{\varepsilon} \times 100 = \pm \frac{0.041}{0.87} \times 100 = \pm 4.71 \ \%$$

A.4.25 <u>Uncertainty of NTU</u>

NTU is expressed as,

$$NTU = \frac{UA}{C_{min}} = \frac{UA}{(\dot{m}c_p)_w} = 2.59$$

The absolute uncertainty for NTU is estimated as,

$$U_{NTU} = \pm \sqrt{\left(\frac{\partial_{NTU}}{\partial_{UA}} U_{UA}\right)^2 + \left(\frac{\partial_{NTU}}{\partial_{\dot{m}_w}} U_{\dot{m}_w}\right)^2 + \left(\frac{\partial_{NTU}}{\partial_{c_{p,w}}} U_{c_{p,w}}\right)^2}$$

$$\frac{\partial_{NTU}}{\partial_{UA}} = \frac{1}{\dot{m}_w c_{p,w}} = \frac{1}{0.02918 X 4165.8} = 0.0082$$

$$\frac{\partial_{NTU}}{\partial_{\dot{m}_w}} = \frac{UA}{\dot{m}_w^2 c_{p,w}} = \frac{UA}{0.02918^2 X 4165.8} = 88.52$$

$$\frac{\partial_{NTU}}{\partial_{c_{p,w}}} = \frac{UA}{\dot{m}_w c_{p,w}^2} = \frac{UA}{0.02918 X 4165.8^2} = 0.00062$$

$$U_{NTU} = \pm \sqrt{(0.0082 \times 12)^2 + 88.52 \times 0.0007)^2 + (0.00062 \times 0.0469)^2} = \pm 0.12$$

The relative uncertainty for effectiveness is estimated as,

$$\frac{U_{NTU}}{NTU} \times 100 = \pm \frac{0.12}{2.59} \times 100 = \pm 4.63\%$$

A.4.26 Uncertainty of the Air Side Heat Transfer Coefficient

The airside heat transfer coefficient (h_a) is calculated from total thermal resistance equation as,

$$\frac{1}{h_a} = \frac{1}{\eta_a A_a (R_{Total} - R_w)} = 0.023$$

The absolute uncertainty for NTU is estimated as,

$$U_{h_a} = \pm \sqrt{\left(\frac{\partial h_a}{\partial \eta_a} U_{\eta_a}\right)^2 + \left(\frac{\partial h_a}{\partial A_a} U_{A_a}\right)^2 + \left(\frac{\partial h_a}{\partial R_{Total}} U_{R_{Total}}\right)^2 + \left(\frac{\partial h_a}{\partial R_w} U_{R_w}\right)^2}$$

$$\frac{\partial h_a}{\partial \eta_a} = \frac{1}{\eta_a^2 A_a (R_{Total} - R_w)}$$

$$\frac{\partial h_a}{\partial A_a} = \frac{1}{\eta_a A_a^2 (R_{Total} - R_w)}$$

$$\frac{\partial h_a}{\partial R_{Total}} = \frac{1}{\eta_a A_a (R_{Total} - R_w)^2}$$

$$\frac{\partial h_a}{\partial R_w} = \frac{1}{\eta_a A_a (R_w)^2} = \frac{1}{(0.99)(0.97)(0.00035)^2}$$

$$U_{h_a} = \pm 2.15$$

The relative uncertainty for the total thermal resistance is estimated as,

$$\frac{U_{h_a}}{h_a} \times 100 = \pm \frac{2.15}{43.48} \times 100 = \pm 4.94 \ \%$$

A.4.27 Uncertainty of the Airside Nusselt Number

The air-side Nusselt number is expressed as,

$$Nu_a = \frac{h_a D_{h,a}}{k_a} = 5.86$$

Therefore, the absolute uncertainty for the airside Nusselt number is estimated as,

$$U_{Nu_a} = \pm \sqrt{\left(\frac{\partial Nu_a}{\partial h_a} U_{h_a}\right)^2 + \left(\frac{\partial Nu_a}{\partial D_{h,a}} U_{D_{h,a}}\right)^2 + \left(\frac{\partial Nu_a}{\partial k_a} U_{k_a}\right)^2}$$

$$\frac{\partial_{Nu_a}}{\partial_{h_a}} = \frac{D_{h,a}}{k_a} = \frac{0.00349}{0.0264} = 0.13$$

$$\frac{\partial_{Nu_a}}{\partial_{D_{h,a}}} = \frac{h_a}{k_a} = \frac{44.35}{0.0264} = 1679.92$$

$$\frac{\partial_{Nu_a}}{\partial_{k_a}} = -\frac{h_a D_{h,a}}{k_a^2} = \frac{44.35 X 0.00349}{0.0264^2} = 222.08$$

$$U_{Nu_a} = \pm 0.46$$

The relative uncertainty for the airside Nusselt number is found as,

$$\frac{U_{Nu_a}}{Nu_a} \times 100 = \pm \frac{0.46}{5,86} \times 100 = \pm 7.85\%$$

A.5 Overall Uncertainties for All Operating Conditions

The uncertainties are estimated for all operating conditions as shown in Table A.3.

Table A.3 Overall experimental uncertainty

Key parameters	Relative uncertainties of the mean value
ΔP_a	±5.49%
Re_a	±3.03%
$\dot{Q}_a$	±7.82%
h_a	±4.94 %
Nu_a	±7.85%
$\dot{m}_w$	±2.41 %
Re_w	±4.57%
$\dot{Q}_w$	±8.5%
$\dot{Q}_{Overall,a}$	±5.79%
h_w	±6.74 %
Nu_w	±8.91%
R_{Total}	±8.01 %
ε	±4.71 %
NTU	±4.63%

REFERENCES

American Society of Mechanical Engineers. "Air Cooled Heat Exchangers" An American National Standard, Performance Test Code (PTC) 30-1991. ASME: NY, USA, 1991.

Bahrami, M., Yovanovich, M., and J.R., Colham. "A Novel Solution for Pressure Drop in Singly Connected Microchannel of Arbitrary Cross Section" International Journal of Heat and Mass Transfer, 50:2492-2502, 2006.

Bahrami, M., Tamayol, A., and P., Taheri. "Slip-Flow Pressure Drop in Microchannels of General Cross Section" Transactions of the ASME 031201-8, Vol. 131, March 2009.

Bier, W. "Manufacturing and Testing of Compact Micro Heat Exchangers with High Volumetric Heat Transfer Coefficients" American Society of Mechanical Engineers, dynamic Systems and Control Division, DSC 19: 189-197, 1990.

Bowman, R. A., Mueller, A. C., and W. M., Nagle. "Mean Temperature Difference in Design" Transactions of the ASME 62(1): 283-294, 1940.

Cao, H., Chen, G. and Q., Yuan. "Thermal Performance Of Cross Flow Microchannel Heat Exchangers" Industrial Engineering Chemical Resource. 49(13): 6215-6220, 2010.

Carrier. "Microchannel Technology - More Efficient, Compact, and Corrosion Resistant Technology for Air-Cooled Chiller Applications" Carrier Corporation, New York, USA, 2006.

Celata, G. P., Morini, G.L., Marconi, V., McPhail, S.J., and G. Zummo. "Using Viscous Heating to Determine the Friction Factor in Microchannels an Experimental Validation" Experimental Thermal and Fluid Science, 30(8):725–731, 2006.

Celata, G.P., Cumo, M., Guglielmi M., and G. Zummo. "Experimental Investigation of Hydraulic and Single phase Heat Transfer in 0.130-mm Capillary Tube", Microscale Thermophysical Engineering, 6(2):85–97, 2002, DOI: 10.1080/1089395029005323 1.

Cengel, Yunus. A. "Heat Transfer - a Practical Approach" McGraw-Hill, New York, ISBN 0-07-245893-3, 2007.

Çengel, Y.A., and A.J. Ghajar. "Heat and Mass Transfer: Fundamentals and Application" p. 374--403. Fourth edition McGraw Hill, New York. 2010.

Cole, K. D., and B., Cetin. "The effect of axial conduction on heat transfer in a liquid microchannel flow" International Journal of Heat and Mass Transfer 54(11-12): 2542–2549, 2011.

Coleman, H.W., and W.G., Steele. "Experimentation and uncertainty analysis for engineers" John Wiley & Sons: New York. 1989.

Dasgupta, Eng. Sarbadaman. "Experimental Study on Heat Transfer and Flow Characteristics of Air Cooling through Cross-flow Microchannel Heat Exchanger"

M.A.Sc. Thesis, Mechanical Engineering Department, University of Windsor, Canada, 2011.

Dasgupta, E. S., F.A., Siddiqui, and A., Fartaj. "Experimental study on air-side heat transfer & fluid flow characteristics of microchannel heat exchanger" Published by the Society of the Automotive Engineers Inc.PA, DOI: 10.4271/2011-01-1166. (Originally presented at the SAE 2011 World Congress, April 14, 2011 Detroit, MI, USA, SAE Paper # 2011-01-1166.Apr 2011.

Dasgupta, E. S., F.A., Siddiqui, and A., Fartaj. "Experimental Study on Air Cooling via a Multiport Mesochannel Cross-Flow Heat Exchanger" ASME 9th International Conference on Nanochannels, Mesochannels, and Minichannels (ICNMM), Paper # ICNMM2011-58257, Edmonton, Alberta, Canada, 2011.

Dean, W. R. "The streamline motion of fluid in a curved pipe" Philosophical Magazine. Series 7, V5 (30): 673-695, 1928.

Dehghandokht, M., Khan, M. G., and A., Fartaj. "Numerical Study of Fluid Flow and Heat Transfer in a Multi-Port Serpentine Meso-Channel Heat Exchanger" Journal of Applied Thermal Engineering, 31(10):1588-1599, 2011

Dehghandokht, M., Khan, M. G., and A., Fartaj. "Flow and Heat Transfer Characteristics of Water and Ethylene Glycol-water in a Multi-Port Serpentine Meso- Channel Heat Exchanger" International Journal of Thermal Sciences 50(8): 1615-1627, 2011.

Dittus, F.W., and L.M.K., Boelter. "Heat transfer in automobile radiators of the Tubular types" University of California Publication Engineering, 12(1):443. 1930.

Dong, J., Chen, J.P., Chen, Z.J., Zhou, Y.M., and W.F. Zhang. "Heat transfer and pressure drop correlations for the wavy fin and flat tube heat exchangers" Applied Thermal Engineering. 27(11-12): 2066-2073, 2007.

Dong, J., Chen, J., Chen, Z., and Y. Zhou. "Air-side thermal hydraulic performance of offset strip fin aluminum heat exchangers" Applied Thermal Engineering, 27(2-3): 306-313, 2007.

American Society of Mechanical Engineers. "Policy on reporting uncertainties in experimental measurements and results" Transactions of the ASME, Journal Fluids Engineering (Journal of heat transfer), 113: 313-314, 1991.

American Society of Mechanical Engineers. "Policy on reporting uncertainties in experimental measurements and results" Transactions of the ASME, Journal of Heat Transfer, 115: 5-6, 1993.

El-Shaboury, A.M.F., and S. J., Ormiston. "Analysis of laminar forced convection of air cross-flow in in-line tube banks with non-square arrangements" Numerical Heat Transfer, Part A, 48(2): 99-126, 2005.

Fan, Y., and L. Luo. "Recent Applications of Advances in Microchannel Heat Exchangers and Multi-Scale Design Optimization" Heat Transfer Engineering, 29(5):461–474, 2008, DOI: 10.1080/01457630701850968.

Figliola, R.S. and D.E. Beasley. "Theory and design for mechanical measurements" John Wiley & Sons, Inc.: NewYork. 2nd Edition, 171-209, 1995.

Fox, R. W., A. T. , McDonald, P. J., Pritchard. "Introduction to Fluid Mechanics, 8[th]Edition" John Wiley & Sons Inc., ISBN-13 9780470547557:328-402, 2010.

Gamrat, G., M., Favre-Marinet and D., Asendrych. "Conduction and entrance effects on laminar liquid flow and heat transfer in rectangular microchannels" International Journal of Heat and Mass Transfer 48 (14): 2943–2954, 2005.

Genhart, B. "Effects of viscous dissipation in natural convection" Journal of Fluid Mechanics, 14: 225-232, 1962.

Geankoplis, Christie John. "Transport processes and separation process principles" Upper Saddle River, NJ: Prentice Hall Professional Technical Reference. 4th edition, ISBN 013101367X, 2003.

Giudice, S. D., C., Nonino and S., Savino. "Effects of viscous dissipation and temperature dependent viscosity in thermally and simultaneously developing laminar flows in microchannels" International Journal of Heat and Fluid Flow, 28: 15–27, 2007.

Harris, C., M., Despa, and K., Kelly. "Design and fabrication of cross flow micro heat exchanger" Journal of Microelectromechanical systems 9: 502-508, 2000.

Herwig, H. and O. Hausner. "Critical view on ''new results in micro-fluid mechanics: an example" International Journal of Heat and Mass Transfer 46(5): 935–937, 2003.

Hetsroni, G., Mosyak, A., Pogrebnyak, E., and L.P. Yarin. "Heat transfer in micro-channels: Comparison of experiments with theory and numerical results" International Journal of Heat and Mass Transfer, 48(25-26): 5580-5601, 2005.

Incropera, F.P., D.P., DeWitt. "Introduction to Heat Transfer" John and Sons, New York. 4th edition, 347- 350, 2002.

Johnson, M., and R. D., Kamm. "Numerical Studies of Steady Flow Dispersion at Low Dean Number in a Gently Curving Tube" Journal of Fluid Mechanics 172: 329-345, 1986.

Kakac, S. and L., Hongtan. "Heat Exchangers: Selection, Rating and Thermal Design" CRC: New York, ISBN 9780849309021, 2002.

Kandlikar, S. G., and W. J., Grande. "Evolution of Microchannel Flow Passages-Thermohydraulic Performance and Fabrication Technology" Journal of Heat Transfer Engineering, 24(1):3-17, 2003.

Kandlikar, S.G., and H.R., Upadhye. "Extending the heat flux limit with enhanced mesochannels in direct single-phase cooling of computer chips" IEEE SEMI-THERM Symposium 21: 8-15, 2005.

Kandlikar, S.G., and M.R., King. "Heat transfer and fluid flow in minichannels and micrrochannels" Elsevier, Great Britain, ISBN 0-0804-4527-6, P3, 2006.

Kang, S. W., Chang, Y. T., and G. S., Chang. "The Manufacture and Test of (110) Orientation Silicon Based Micro Heat Exchanger" Tamkang Journal of Science and Engineering, 5(3):129–136, 2002.

Kays, W. M., and A. L., London. "Compact Heat Exchangers: Third Edition" Krieger Publishing Company, Florida, ISBN 1-57524-060-2:102-107, 1998.

Khan, M.G. and A., Fartaj. "Heat Transfer Experiments of Ethylene Glycol-Water Mixture in Multi-Port Serpentine Meso-Channel Heat Exchanger Slab" 3rd Joint US-European Fluids Engineering Summer Meeting (FEDSM) and 8th International Conference on Nanochannels, Mesochannels, and Minichannels (ICNMM), ASME, Montreal, Quebec, CANADA.FEDSM-ICNMM2010-31131 pp. 1569-1582, 2010.

Khan, M.G. and A., Fartaj. "Experiments of ethylene glycol-water mixture in multi-port circular straight microchannel slab" Proceedings of the Society of Automotive Engineers (SAE) Technical Paper 2010-01-0326, 2010, doi: 10.4271/2010-01-0326.

Khan, M. G., and A., Fartaj. "A Review on Microchannel Heat Exchangers and Potential Applications" International Journal of Energy Research 35(7): 553-582, 2010, doi: 10.1002/er.1720.

Kim, J-H., and E. A., Groll. "Microchannel Heat Exchanger Defrost Performance and Reliability (ASHRAE 1195-RP)" Final report, Ray W. Herrick Labs, Purdue University, 2003.

Kline, S.J. and F.A., McClintock. "Describing uncertainties in single-sample side experiments" Mechanical Engineering 75: 3-8, 1953.

Koo, J., and C. Kleinstreuer. "Viscous dissipation effects in microtubes and microchannels" International Journal of Heat and Mass Transfer 47(14-16):3159–3169, 2004.

Kumar, V, and K.D.P., Nigam. "Laminar convective heat transfer in chaotic configuration" International Journal of Heat and Mass Transfer, 50(13-14): 2469–2479, 2007.

Li, J., Wang, Shuangfeng, and Weijun, Zhang. "Air-side thermal hydraulic performance of an integrated fin and micro-channel heat exchanger" Energy Conversion and Management, 52(2): 983-989, 2011.

Lienhard, John. H. "A Heat Transfer Textbook" Phlogiston Press, Cambridge, MA, ISBN 13: 9780133850895.

Luo, L., Y., Fan, and D., Tondeur. "Heat Exchanger: From Micro - to Multi - Scale Design Optimization" International Journal of Energy Research, Wiley Online Library, 31: 1266-1274, 2007.

Ma, Allen. "Density of DI-Water" The Physics Factbook, 2007. 18 Jun 2012. <http://hypertextbook.com/facts/2007/AllenMa.shtml>.

Maranzana, G., Perry, S., and D. Maillet. "Mini- and micro-channels: influence of axial conduction in the walls" International Journal of Heat and Mass Transfer, 47(17-18): 3993–4004, 2004.

Mehendale, S.S., Jacobi, A. M., and R.K., Shah. "Fluid Flow and Heat Transfer at Micro- and Meso-scales with Application to Heat Exchanger Design" ASME Applied Mechanical Review, 53(7):175-193, 2000, doi:10.1115/1.3097347.

Moffat, R.J. "Describing the uncertainties in experimental results" International Journal of Thermal Fluid Science, 1: 3-7, 1998.

Mott, R. L. "Applied Fluid Mechanics" Pearson Prentice Hall, Upper Saddle River, New Jersey, ISBN 0-13-114680-7, 2006.

Morini, Gian, Luca. "Viscous heating in liquid flows in micro-channels" International Journal of Heat and Mass Transfer, 48(17): 3637–3647, 2005.

Murakami, Y., and B. B., Miki´C. "Parametric Investigation of Viscous Dissipation Effects on Optimized Air Cooling Microchanneled Heat Sinks" International Journal of Heat Transfer Engineering, 24(1):53–62, 2003.

Muzychka, Y. S., and M. M., Yovanovich "Pressure Drop in Laminar Developing Flow in Noncircular Ducts: A Scaling and Modeling Approach" Journal of Fluids Engineering, Vol. 131 / 111105-1, 2009

Muzychka, Y. S. "Generalized Models for Laminar Developing Flows in Heat Sinksand Heat Exchangers" Proc. 9th International Conference on Nanochannels, Microchannels and Minichannels, M.E. Alberta, Canada, ICNMM2011-58294, June 19-22, 2011.

Nuntaphan, A., T., Kiasiriroat, and C.C., Wang. "Air side performance at low Reynolds number of cross-flow heat exchanger using crimped spiral fins" International Communications in Heat and Mass Transfer 32(1-2): 151-165, 2005.

Owhaib, W., and B. Palm. "Experimental investigation of single-phase convective heat transfer in circular mesochannels" Journal of Experimental Thermal and Fluid Science, 28: 105-110, 2004.

Obot, N. T., Das, L. Vakili, D.E., and R.A. Green. "Effect of Prandtl Number on Smooth-Tube Heat Transfer and Pressure Drop" International Communications in Heat and Mass Transfer, 24(6):889-896, 1997.

Park, Y.G., and A.M., Jacobi. "The Air-Side thermal-hydraulic performance of flat-tube heat exchangers with louvered, wavy, and plain fins under dry and wet conditions" Journal of Heat Transfer, 131(6): 1-13, 2009.

Paeng, J.G., Kim, K.H., and Y.H. Yoon. "Experimental measurement and numerical computation of the air side convective heat transfer coefficients in a plate fin-tube heat exchanger" Journal of Mechanical Science and Technology, 23(2): 536-543, 2009.

Raschke. K. "Heat Transfer between the Plant and the Environment" Annual Review of Plant Physiology, 11: 111-126, 1960, DOI:10.1146/annurev.pp.11.060160.000551.

Petukhov, B.S. "Heat transfer and friction in turbulent pipe flow with variable physical properties" Advances in Heat Transfer, 6: 503-564, 1970.

Rugh, J.P., Pearson, J.T., and S., Rarnadhyani. "A study of a very compact heat exchanger used for passenger compartment heating in automobiles" Compact Heat Exchangers for Power and Process Industries, Heat Transfer Division, ASME 201: 15-24. 1992.

Schmidt, T.E. "Heat transfer calculations for extended surfaces" Refrigerating Engineering, 57:351-357, 1949.

Siddique, F.A., Dasgupta, E. S., and A. Fartaj. "Experimental investigation of air-side heat transfer and fluid flow performances of multi-port serpentine crossflow mesochannel heat exchanger" International Journal of Heat and Fluid Flow, 33(1): 207–219, 2012.

Shah, R.K., and A. L. London. "Laminar flow forced convection in ducts" Advanced Heat Transfer, Academic Press, New York, 1978.

Shah, R. K., and R. L., Webb. "Compact and Enhanced Heat Exchangers" Hemisphere Publication Corporation, ISSN: 961- 91393-0-5: 425-468, 1983

Shah, R. K., and D.P. Sekulic. "Fundamentals of Heat Exchanger Design" John Wiley & sons, ISSN: 0-471-32171-0, 2003.

Soares, A. A., Ferreira , J.M., Carameloa, , L. , Anacleto, J., and R.P. Chhabra. "Effect of Temperature-Dependent Viscosity on Forced Convection Heat Transfer from a Cylinder in Crossflow of Power-Law Fluids" International Journal of Heat and Mass Transfer, 53(21-22):4728-4740, 2010.

Sobhan, C. B., and S. V. Garimella. "A Comparative Analysis of Studies on Heat Transfer and Fluid Flow in Microchannels" CTRC Research Publications, MicroscaleThermophysical Engineering, 5(4):293–311, 2001.

Steinke, M. E., and S.G., Kandlikar. " Review of single-phase heat transfer enhancement techniques for application in microchannels, minichannels and microdevices" International Journal of Heat Technology, 22: 3-11, 2004.

Steinke, M. E., and S. G. Kandlikar. "Single-Phase Liquid Heat Transfer in Plain and Enhanced Microchannels" ICNMM2006-96227, Fourth International Conference on Nanochannels, Microchannels and Minichannels, Limerick, Ireland, 943-951, 2006.

Tailor, J., Carrano, A.L., and S. G. Kandlikar. "Characterization of the effect of surface roughness and texture on fluid flow—past, present, and future" International Journal of Thermal Sciences, 45: 962–968, 2006.

Taler, David. "Prediction of heat transfer correlations for compact heat exchangers" International Journal of Heat and Mass Transfer, 69(3): 137-150, 2005. DOI: 10.1007/s10010-004-0148-5

Tang, S. and K.T. Yang. "Thermal performance of a single-row fin-and-tube heat exchanger" International Journal of Thermal Science, 14(2): 172-180, 2005.

Tang, L.H., Zeng, M., and Q.W. Wang. "Experimental and numerical investigation on air--side performance of fin-and-tube heat exchangers with various fin patterns" Experimental Thermal and Fluid Science, 33(5): 818 – 827, 2009.

Tao, Y.B., He, Y.L., Huang, J., Wu, Z.G., and W.Q. Tao. "Numerical study of local heat transfer coefficient and fin efficiency of wavy fin-and-tube heat exchangers" International Journal of Thermal Sciences, 46(8):768-778, 2007.

Tiselj, I., Hetsroni G., Mavko, B., Mosyak, A., Pogrebnyak E., and Z. Segal. "Effect of axial conduction on the heat transfer in micro-channels" International Journal of Heat and Mass Transfer, 47 (12-13): 2551–2565, 2004.

Tian, L., He', Y., Tao, Y., and W. Tao. "A comparative study on the air-side performance of wavy fin-and-tube heat exchanger with punched delta winglets in staggered and in-line arrangements." International Journal of Thermal Sciences, 48(9): 1765-1776, 2009.

Tso, C.P., and S.P. Mahulinkar. "Experimental verification of the role of Brinkman number in microchannels using local parameters" International journal of Heat and Mass Transfer.43 (10): 1837-1849, 2000.

Tso, C.P., and S.P. Mahulinkar. "The use of the Brinkman number for single phase forced convective heat transfer in microchannels" International journal of Heat and Mass Transfer.41 (12): 1759-1769, 1998.

Tso, C. P., and S. P. Mahulikar, "Experimental Verification of the Role of Brinkman Number in Microchannels Using Local Parameters" International Journal of Heat and Mass Transfer, 43(10): 1837-1849, 2000.

Tunc, G., and Y. Bayazitoglu. "Heat transfer in microtubes with viscous dissipation" International Journal of Heat and Mass Transfer, 44(13): 2395–2403, 2001.

Tuckerman, D.B., and R.F.W. Pease. "High-performance heat sinking for VLSI" IEEE Electron Device Letter, VOL.EDL 2(5):126-129, 1981.

Wang, Chi-Chuan. "Recent progress on the air-side performance of fin-and-tube heat exchangers" International Journal of Heat Exchangers, 1: 49-76, 2000.

Wang, C.C., and K.Y. Chi. "Heat transfer and friction characteristics of plain fin-and-tube heat exchangers" part I: new experimental data. International Journal of Heat and Mass Transfer, 43: 2681 – 2691, 2000.

Wang, C.C., Webb, R.L., and K.Y. Chi. "Data reduction for air-side performance of fin-and- tube heat exchangers" Journal of Experimental Thermal and Fluid Science, 21, 218-226, 2000.

Westphalen, D., Roth, K. W., and J. Brodrick. "Emerging Technologies: Microchannel Heat Exchangers" ASHRAE Journal, 45(12):107-109, 2003.

White, Frank. M. "Fluid Mechanics", McGraw-Hill Companies, Burr Ridge, IL, ISBN13: 9780072402179, 2003.

Xu, B., Ooi, K.T., Mavriplis, C., and M.E. Zaghloul. "Viscous Dissipation Effects for Liquid Flow in Microchannels" NSTI. Nano Science and technology institute, Nano technology, 1: 100-103, 2002.

Zhang, Li-Zhi. "Total heat recovery: heat and moisture recovery from ventilation air" p.1-6.Nova Science Publishers, Incorporation, New York, 2008.

Zhuo, L., He, Y., Tang, G., and W., Tao. "Experimental and numerical studies of liquid flow and heat transfer in microtubes" International Journal of Heat and Mass Transfer, 50(17-18): 3447–3460, 2007.

Zimparov, Ventsislav. "Energy Conservation through Heat Transfer Enhancement Techniques" International Journal of Energy Research, 26 (7):675-696, 2002.

VITA AUCTORIS

NAME   Shahram Fotowat

PLACE OF BIRTH   Shiraz, Fars, Iran

YEAR OF BIRTH   1960

EDUCATION

- High school diploma, Shiraz University high school, 1977.

- Bachelor of Applied Science (B. A. Sc.) in Mechanical Engineering from Isfahan University of Technology, Isfahan, Iran, 1985.

- Master of Applied Science candidate in Mechanical Engineering, University of Windsor, Windsor, Ontario, Canada, 2012.

EXPERIENCE

Since 1991, he established and has managed the Zarnegar Engineering & Construction Company in the field of Petrochemical, Oil and Gas, Shiraz, Iran.

MAJOR PROJECTS

- Project manager responsible for installing insulation of pipes and equipments in the 7th refinery contract with TPL (Italy), Arak, Iran.

- Senior manager of Aromatic Petrochemical plant piping project, Bandar Imam Petrochemical Complex, Iran.

- Senior manager of the Parazylene Petrochemical plant piping project, Bandar Imam Petrochemical complex, Iran.

- Project manager of the water distribution Project of Estahban city, Fars, Iran.

- Senior project manager of the water distribution project of Bam city, Kerman, Iran.

- Senior project manager of a large scale gas distribution in Sadra, Shairaz, Iran.

As well as many other projects that could not be included, however, the most recent one is the Dehdasht pipeline project, Kohgiluyeh and Boyer-Ahmad, Iran.